CERN Yellow Reports: Monographs CERN-2024-004

An Accelerator-based Research Infrastructure for Cancer Therapy and Biomedical Sciences with Ion Beams

Editors: Ugo Amaldi, Elena Benedetto, Panagiota Foka, Sandro Rossi, Maurizio Vretenar

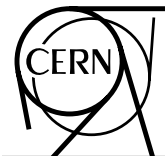

CERN Yellow Reports: Monographs
Published by CERN, CH-1211 Geneva 23, Switzerland

ISBN 978-92-9083-671-1 (paperback)
ISBN 978-92-9083-672-8 (PDF)
ISSN 2519-8068 (Print)
ISSN 2519-8076 (Online)
DOI https://doi.org/10.23731/CYRM-2024-004

This volume should be cited as:
An Accelerator-based Research Infrastructure for Cancer Therapy and Biomedical Sciences with Ion Beams, CERN Yellow Reports: Monographs, CERN-2024-004 (CERN, Geneva, 2024), doi:10.23731/CYRM-2024-004.

Editors: Ugo Amaldi *et al.*
Accepted December, 2024, by the CERN Reports Editorial Board
(contact Carlos.Lourenco@cern.ch).
Published by the CERN Scientific Information Service (contact Jens.Vigen@cern.ch).
Indexed in the CERN Document Server and in INSPIRE.
Published Open Access to permit its wide dissemination, as knowledge transfer is an integral part of the mission of CERN.

An Accelerator-based Research Infrastructure for Cancer Therapy and Biomedical Sciences with Ion Beams

U. Amaldi
TERA Foundation, Novara, Italy
J. Balosso
Department of Radiotherapy and ARCHADE, François Baclesse Centre, Caen, France
E. Benedetto
Fondation Tera-Care, Geneva, Switzerland, and SEEIIST
G. Bisoffi
INFN, Legnaro, Italy, and CERN, Geneva, Switzerland
J. Burgar
Slovenian Engineering Academy, Slovenia
S. Damjanovic
SEEIIST
M. Durante
GSI, Darmstadt, Germany
M. Dosanjh
University of Oxford, UK, and CERN, Geneva, Switzerland
P. Foka
GSI, Darmstadt, Germany
P. Georgieva
SEEIIST
Th. Haberer
HIT, Heidelberg, Germany
L. Litov
SEEIIST
S. Rossi
CNAO Foundation, Pavia, Italy
M. Sapinski
PSI, Villigen, Switzerland, and CERN, Geneva, Switzerland
B. Singers Sørensen
Department of Experimental Clinical Oncology, Aarhus, Denmark
H. Specht †
University of Heidelberg, Germany
M. Vretenar
CERN, Geneva, Switzerland

Editors: Ugo Amaldi, Elena Benedetto, Panagiota Foka, Sandro Rossi, Maurizio Vretenar

†Deceased 20 May 2024

Abstract
This report describes the general framework, research goals, preliminary technical design, and resources required for a novel accelerator-based research infrastructure for cancer therapy and biomedical sciences with ion beams. The information presented is the result of five years of research and design activities conducted by a wide multinational collaboration to address the needs of the South East European International Institute for Sustainable Technologies (SEEIIST), an initiative aiming at the construction in South East Europe of a facility devoted to cancer research and therapy with ion beams. The new design combines the experience of the European ion therapy centres and integrates innovative features that will push the performance much beyond the present state of the art for European carbon ion facilities.

Keywords
Medical physics; Hadron therapy; FLASH; Particle accelerators; Synchrotrons.

Introduction

This report describes the general framework, research goals, preliminary technical design, and resources required for a novel accelerator-based research infrastructure (RI) for cancer therapy and biomedical sciences with ion beams. The information presented is the result of five years of research and design activities conducted by a multinational team to address the needs of the South East European International Institute for Sustainable Technologies (SEEIIST), an initiative aiming at the construction in South East Europe of a facility devoted to cancer research and therapy with ion beams.

Proposed in 2016 at a workshop of the World Academy of Art and Science in Dubrovnik, SEEIIST was officially launched in 2017 with a Declaration of Intent for future collaboration signed between Albania, Bosnia and Herzegovina, Bulgaria, Kosovo[1], Montenegro, North Macedonia, Serbia, and Slovenia; Croatia agreed "ad referendum", while Greece participated as an observer and joined in 2022. In January 2018, the SEEIIST International Steering Committee (ISC) was formed, and its members unanimously selected a facility for cancer research and therapy with ion beams as the core of the institute, devoting 50% of its time to biomedical research and 50% to cancer treatment, focusing in particular on clinical trials. The strategic goals of the institute are both scientific—enhancing the tools and the knowledge needed in the fight against cancer—and political—building international cooperation and scientific capacity in South East Europe, joining countries that were recently at war in the shared mission of promoting science for peace.

The technical document supporting the ISC decision was a conceptual design report prepared in 2017 by a team of experts led by U. Amaldi, submitted to the scientific community and published as a CERN report in January 2019 [1]. The layout described in that document was based on a well-proven synchrotron design derived from the CERN Proton-Ion Medical Machine Study (PIMMS), which had been used for the construction of two European ion therapy facilities, Centro Nazionale di Adroterapia Oncologica (CNAO; Italy, in operation since 2011) and MedAustron (Austria, 2016) [2].

As a next step, since 2018, a large group of medical doctors, scientists, and engineers from different European institutions has been working towards the transformation of this initial design into the preliminary technical design presented in this report, providing at the same time an initial estimate of the resources required in terms of personnel and investment. While keeping the basic PIMMS layout, the new design moves forward by combining the experience from the other two European ion therapy centres—the Heidelberg Ion Therapy Center (HIT) and the Marburg Ion Beam Therapy Center (MIT) in Marburg, both in Germany—and by integrating innovative features that will push the performance much beyond the present state of the art for European carbon ion facilities. Its basic requirements are: acceleration of different types of beams, such as helium, carbon, oxygen, neon, and argon; reaching intensities more than ten times those of present facilities; and the use of advanced dose delivery techniques such as multiple energy extraction, mini-beams, and "FLASH"-type beams. Considering the long time needed for approval and construction of a new facility, the programme included the exploration of more advanced accelerator designs such as a superconducting synchrotron, a configuration that might substantially reduce footprint and cost of the accelerator but requires a considerable R&D effort to be implemented in a new facility. The design of the superconducting alternative, together with the development of a superconducting ion gantry design and of alternative accelerator designs limited to lighter ions, has been integrated into the European project "HITRI*plus*"[2], an integrating activity in the RI programme of Horizon 2020 that started in 2021 and will deliver its final results in 2025.

Cancer is a major concern for society. It is the second leading cause of death globally, and its incidence is expected to continue increasing in relation to the aging populations and aggressive

[1] This designation is without prejudice to positions on status and is in line with UNSCR 1244 and the ICJ Opinion on the Kosovo Declaration of Independence.

[2] Heavy Ion Therapy Research Integration plus, a project receiving funding from the European Union's Horizon 2020 Research and Innovation programme under Grant Agreement No. 101008548 (https://www.hitriplus.eu/).

environmental conditions in developing countries. As a powerful tool to fight this disease, more than 30 years since the first patient treatments in a hospital environment, cancer therapy with particle beams has proven to be a precious alternative to conventional treatment with X-rays, minimising the risk of collateral damage and recurrences for tumours close to critical organs and in paediatric patients, thus improving quality of life after treatment and reducing the social impact of cancer. While therapy with protons has now been taken up by industry and is increasingly available in many countries, therapy with ions heavier than protons is limited by the cost and dimensions of the facilities required, despite the advantages of heavier ions in terms of accuracy in dose deposition and their recognised effectiveness in treating tumours that are resistant to other types of radiation therapy. To fully exploit this precise and effective treatment tool, however, additional research is needed to refine imaging techniques and beam delivery methods, and to precisely assess the effects of ion beams on human biology.

The facility described in this report constitutes a unique opportunity to exploit the most recent techniques for patient treatment, sustaining at the same time an advanced research programme that cannot be addressed in present ion therapy centres devoting most of their operation time to patient treatment. Its design, as presented in this report, is not specific to South East European countries but could be implemented by any national or international community willing to embrace this therapy and research direction. If built in the South East Europe region, however, it could constitute the focal point of a regional hub for biomedical research and therapy with particles, becoming part of a network of medical centres, data-processing centres, accelerator development laboratories, etc., operating at the frontiers between medicine, biology, and physics. This network would constitute a major opportunity for the countries in the region to create peaceful collaboration and regional integration, contributing to the development of local society and helping to reverse brain drain.

At the moment of closing this report, the SEEIIST ISC meets regularly and maintains contact with its partners and with the European Commission, to define a framework for selecting the site and implementing the facility.

Geneva, October 2024

1 General framework and research goals

1.1 Scientific excellence

1.1.1 A multidisciplinary field

In hadron therapy—also called particle therapy or ion beam therapy—tumours are irradiated with subatomic particles (protons or heavier ions) accelerated to energies between 70 and 430 MeV/u by a dedicated particle accelerator. The number of patients already treated worldwide is increasing fast, almost exponentially (410,000[3] by the end of 2023, according to PTCOG statistics), with two ions so far licensed for treatment: protons and carbon ions. However, a vigorous research effort is required to further advance this rapidly progressing field of cancer therapy and fully exploit its potential. The most critical research subjects include radiobiology, accelerator design and dose delivery systems, dosimetry, tracking tumours in moving organs, and clinical comparison of different ions.

1.1.2 Scientific vision and mission

In Europe, there are 32 clinical centres that use protons for cancer treatment, but only four also provide the more expensive treatment with heavier ions (carbon), despite the many advantages of carbon ion therapy with respect to proton therapy. These four European centres are HIT in Heidelberg[4], CNAO[5] in Pavia, MIT[6] in Marburg, and MedAustron[7] in Wiener Neustadt. Outside Europe, ten carbon therapy centres are in operation in Asia, with one more under construction. The first carbon therapy centre in the USA is also under construction. In total, by the end of 2023, more than 57,000 patients had been treated with carbon ions worldwide, and approximately 10,000 new patients are added every year.

Typically, these centres run five days a week, 10–12 h per day, for patient treatments. Only nights and weekends are devoted to non-clinical research programmes, in a single, not very large, experimental room. Clearly, the main factors limiting the diffusion of ion therapy are the cost and the lack of clinical and pre-clinical experimental data on different ions and treatment modalities. Therefore, in this report, we propose a new "next-generation" facility, setting ***research as a priority and one of its main missions, in parallel with patient treatment***. For this reason, the overall concept for the design of the proposed facility is based on six basic choices:

1. The facility will be equipped with five 70–430 MeV/u ion beamlines, with three used for patient treatment and two used for the experimental programme.
2. The experimental programme will be based in a large experimental hall with two beams—from which additional beams can be branched out—and a crane for mounting two separate caves with movable shielding, which can be adapted to the changing needs of a long-term multidisciplinary programme.
3. The beam-sharing is based on the concept that about 50% of the daytime, and all nights and weekends, will be used for the non-clinical research programmes, while the remaining 50% of the daytime will be devoted to therapy for patients, who will be mostly enrolled in clinical research protocols.
4. Internal and external animal facilities will be available, thus allowing extended research programmes requiring the irradiation of small and large animals.
5. An additional research programme focused on new radioisotopes for imaging and cancer treatment could be supported by a dual-mode, low-energy injector accelerator. A specially designed linear accelerator (linac) would produce radioisotopes in parallel with its standard

[3] All patient data in this report are referred to the 2023 particle therapy patient statistics collected by the Particle Therapy Co-Operative Group (PTCOG), available at https://ptcog.site/
[4] http://www.hit-heidelberg.com
[5] https://www.fondazionecnao.it/
[6] https://www.mit-marburg.de/
[7] https://www.medaustron.at/

operation, generating beams to be accelerated to higher energies for the research and therapy facility.

6. The accelerator design benefits from the experience of the existing European centres and integrates the most advanced beam delivery techniques so as to allow (i) dose delivery in a single synchrotron cycle with tens of different energies and (ii) fast extraction and shaping of the ion beam for FLASH therapy, which requires dose rates 100 to 1000 times those used in standard treatments.

These choices have two very relevant consequences:

- many groups of excellent scientists and medical doctors would be motivated to bring their ideas, expertise, and instrumentation to perform experiments at the proposed new facility;
- the treatment of 375 patients/year (estimated to be treated during 50% of daytime hours on weekdays) could produce a level of revenue that is expected to cover at least half of the running costs of the facility.

The proposed facility is conceived to cover a broad and diversified experimental programme, aiming to boost research in this rapidly evolving multidisciplinary field, focusing on the following five research areas.

Radiobiology—Pre-clinical radiobiology is an essential tool for supporting new therapy solutions, such as the novel combined use of particle therapy with immunotherapy and radiogenomics for personalised medicine and patient selection. New therapy techniques, such as ultra-high-dose-rate (FLASH) irradiations and mini-beam radiotherapy (MBRT) need extensive pre-clinical testing. Basic radiobiology studies are also important for protection from space radiation.

Animal studies—The majority of radiobiology studies need animal models, generally rodents, including genetically modified animals. The new facility would incorporate on-site state-of-the-art animal facilities to enable modern radiobiology research. Moreover, it could offer a unique programme in Europe for treatment of large sick animals, in collaboration with external veterinary departments, with the aim of running comparative trials in pets.

Clinical trials—The majority of patients can be enrolled in clinical trials. In the first two years, the programme would focus on phase-I/II trials in tumour sites traditionally treated with protons and carbon ions. Later, the programme would also include a number of phase-III trials comparing carbon ions with other ions and ions with conventional intensity-modulated radiation. These trials will extend to treating locations with high mortality, such as the pancreas and lung.

Medical physics—Very promising ultrafast dose delivery methods can extend ion therapy to the challenging group of moving organs, while new synchrotron extractions and delivery systems will allow FLASH irradiations. Tomography with helium ions—possibly extracted alongside carbon ions—together with ion-acoustic imaging, promise to reduce range uncertainties. Moreover, in-beam MRI can generate precious real-time information and pave the way for adaptive treatments.

Materials science—Material research, using high-energy ions, is distinct from ion beam analysis and particle-induced X-ray emission, which are widely used with low-energy accelerators. The beams extracted from the accelerator will give the opportunity for testing the radiation hardness of shielding materials, space microelectronics, and the production of nanotubes.

1.1.3 Science community

A new European RI for cancer therapy and biomedical sciences with ion beams will clearly benefit from the experiences of existing ion therapy centres and established networks. Hence, it should be strongly connected with the four European carbon ion therapy centres, and it should be embedded in the five European networks active in the field: the European Network for Light Ion Hadron Therapy

(ENLIGHT)[8], the Infrastructure in Proton International Research (INSPIRE)[9] project, the European Particle Therapy Network (EPTN)[10], the International Biophysics Collaboration (IBC)[11], and the Heavy Ion Therapy Research Integration plus (HITRI*plus*)[12] project.

The ENLIGHT scientific network was established in 2002 to coordinate European efforts in hadron therapy, and it continues to meet annually and to organise educational sessions, focusing primarily on basic and translational research topics.

INSPIRE was funded by EU FP7 for the period 2018–2021, as an infrastructure—led by the University of Manchester—at which researchers of clinical proton therapy centres, universities, and industries could conduct their research.

EPTN—an official task force of the European Society for Radiotherapy and Oncology—was established in 2015 to foster cooperation among the increasing number of centres and to integrate particle therapy into the framework of existing radiation oncology research networks.

IBC was established at the Facility for Antiproton and Ion Research (FAIR) with the goal of creating a network for new and existing accelerator-based research facilities and coordinating their biomedical programmes.

HITRI*plus* is an integrating activity, launched in 2021, within the Horizon 2020 framework programme of the European Commission, aiming to structure and advance research on cancer therapy with heavy ions and its instruments.

1.1.4 Science highlights and technologies

From a clinical point of view, the biological effects of proton beams are similar to those of X-ray beams, which are commonly used in radiation therapy for cancer, but the surrounding healthy tissues are better spared. This is because for protons, as well as for heavier ions, the energy deposited per unit length, being inversely proportional to the square of their velocity, increases slowly with the penetration depth and reaches a peak at the point where it stops, a well-defined penetration depth determined by their energy. This enables the treatment of deep-seated tumours while sparing the healthy tissues both before and after the target tumour.

Carbon and other ions are more precise than protons due to their lower lateral scattering; moreover, they produce biological damage that is quantitatively and qualitatively different from that caused by X-rays or protons, meaning that they can be considered like a *different drug* in oncology. This increased efficacy is the basis of the clinical use of ions, and it can allow the control of so-called "radioresistant tumours" that are poorly controlled by either X-rays or protons.

The proposed RI features 70–430 MeV/u ion beamlines that can be used not only to host a number of phase-III trials comparing carbon and other ions with other radiations but also to tackle experimental programmes that go far beyond the usual clinical studies needed to expand ion beam indications.

Radiobiology experiments will support new therapy solutions, such as the novel combined use of ion therapy with immunotherapy and radiogenomics for personalised medicine and patient selection. In addition, they will allow radiobiology studies, which are important for space radiation protection. Experiments, both in vitro and in vivo, and the development of new extraction methods and beam delivery systems, will allow possibly disruptive FLASH radiotherapy with ion beams.

[8] https://enlight.web.cern.ch
[9] https://www.protonsinspire.eu/
[10] https://www.estro.org/Science/EPTN
[11] https://www.gsi.de/bio-coll
[12] https://www.hitriplus.eu/

1.1.5 Prospective users of the RI

The present study has been developed under the impulse, and with the strong support, of SEEIIST[13], which has adopted this accelerator-based RI for cancer therapy and biomedical sciences with ion beams as its main scientific programme. However, it is available to be implemented by any other institution, inside or outside Europe, that is willing to engage in the direction of cancer treatment and research with ions heavier than protons.

SEEIIST is an ambitious initiative aiming at two strategic goals: (a) enhancing the tools and the knowledge needed in the fight against cancer, and (b) simultaneously building international cooperation and scientific capacity in South East Europe. Proposed in 2016 at a workshop of the World Academy of Art and Science in Dubrovnik, SEEIIST was officially launched in 2017 with a declaration of intent for future collaboration signed between Albania, Bosnia and Herzegovina, Bulgaria, Kosovo[14], Montenegro, North Macedonia, Serbia, and Slovenia; Croatia agreed "ad referendum", while Greece joined as a full member in 2021. In January 2018, the SEEIIST ISC was formed, and its members unanimously selected a facility for cancer research and therapy with ion beams as the core of the institute, devoting 50% of weekdays, along with nights and weekends, to non-clinical research, and the remaining 50% of weekday time to cancer treatment, in particular clinical trials.

The technical document supporting the SEEIIST decision was a conceptual design report prepared in 2017 by a team of experts, submitted to the scientific community and published as a CERN report in January 2019: "A Facility for Tumour Therapy and Biomedical Research in South-Eastern Europe" [1].

The complete and detailed layout described in that document is based on the well-proven synchrotron design derived from the CERN PIMMS—which has already been used for the construction of CNAO and MedAustron—with the addition of some advanced accelerator components and operational features studied since 2018 by a large European collaboration built around the Next Ion Medical Machine Study (NIMMS)[15] initiative of CERN.

1.2 General framework and contents of the report

1.2.1 General framework

In Europe, about 50% of all cancer patients are irradiated with X-ray beams. These beams are produced when electrons, accelerated by a linear accelerator to about 10 million electronvolts (10 MeV), bombard a heavy metal target. This very successful radiation modality is almost 70 years old, and new techniques are constantly being developed, resulting in continuous increases in cure rates. In addition, they promise further substantial improvements in the reduction of secondary effects, as is the case with recent techniques such as image-guided radiotherapy (IGRT) and the very novel FLASH technique for "flash radiotherapy" [3] [4].

Radiation oncologists worldwide use about 10,000 electron linacs, corresponding to about half of all the running accelerators with energies larger than 1 MeV [5]. Today, radiation therapy with X-rays is by far the most cost-effective cancer treatment.

[13] https://seeiist.eu/
[14] This designation is without prejudice to positions on status and is in line with UNSCR 1244 and the ICJ Opinion on the Kosovo Declaration of Independence.
[15] https://nimms.web.cern.ch/

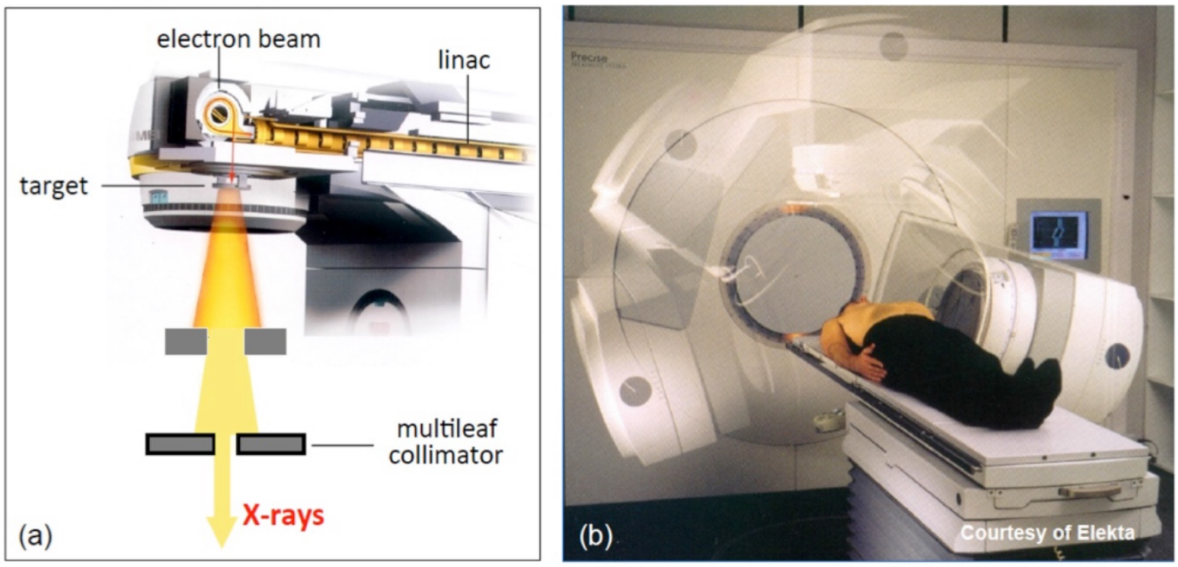

Fig. 1: (a) A sketch and (b) photograph of a clinical electron linear accelerator (linac). The magnet that deflects the electron beam by 270°, the target, and the collimators are mounted on a "gantry" that rotates around the patient.

A typical clinical electron linac is shown in **Fig. 1**. This is usually a small and lightweight device. The heart of such a linac is a very special, 1-m-long, copper accelerating tube with a diameter of about 10 cm, mounted on a gantry that rotates around the couch on which the patient is lying (**Fig. 1b**). However, for the treatment of deep-seated tumours, it is beneficial to use ions to ensure lower irradiation of the healthy tissues. Hence, hadron accelerators are needed to provide them at the energies required for treatment. Hadron accelerators are considerably larger, weightier, and costlier than electron linacs, because a proton (carbon ion) has 2000 (24,000) times the mass of an electron. Consequently, to treat a 30-cm-deep tumour, they have to be accelerated to about 200 MeV (5000 MeV). These large energies, which are required for treating deep-seated tumours with protons and other ions, can only be obtained with circular accelerators—cyclotrons, synchrocyclotrons, and synchrotrons—in which bunches of particles are bent by powerful magnets on a circular path and receive a small energy increase at every turn. Long linear accelerators have also been proposed, but so far, no proton or ion linac for therapy is in operation.

Current proton therapy cyclotrons (and synchrocyclotrons) are generally superconducting, with a diameter of about 1.5 m. Synchrotrons are also used, with a typical 230 MeV therapy synchrotron for protons having a diameter of 6–8 m, and its magnets, which bend the beam on a circular path, weigh tens of tonnes. Since a carbon ion is made up of six protons and six neutrons, to treat the same tumour target, the diameter of an ion synchrotron has to be about three times larger, i.e. 18–25 m. Typical therapy synchrotrons accelerate carbon ions to 430 MeV/u, i.e. to 5160 MeV total energy. As an example, the layout of the HIT is shown **Fig. 2**. More compact superconducting synchrotrons are under development and will be discussed in Section 3.4.5.

In synchrotrons, groups of particles are typically injected at energies of 5–7 MeV/u (60–84 MeV) by a special "injector" linac and circulate for about 1 s, corresponding to about one million turns. The configurations of all the ion synchrotrons are similar, including that of the proposed RI. Typically, they feature one or more horizontal beamlines and a vertical beamline, as shown in **Fig. 3**. In some centres, a carbon ion "gantry" rotates around the patient couch. The developments in the design of a new "lightweight" superconducting gantry are presented in Section 3.6.

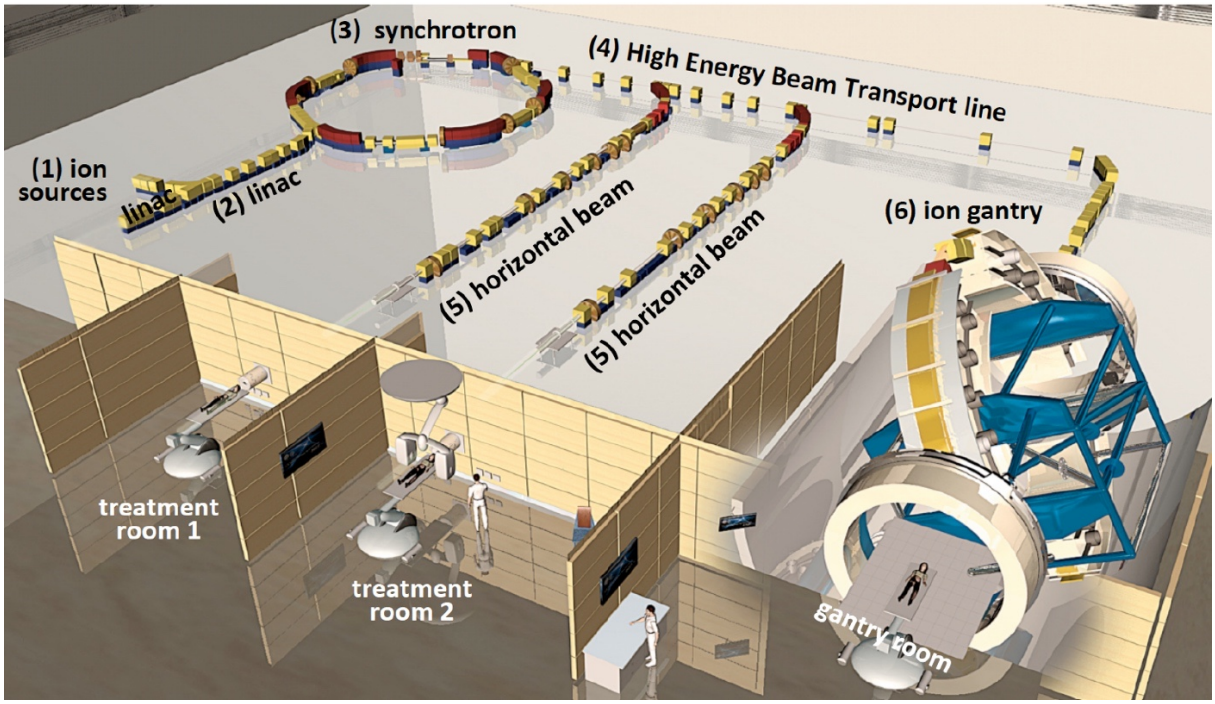

Fig. 2: Layout of the HIT centre, in Heidelberg, which was the first European carbon ion and proton centre. By the end of 2023, HIT had treated about 5200 patients with carbon ions.

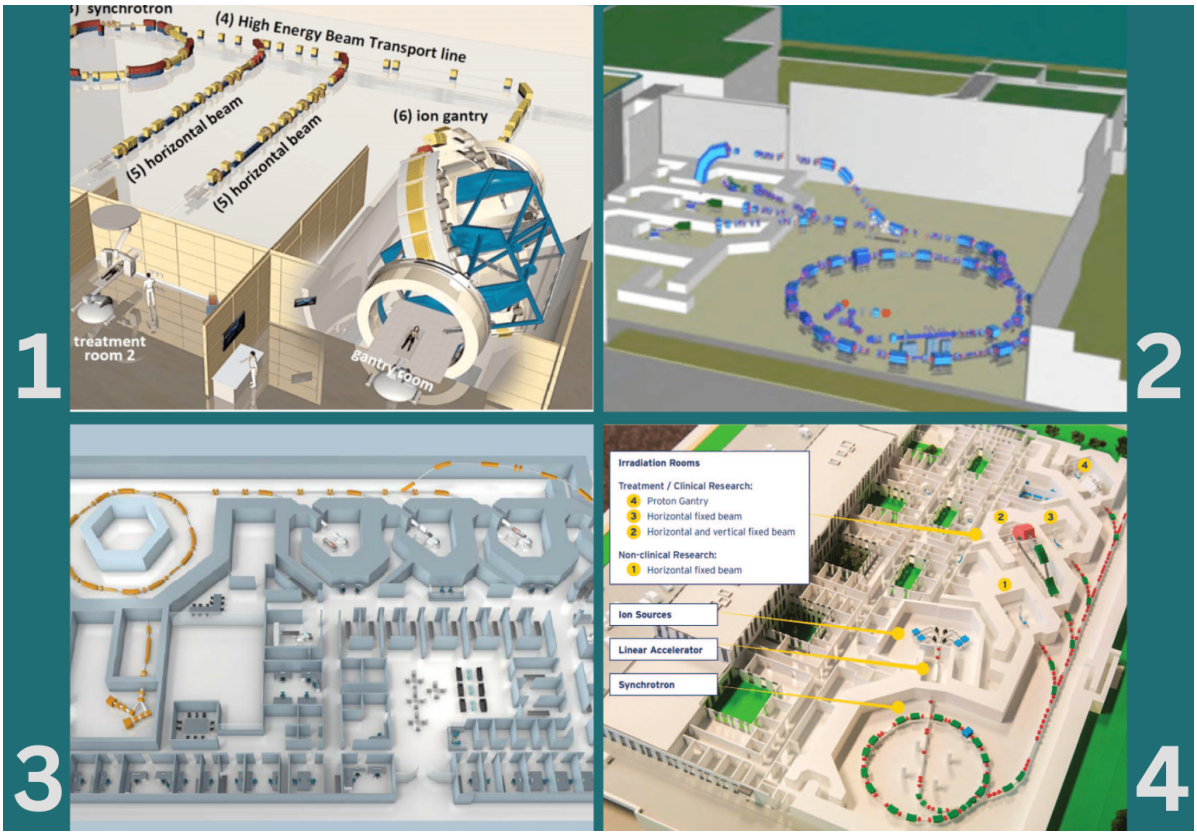

Fig. 3: Layouts of the four European carbon ion facilities: (1) HIT, (2) CNAO, (3) MIT, and (4) MedAustron.

The results of PIMMS [6] [2] have been used as a *baseline design* for the proposed new RI. PIMMS was developed at CERN from 1996 to 2000, and it gave birth to CNAO (Pavia, Italy) and MedAustron (Wiener Neustadt, Austria).

Synchrotrons such as those shown in **Fig. 3** can accelerate protons and C-ions to the 70–430 MeV/u range, but they can also accelerate many other types of ions between protons and oxygen ions. In the proposed facility, this range is foreseen to be enlarged, up to argon—for instance—when the ions are not fully stripped, to perform topical experiments in the five research areas discussed in Section 1.1.2.

1.2.2 Worldwide facilities and number of treated patients

Since the beginning of the new millennium, cancer tumour therapy with particle beams has gained huge momentum. Many new particle therapy facilities have been built, and many more are under construction (**Fig. 4**). In June 2024 (according to PTCOG), there were 127 facilities in operation worldwide, and another 66 were under construction or at the planning stage. Most of these are proton centres: 48 in the USA (protons only), 32 in Europe (of which four are *dual* centres for protons and carbon ions), 25 in Japan (of which six are carbon and one is dual), seven in China (of which one is carbon, and one is triple p and C-ion boosted), five in Taiwan (of which one is carbon), and ten (protons only) in other parts of the world. The locations of the European proton and carbon ion therapy centres are shown in **Fig. 5**.

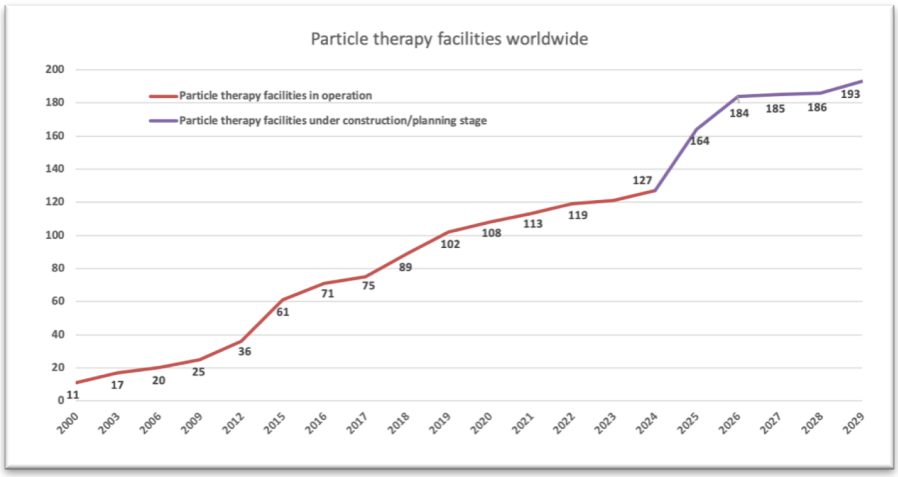

Fig. 4: Hadron therapy facilities in operation, under construction, and in the planning stage worldwide as of June 2024 (https://www.ptcog.site/).

Fig. 5: European hadron therapy facilities in operation in 2024.

The growth in the number of treated patients is almost exponential, in particular for protons, as shown in **Fig. 6**. At the end of 2007, the number of patients was 58,500, of which 54,000 were treated with protons and 4500 with carbon ions. At the end of 2023 (according to PTCOG), the number had

grown to 411,421 (350,336 with protons, 57,498 with carbon ions, and the rest with other ions such as helium, pions, and others).

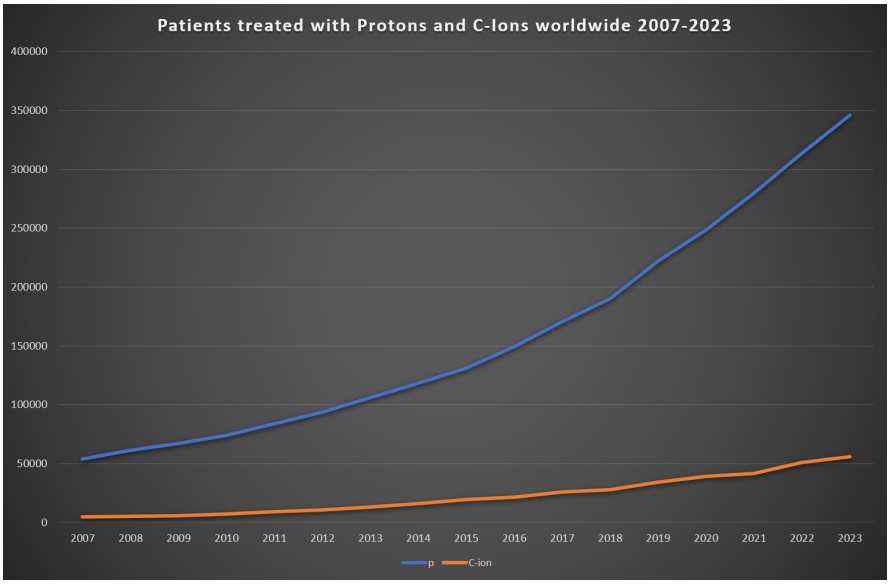

Fig. 6: Numbers of patients treated with proton and carbon ion beams worldwide to the end of 2023 (PTCOG).

1.2.3 Contents of the report

This report is subdivided in two parts. Part I is devoted to the description of the bases of hadron therapy and of the five research programmes that can be tackled with these beams. Part II describes the proposed facility, with its various extraction schemes, underscoring the novelty of its design, the ongoing development work, the foreseen organisation, and the needed investments.

In particular, Section 1.2 describes the world centres and Section 2.1 presents the physical and radiobiological bases of all radiation therapies. The clinical results obtained with proton and carbon ion beams are presented in Section 2.2. Sections 2.3 to 2.8 are devoted to detailed descriptions of the programmes in patient treatment, radiobiology, animal studies, medical physics, and materials science.

Section 3.2 of Part II justifies the choice of the baseline design based on warm-magnet technology, which is discussed in detail in Sections 3.3 to 3.5. Alternative superconducting solutions, under development in the NIMMS framework, are presented in Section 3.4.5. In Section 3.6, the superconducting alternatives for the rotating C-ion gantry are discussed. The very complex dedicated software needed to control the facility is presented in Section 3.8. Section 3.9 is devoted to the description of the building and of the site it requires. Environmental considerations are treated in Section 3.10. An estimate of the investments needed for both the construction and the running of the RI, based on the CNAO experiences, in the configuration chosen for SEEIIST is presented in Section 3.11.

2 Clinical and research programme

2.1 Physical and radiobiological bases of X-ray and hadron therapies

2.1.1 Fundamentals of tumour radiotherapy with X-rays

The aim of a radiation treatment is to deposit a large enough energy in a tumour target per unit mass—a quantity specified by the “radiation dose”, which is the energy absorbed by a unit of mass and is measured in “grays”: 1 Gy = 1 J/kg. In the case of a “conventional” irradiation, this energy is not transferred directly by the 1–10 MeV photons constituting the X-ray beam but indirectly by the

"secondary" electrons that are set in motion by the photons. Before coming to a stop, over a tortuous path of about 10 mm, these electrons lose energy in two ways:

(i) by promoting the electrons of the traversed atoms and molecules to a state of higher energy—molecular "excitation";

(ii) by ejecting atomic electrons, most of which, in turn, excite atoms and eject other electrons—molecular "ionisation".

Immediately afterwards, the excited molecules go back to their normal states, such that the main result of a radiation beam crossing a piece of matter is the deposition of energy in the form of ionisation of its atoms and molecules. The local radiation "dose" can be conveniently thought of as the energy left by the beam, in the form of ionisation, in a unit mass of tissue.

In the case of X-rays, the ionisation phenomena are characterised by the fact that the secondary electrons producing them are a "sparsely ionising" radiation, which means that two successive ionisations—along the electron paths—are separated by a distance larger than the 2-nm diameter of a DNA double helix. The average distance is determined by the values of the linear energy transfer (LET), which is the ratio between the energy loss ΔE and the length of track Δx over which the loss ΔE occurs:

$$\text{Linear energy transfer} = \text{LET} = \Delta E/\Delta x, \qquad (1.1)$$

which is usually measured in keV/μm.

In therapeutic X-ray irradiations with a linac (**Fig. 1**), the LET values along the paths of all secondary electrons are *consistently less than 10 keV/μm*. For these *sparsely ionising* radiations, about 70% of the energy is absorbed by water molecules and produces reactive oxygen species (ROS), i.e. simple molecules containing oxygen, which are chemically very aggressive and are usually called "free radicals" or "oxidants". By diffusing in the cell, these radicals can arrive on DNA molecules and break them, either on one strand (single-strand break, SSB) or on both strands (double-strand break, DSB). Because of its importance, the DNA molecule is protected by an elaborate repair system that restores, with high fidelity, the SSBs and most of the DSBs. The unrepaired breaks can cause the death of a cell.

ROS are activated in oxygenated tissues and deactivated in hypoxic ones. For this reason, hypoxic tumour cells tend to be "radioresistant", and therefore, they require larger X-ray doses to be severely damaged. Hypoxic cells are found at the centre of some large tumours, but there are also tumours that are radioresistant without being hypoxic. Many radiation oncologists state that about 5% of the tumours treated with radiation are radioresistant, but this fraction is not universally accepted by experts. In any case, radioresistance is the major problem of conventional radiotherapy: for radioresistant tumours, the cure rate is low because the X-ray dose cannot be increased to the level required for their control without irradiating nearby critical organs at risk (OARs) that cannot be irradiated because the patient's quality of life would be compromised.

2.1.2 Dose distribution and treatment schemes in X-ray therapy

As shown by the blue curve in **Fig. 7**, the depth–dose distribution of a conventional X-ray beam, after reaching a maximum at a depth of a few centimetres (the build-up effect), is characterised by an almost exponential attenuation and absorption of the dose, resulting in the maximum dose being delivered near the beam entrance.

Because the relative dose decreases with depth after 10–20 mm, the clinical effects also decrease. To concentrate the dose and produce the largest curative effects in the tumour target, the X-ray dose is given from many directions by rotating the electron linac around the patient and modulating the shape and intensity of each beam using computer-controlled "multileaf" collimators (**Fig. 1**).

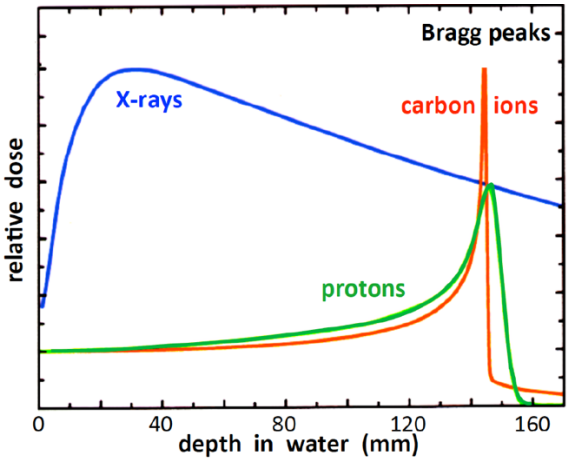

Fig. 7: Comparison of depth–dose profiles of high-energy photon (X-rays, in blue), proton (green), and carbon ion (red) beams. The abscissa shows the depth in water or in soft tissues.

The X-ray dose determines the clinical effects of the treatment, which are well documented for both normal and cancerous tissues thanks to more than 100 years of study. In a typical treatment with X-rays, a total dose of 60–70 Gy is deposited in a tumour target in 25–35 daily fractions over 5–7 weeks to allow for unavoidably irradiated healthy cells and tissues to repair the radiation damage. In fact, in about 95% of all solid cancers, the tumour cells are more "radiosensitive" than the normal cells. However, the cells of about 5% of tumours are more radioresistant than the normal cells, meaning that dose fractionation not only fails to help but may even be deleterious. Radioresistance is often due to a lack of cell oxygenation (which sometimes happens at the centre of a tumour) and is a serious limitation of conventional radiotherapy with X-rays. This can be overcome—as discussed in the next sections—by using carbon or other ions.

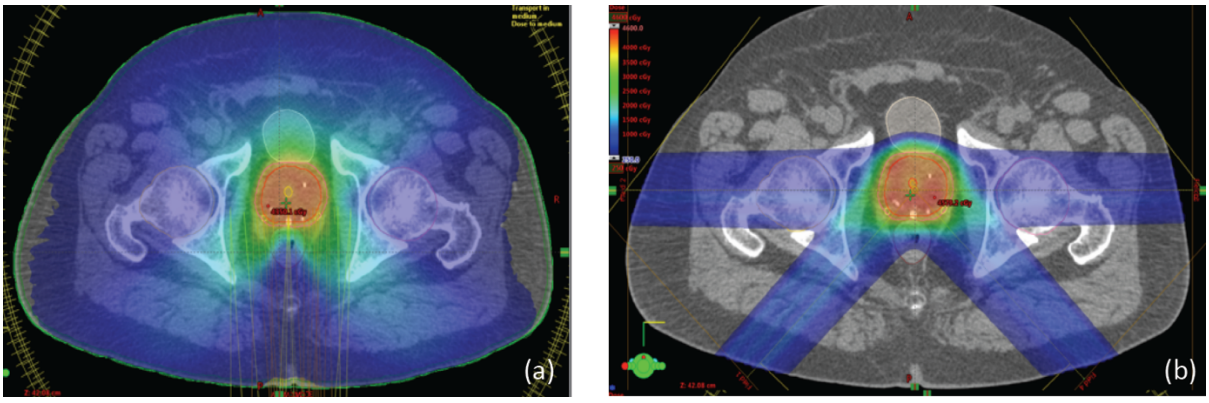

Fig. 8: Density of dose distribution for irradiation of prostate cancer: (a) TrueBeam (Varian Medical Systems) photon plan delivered using two nonplanar volumetric arcs (X-ray-based volumetric arc therapy) [7]; (b) 4-field proton plan (Varian Medical Systems) delivered as intensity-modulated proton therapy.

If the linac rotates around the patient **(Fig. 1b)**, with modern treatments, the conformality of the dose can be excellent, as shown in **Fig. 8a** for a prostate cancer. However, this outstanding target coverage comes at the cost of a large "dose bath", i.e. a very large volume receiving moderate to low doses. Unavoidably, these doses cause toxicity.

2.1.3 Physical bases of hadron therapy

In contrast to the X-ray treatment plan of **Fig. 8a**, the proton plan of **Fig. 8b** much better spares the rectum, which is in this case the main OAR. This is because charged hadrons move in practically straight lines in matter, and the largest ionisation density occurs just before the particles stop, in a well-defined "spot" determined by their energy, as shown in **Fig. 9**. When projected on the longitudinal plane, this spot is at the origin of the Bragg peaks of **Fig. 7**.

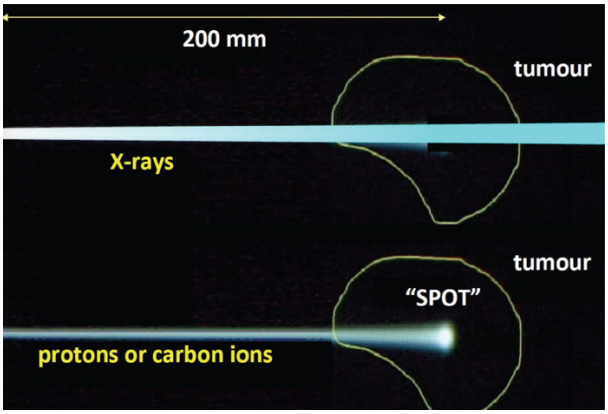

Fig. 9: X-rays traverse a tumour and also deposit their energy before and after the target volume (top), while protons and carbon ions deposit their energy in a well-defined spot (bottom). In water (and also in soft tissues), the 3D spot is at a depth of 200 mm when the energies of protons and carbon ions are 170 and 4000 MeV (i.e. 330 MeV/u), respectively.

In contrast to X-rays, heavy charged particles are "directly ionising radiation". After entering a target, they move in almost straight lines and *continuously* lose kinetic energy at the spatial rate $\Delta E/\Delta x$ by electrically interacting with the electrons of the tissue until they stop. In fact, the LET = $\Delta E/\Delta x$ is inversely proportional to the *square of the velocity* of the charged particle, so the energy deposited by a mono-energetic beam becomes increasingly larger towards the end of the range in matter as the particles slow down before stopping.

Both the longitudinal and lateral dose profiles—resulting from the interaction of charged particles with atomic electrons and the nuclei of the traversed tissues, respectively—are important in hadron therapy.

The longitudinal profile (**Fig. 10**) is dominated by the inelastic electromagnetic interaction with atomic electrons, leading to the Bragg peak. Because of the large mass of C-ions, the longitudinal width of the peak is greater for protons than for C-ions, as shown in **Fig. 7**. This is determined by the fluctuations resulting from infrequent large losses that set energetic electrons in motion in a phenomenon called "straggling". The transverse dimensions of a 200–300 mm-deep beam spot are about 10 mm in the case of protons and about 4 mm in the case of carbon ions. The lateral profile is caused by elastic scattering on target nuclei ("multiple scattering"), which leads to a broadening of the beam. Nuclear interactions reduce the intensity of the primary beam and contribute to both the longitudinal and lateral profiles.

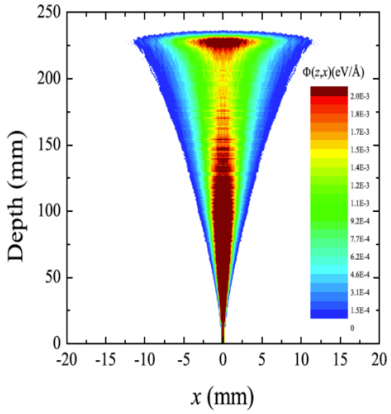

Fig. 10: Monte Carlo simulation of the longitudinal and lateral dose spread of a 160-MeV proton beam in water. Here, $\Phi(z,x)$ is the dose at depth z and lateral distance x.

Another difference between protons and carbon ions, which appears in **Fig. 7**, is that interactions with nuclei generate slow target fragments, which give a small contribution to the dose but can have high biological effectiveness. If particles heavier than protons are used, projectile fragmentation

produces fast fragments with a mean velocity similar to the velocity of the primary ions. These fragments have lower mass and, therefore, a greater range than the primary ions, thus generating a longitudinal tail in the Bragg curve, as shown by the red curve in **Fig. 7**. The angular distribution of these fragments is narrow in the forward direction, but the spread of the lighter fragments (protons and helium) contributes to the lateral widening of the beam.

The exploitation of the proton Bragg peak makes it possible to have the same conformality to the tumour target as with X-rays, but with a far lower number of external beams—e.g. four in **Fig. 8b**. This means that with charged particles, the tumour control probability (TCP) will be the same, but the normal tissue complication probability (NTCP) will be lower. If the TCP with X-rays is low, one can increase the target dose to reach the same NTCP as with X-rays but with a higher TCP. Non-malignant tissue can thus be spared by using charged particles due to their physical properties.

The treatment plan shown in **Fig. 8** represents a hypofractionated planning target volume dose prescription of 36.25 Gy to be administered in five fractions to a patient with prostate cancer, with a simultaneous integrated boost to the prostate gland of 40 Gy. The two plans delivered the same target dose, but the integral delivered dose was much lower with protons than with X-rays, and—as already said—the rectum is better spared from radiation.

The physics of hadron therapy is elegantly described in several books [8] [9] [10] [11] and in many review papers [12] [13] [14] [15] [16] [17] [18]. In the following, the physics bases are briefly described, and the open issues are treated in detail.

Generally speaking, the physics processes are fairly well understood, even if this is often not with the accuracy desirable for cancer treatment. The particle range in the Bragg-peak region, which is essential for irradiating the tumour and not the surrounding OARs, can be calculated by the stopping power. As shown in **Fig. 11a**, the narrow pristine Bragg peak must be extended by superposing many longitudinally narrow peaks to cover the entire tumour volume (spread-out Bragg peak, SOBP). **Figure 11b** shows that carbon ions, for the same iso-effective dose, spare the normal tissues located upstream of the tumour target better than protons, due to the larger relative biological effectiveness (RBE) of carbon ions with respect to protons, which is discussed in Sections 2.1.4 and 2.1.5.

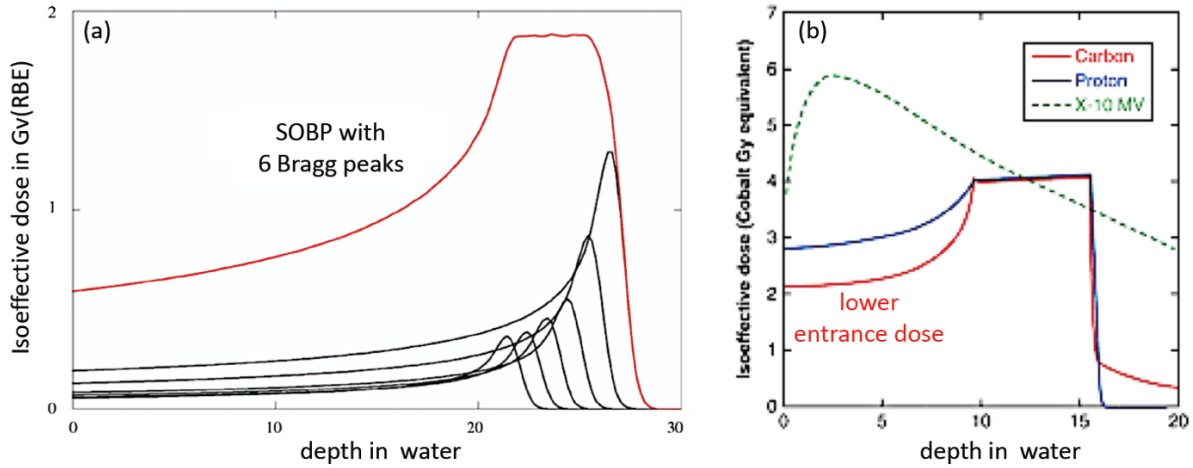

Fig. 11: (a) By superimposing several proton Bragg peaks, it is possible to create a spread-out Bragg peak (SOBP). (b) By considering the relative biological effectiveness (RBE) of carbon ions, a longitudinally uniform iso-effective dose can be delivered to the whole tumour, as is possible with protons.

The spreading of the Bragg peak can be achieved either by passive modulation of the primary-beam energy or by changing the energy while raster scanning tumour slices with a pencil beam (**Fig. 12**).

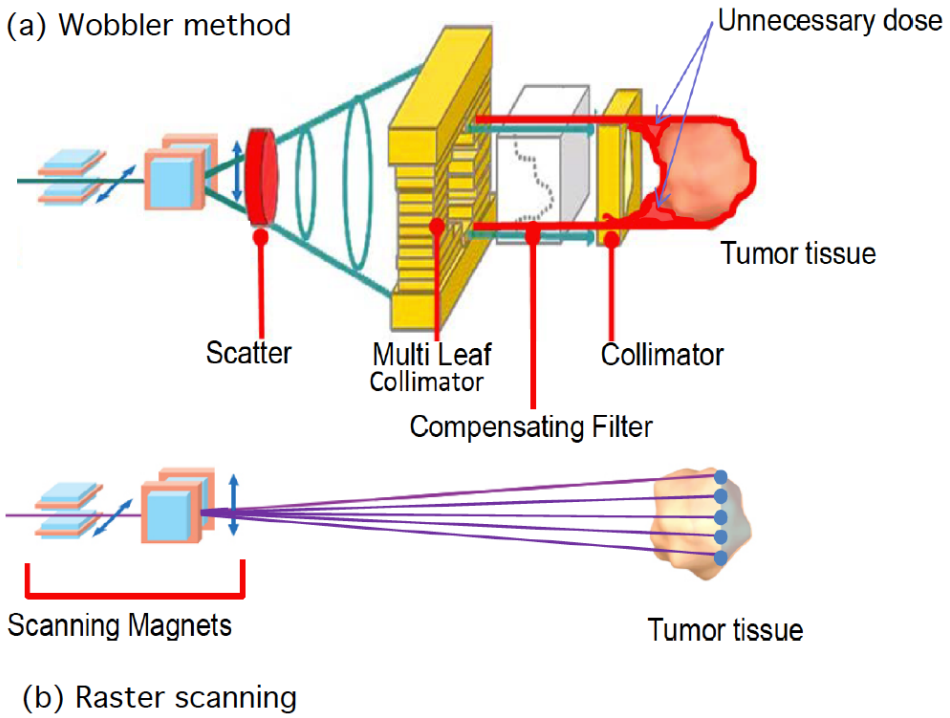

Fig. 12: Passive and active charged particle beam delivery systems. (Courtesy of Toshiba, Japan.)

Pencil-beam scanning has several advantages compared to passive scattering including: (1) high beam efficiency; (2) uniform coverage of tumours with complex shapes; (3) daily adaptive planning; (4) no extra dose in the proximal region; (5) no need for bolus and multileaf collimators; (6) reduced production of neutrons, which may represent a risk for second cancers.

Scanning provides superior dose distributions when compared to passive modulation. However, the interplay between pencil-beam scanning and organ movement (**Fig. 13**) caused by breathing may jeopardise the dose distribution, and this makes treatment of moving targets—e.g. lung tumours—with spot scanning much more complicated than with passive modulation [19].

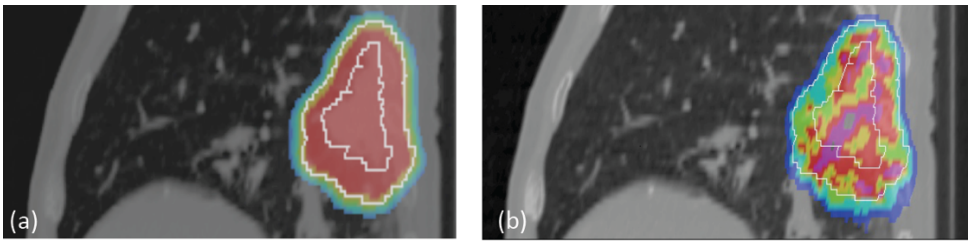

Fig. 13: (a) In a lung tumour treated with beam scanning, a uniform dose can be delivered to the clinical and planning target volumes, delimited by the two white lines, in the case of no motion (due to, for instance, extremely fast delivery). (b) The patient's breathing causes a non-uniform dose distribution. (Courtesy of Christoph Bert, University of Erlangen, Germany.)

Another cause of deterioration of the dose distribution is the range uncertainty due to organ movements and other reasons, which requires the deliberate delivery dose to a larger range than prescribed in order to avoid missing parts of the tumour. This, in turn, can move the SOBP into an OAR, thus increasing toxicity.

Lateral scattering broadens the beam and creates an undesired penumbra. **Figure 14** shows the transverse full width at half maximum (FWHM) values of different beams; these calculations were conducted using the Monte Carlo code Geant4[16]. The *y* axis shows the results of Gaussian fits to the beam distributions.

[16] https://geant4.cern.ch

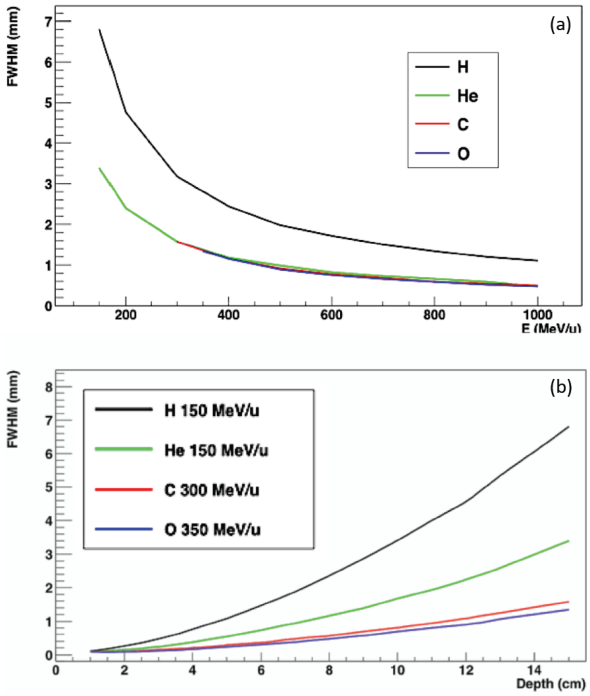

Fig. 14: Lateral spreads of different ion beams in water. (a) Transverse FWHM as a function of the depth for beams of different energy, having the same range of 15 cm in water. (b) Transverse FWHM values for beams of different energies having a 15-cm range in water.

Hirohiko Tsuji and other Japanese radiotherapists elected to use C-ions, and they started a programme at the National Institute for Radiological Sciences (NIRS) in Chiba in 1994, as reported in [18], for almost all kinds of solid tumours in different regions [20], treating about 15,500 patients since then. The success of the NIRS programme led to widespread use of carbon therapy in other such facilities in Asia and Europe. The USA is also constructing a C-ion therapy facility, which is being built by Mayo Clinics in Jacksonville, Florida. This is the first to be constructed after the termination of the clinical trials at the Lawrence Berkeley National Laboratory with helium and neon ions. Radiation oncologists only have experience with carbon ions; however, other ions with $1 < Z < 6$ (especially ^{4}He) or slightly heavier than ^{12}C (e.g. ^{16}O) can play a role in hadron therapy.

2.1.4 Radiobiological bases of hadron therapy

The biological effects of densely ionising radiation have been studied since the beginning of radiobiology. As a matter of fact, alpha particles (i.e. helium nuclei) deliver the main contribution to the background radiation dose on Earth due to indoor inhalation of radon. Neutrons have also been extensively studied, because of the need to protect workers in nuclear power plants, the use of fast neutrons in radiotherapy, and the exposure of the survivors of the atomic bombs that were dropped on Hiroshima and Nagasaki. The study of the biological effects of charged particles is more recent, and it depends on the availability of accelerators.

Most of the early studies focused on the measure of the RBE, which is defined as the ratio of a reference dose D_X (usually that due to X-rays produced by 200–250 keV electrons) to the dose D_{ion} necessary to produce the *same* biological effect with ion irradiation:

$$\mathrm{RBE} = [D_X/D_{ion}]_{\text{same effect}}. \qquad (1.2)$$

Often, the endpoint is chosen at 10% cell survival, but the RBE of course varies with the cell type and the effect considered.

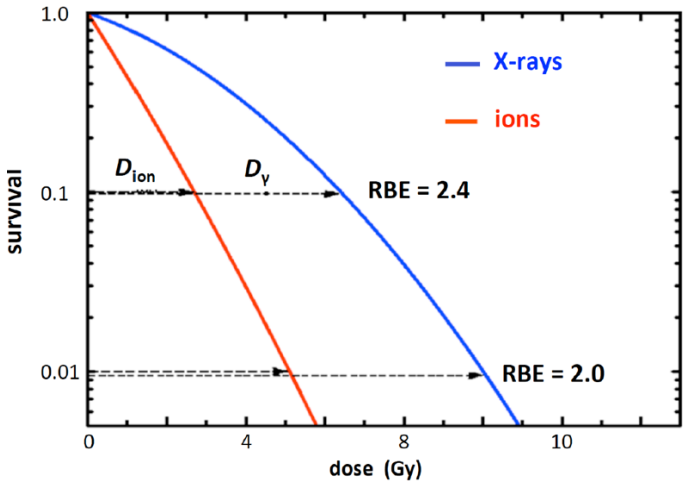

Fig. 15: Example showing the calculation of two RBE values from the survival curves of cultivated cells irradiated with X-rays and a carbon ion beam having a very large linear energy transfer (LET = 200 keV/µm).

Two typical dose–response curves are shown in **Fig. 15**. Here, the blue line refers to X-rays and features a "shoulder" that is due to the repair mechanism of the DSBs of the cellular DNA induced by sparsely ionising radiations (LET < 10 keV/µm), which are the fast electrons set in motion by the X-ray photons. Instead, for carbon ions (red curve) the shape of the dose–response curve is almost linear (in logarithmic scale) because the clustered damage produced by densely ionising radiation is not repaired. These different shapes are the reason that the RBE value depends on the chosen survival rate, i.e. on the dose per session: 2.4 (2.0) for a survival rate of 10% (1%).

Typically, the RBE of protons is within 10% of the RBE of X-rays; this is because protons, which have LET values of *less than 10 keV/µm* for most of their range in the patient's body, are sparsely ionising, like the electrons set in motion by X-ray photons. Instead, carbon ions have—in the last centimetres of their range—a LET *greater than 10 keV/µm* and behave as "densely ionising" radiation, producing physical, chemical, and biological effects in the traversed cells that are different from those of either X-rays *or* protons. Indeed, in the case of carbon ions, only about 30% of the deposited dose in the traversed cells produces free radicals, which *indirectly* induce SSBs and, more rarely, DSBs. Complementarily, 70% of the deposited dose *directly* produces closely spaced damage that, not being mediated by ROS, is insensitive to the oxygen content of the tissue and is not repaired by the cellular mechanisms. Because of this behaviour, the tumours that are radioresistant to both X-rays and protons—i.e. about 5% of all solid tumours—are the elective targets of carbon and other ions.

Overall, X-rays and protons act mainly *indirectly* on the DNA and through *chemical* processes, while carbon ions act mainly *directly* and through *physical* processes. As a consequence, the survival curve of densely ionising ions is linear, and the ion RBE values can be in the range 2–3 (as shown in **Fig. 15**); this results in an increased plateau/peak ratio—in other words, it is the equivalent of giving a higher dose to the tumour without increasing the dose delivered to the traversed tissues, as indicated in **Fig. 11b**.

Figure 16 shows a comparison of the effectiveness of protons and C-ions for cell killing in a radioresistant cell line (Chinese hamster ovary cells V79) with two opposite beams [21]. The measurements show that at the same survival in the plateau, C-ions induce more cell killing in the target region. Therefore, carbon and other ions allow a widening of the therapeutic window beyond the possibility offered by conformality of the dose.

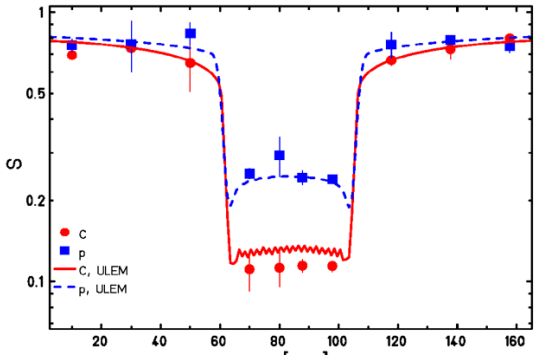

Fig. 16: Survival of V79 hamster cells irradiated with two opposite beams of either protons (blue) or C-ions (red). The curves are predictions using the local effect model (LEM) mode developed at GSI by G. Kraft and collaborators [22].

Notwithstanding many years of studies, starting at the Lawrence Berkeley Laboratory (LBL) in the 1970s and then at GSI in Germany, the Heavy Ion Medical Accelerator in Chiba (HIMAC) in Japan, Brookhaven National Laboratory (BNL) in the USA, and many other accelerators, uncertainty regarding RBE values is still high. In proton therapy, a constant value of 1.1 is used all along the SOBP, but it is generally acknowledged that corrections should be used, at least in the distal part of the SOBP, where radiobiology shows that slow protons have increased effectiveness.

The RBE clearly has a much greater impact when heavier ions are used, because in this case, the LET varies along the SOBP. For carbon ions, the dose in the SOBP is modulated using appropriate models for the RBE. Different models are used in Europe and Japan, and the calculated doses in Gy (RBE) can differ significantly. Uncertainty regarding the RBE is often quoted as a major hindrance to the widespread use of heavy ions in radiotherapy and is a source of concern in terms of potential late effects. For instance, C-ions have been used very little in paediatric patients, mostly due to concerns about the high risk of secondary effects, but also because of uncertainties related to an RBE value that is different from 1.

Many years of in-vitro studies on the RBE for cell killing consistently show a bell-shaped dependence on LET (**Fig. 17**) [23], along with a significant dependence on the particle charge. Data mining of survival curves for cell cultures exposed to charged particles has confirmed the spread in the RBE–LET relationship originally measured at LBL. The blue curves in **Fig. 17** describe the approximated band of Chinese hamster V79 survival data, and the red curves include the data on different in-vitro cell lines collected at LBL in the 1970s.

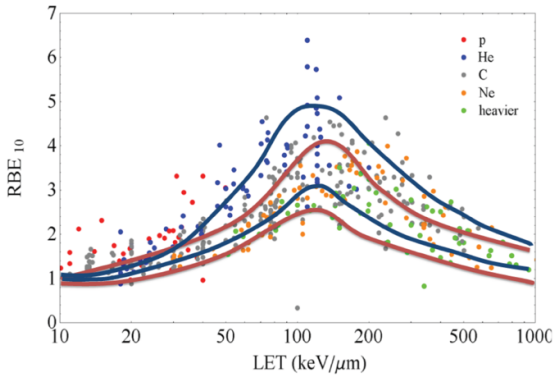

Fig. 17: Variability in the relative biological effectiveness (RBE; calculated at 10% survival level) versus LET, the linear energy transfer, in water measured in keV/µm, for in-vitro data. Points are extracted from the large PIDE database[17] developed at GSI. Different colours correspond to different ions [23].

[17] https://www.gsi.de/bio-pide

2.1.5 RBE-weighted dose

In treating patients with carbon and other ions heavier than protons, understanding the radiobiological effectiveness, applying to both tumour and normal tissues, is crucial because the radiation field must be quantified by giving the "RBE-weighted" dose:

$$D_{\mathrm{RBE}} = \mathrm{RBE} \times D, \tag{1.3}$$

which is reported as Gy (RBE) and is obtained by multiplying the physical dose (measured in Gy = J/kg) by the RBE value of that particular tissue.

Although conceptually simple, Eq. (1.3) needs to be applied with caution in the clinical environment because the RBE of a tissue is not only characterised by a single value but depends on several factors: first of all on the LET and the considered effect level, but also on the dose rate, the oxygenation of the tissue, the irradiation history, and so on. Moreover, due to the many different energies of the particles traversing a small volume of a tissue, the RBE varies within the irradiated target, whereas for photons, the RBE can be taken to be equal to 1 throughout the entire irradiated volume.

When applying Eq. (1.3), the percentage error in the RBE-weighed dose D_{RBE} is equal to the percentage error in the RBE itself. Thus, the precise characterisation of the RBE, and its dependencies on the relevant physical and biological factors, are of utmost importance. Data for cells cultivated in vitro are available, such as those shown in **Fig. 17**. However, cells and tissues in vivo may behave differently; therefore, only systematic animal studies and accumulated human-treatment data can provide the information needed for planning the irradiation of human patients. A reduction of uncertainties is highly desirable, and many well-conceived experiments are thus needed to gather enough information and reduce the error in D_{RBE} to less than ±5%. Note that in X-ray treatments, the error in the dose D, which is the only relevant quantity, is required to be smaller than ±2.5%.

In a treatment-planning software, the increased radiobiological effectiveness of ions is integrated into a model that describes the radiosensitivity of normal and cancerous tissues. The most used of these in Europe is the local effect model (LEM) developed at GSI by Gerhard Kraft and collaborators [22]. This model is based on the complete 3D distribution of the ionisation, and damage, around the track, along with knowledge about the photon dose–response curve for the endpoint of interest. Thus, it allows the description of biological effects both in vitro and in vivo.

In summary, carbon ion beams of about 5000 MeV are indicated for treatment of deep-seated tumours that are radioresistant to both X-rays and to protons. These types of tumour are thus the elective targets in a carbon ion facility.

In general, the major determinants that need to be considered are:

(i) the enhancement of RBE, which is particularly pronounced in the Bragg peak and which varies with the residual range of the particle;

(ii) the decrease of the RBE of ions with increasing dose per session; thus, the subdivision of the total dose in fractions is an important parameter that affects the RBE;

(iii) the higher RBE of ions for cells that manifest a higher repair capacity and are thus resistant to photon radiation as compared to cells showing a higher sensitivity to photon radiation;

(iv) the biological effects of ions being less sensitive to oxygen concentration as compared to conventional radiation.

The relevance of these factors has been clearly demonstrated in numerous in vitro and in vivo experimental approaches, but many experiments still need to be performed, both with cell monolayers in vitro and with small animals in vivo. Modelling will always be necessary for incorporating RBE into treatment planning, and there is room for improvement here in switching from phenomenological to mechanistic models.

It is worth noting that even though the uncertainty in RBE is certainly an issue to be better understood in C-ion therapy, it should not prevent the use of this treatment modality, given the lack of significant side effects observed so far in Japan and Europe. Centres such as NIRS, HIT, and CNAO, where patients are treated with C-ions, all use phase-I/II dose-escalation trials to find optimal protocols. At IMPCAS in Lanzhou, China, patients are treated with C-ions without any biological modulation, i.e. with a flat SOBP in terms of dose, apparently with no major toxicity.

The LEM, which is widely used in Europe, is very detailed and cannot be described here. However, some simple considerations allow an understanding of the values of LET at which the RBEs of **Fig. 17** become different from 1. The most important parameter is the diameter of the DNA molecule—about 2 nm—as DNA represents the main target of the radiation attack inside the cell. (However, other scales, such as the level of chromatin organisation—so-called "giant loops" with a size of the order of 1 µm—and the cell nucleus size, about 10 µm, are also known to be of relevance.) The importance of the nanometre scale is illustrated in **Fig. 18**, which indicates the decrease of the average distance between two successive ionisations (indicated by the letter *d*) when a carbon ion penetrates the patient's body, losing energy until it stops.

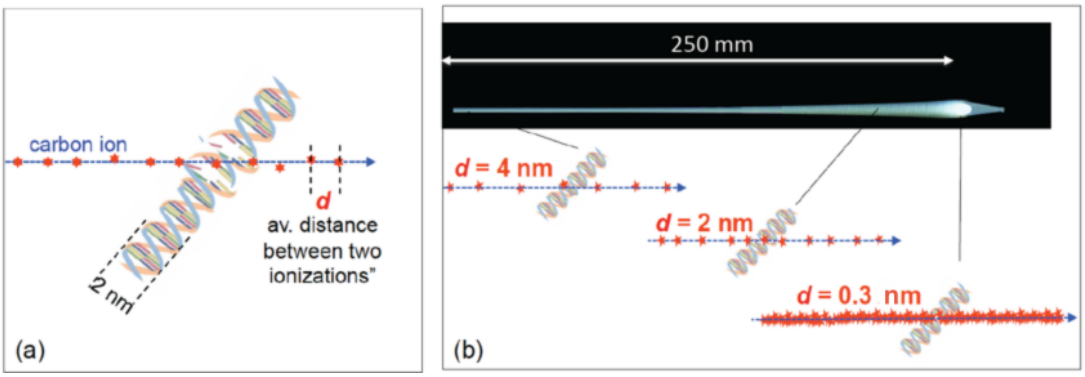

Fig. 18: (a) One simple parameter defining the biological effect is the average distance *d* between two ionisations. (b) The value of *d* decreases when the energy of the ion decreases during the slow-down process and is equal to 2 nm for a residual range $R = 40$ mm.

Figure 17 shows that when the LET becomes larger than 30 keV/µm during the slow-down process, the RBE increases sharply, attaining values larger than 3 for LET ≈ 150 keV/µm and—for some cell types and endpoints—it then drops towards higher LET values as a consequence of saturation effects that are equivalent to a waste of energy (so-called "overkill").

The value 30 keV/µm can be qualitatively understood because a particle with LET = 30 keV/µm (30 eV/nm) leaves, on average, 60 eV in the 2-nm double helix, and about 30 eV are needed to produce one ionisation. For densely ionising radiation, with a LET larger than about 30 eV/nm, the ionisations occur close together along the ion track, since *d* is less than 1 nm on average. This corresponds to a few ionisations per nanometre, which is of the order of magnitude required to induce severe, clustered, non-reparable damage. Such damage hinders the cell cycle and stops tumour growth, and it may also induce the cell's internal programme for its own destruction (apoptosis), yielding rapid tumour regression. Most cells and tissues show this general behaviour; however, for different cells and endpoints, the exact shape and position of the LET dependence of RBE may vary.

The images in **Fig. 18** are qualitative; however they do consider one very important aspect of dose delivery at the microscopic level: the ionisation of carbon ions is strongly concentrated around the ion trajectory. This property of the "track structure" is essential for determining the biological effects when the ion traverses the cellular DNA. By considering the track structure, the LEM, mentioned above, computes the RBE values for ions of any charge and energy, and for cells of different radiosensitivity, and it is used by practically all European treatment planning systems (TPSs).

As shown in **Fig. 19a** [24], the RBE increases at the end of the ion range in a tissue because the LET increases when the charged particle is slowed by colliding with atomic electrons. As a

consequence, to obtain a longitudinally uniform "effective" dose (the blue curve in **Fig. 19b**, the "physical" dose has to decrease with the depth, as shown by the red curve).

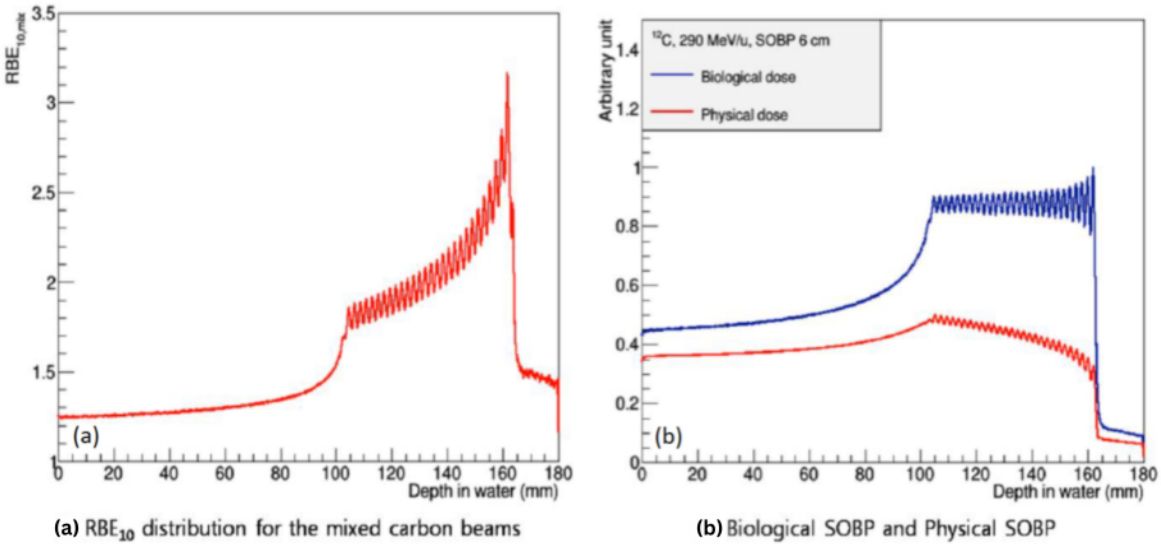

(a) RBE_{10} distribution for the mixed carbon beams (b) Biological SOBP and Physical SOBP

Fig. 19: Depth distributions of (a) the RBE of carbon ions interacting with human salivary gland cells and (b) the physical (red) and effective (blue) doses.

The average RBE is about 2 on the SOBP and 1.3 in the entrance channel, while protons have RBE ≅ 1 everywhere because they are sparsely ionising radiation, as are X-rays. This is why carbon ions spare the normal traversed tissues better than protons, as shown in **Fig. 11b**.

In summary, the radiobiological and clinical effects of carbon ions are different because they are densely ionising. In particular, in the last 3–4 cm of their range, where the tumour tissues are located, *d* is smaller than 1 nm and the ionisations lie close to the particle trajectory, meaning that they behave as a *different type* of radiation with respect to X-rays and protons; in particular, about 70% of the deposited dose *directly* produces closely spaced damage.

In X-ray and proton treatments, the total dose is deposited in many sessions to allow the normal cells to repair during the intervening days. Conversely, with carbon ions, such repair mechanisms are not as active; when using carbon ion beams, it is therefore possible to reduce the number of sessions from 25–30 to 10–15, thus reducing the stress for the patient and lowering the treatment cost. It is worth mentioning that, recently, lung tumours have been treated at NIRS (Japan) in just one session, with good results. Therefore, the important topic of hypofractionation is a priority item to be included in clinical studies.

Clearly, such open questions require a strong radiobiology programme that needs dedicated time and effort. This underlines the need for a next-generation facility focusing on research, such as that proposed in this report, that could implement such programmes for the benefit of the broader community and eventually for the benefit of patients.

2.2 Medical programme and clinical research

2.2.1 Outcomes in patients treated by ion therapy and early clinical trials

About 50% of the patients who have been treated with C-ions worldwide (reaching more than 57,000 by the end of 2023), were treated in Japan, with 15,500 of those patients having been treated at NIRS in Chiba. The results have been described in a book [20] and in two journal articles [25] [26], and they have been reviewed by an independent panel [27]. Excellent results are described for locally advanced non-squamous cell tumours such as adenocarcinoma, adenoid cystic carcinoma, malignant melanoma, hepatocellular carcinoma, and bone and soft-tissue sarcomas. Very promising results were obtained in tumours with high mortality, such as pancreatic cancer and locally recurrent rectal cancer. The exciting

results from Chiba have been essentially confirmed in other Japanese centres [28] [29] and in Europe at HIT [30] and CNAO [31] in retrospective analyses. Prospective confirmative trials are ongoing.

The Japanese experience is based on phase-I/II dose-escalation trials, not on phase-III comparative trials [32] [33]. Some retrospective studies have been conducted in the Hyogo Ion Beam Medical Center (HIBMC), the only Japanese facility having the capability to treat patients with both protons and C-ions [29] (**Fig. 20**).

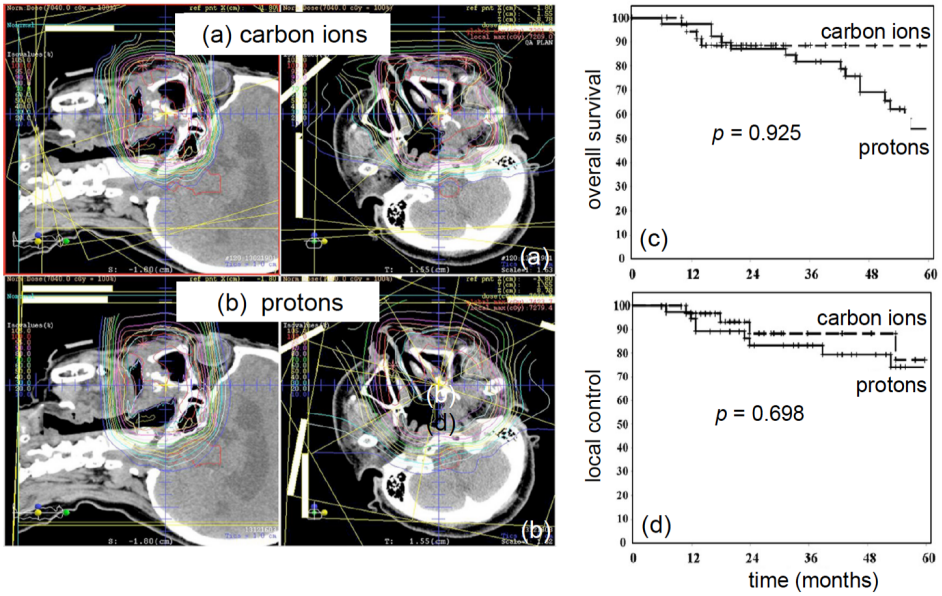

Fig. 20: Comparison of (a) carbon ion and (b) proton treatment plans for adenoid cystic carcinoma of the nasopharynx treated at HIBMC, Japan. (c) Overall survival and (d) local control in 40 patients treated for C-ions versus 40 patients treated with protons for histologically confirmed adenoid cystic carcinoma of the head-and-neck region [28].

The retrospective comparison of the patients treated at the HIBMC in Japan with protons or C-ions for head-and-neck tumours found similar results for local control but a higher survival rate in the patients treated with C-ions. Because the prescribed target dose was the same, the similar local control dose demonstrates that the calculated Gy (RBE) values are reasonably correct, i.e. that the models used to calculate them for protons (using a uniform 10% increase compared to X-ray dose along the whole SOBP) and carbon ions (at HIBMC, the Kanai model [34] is used) are solid and provide consistent clinical results. The improved survival rate may instead reflect a systemic response, specifically an immune response.

Several problems are encountered in comparative trials with different ions [35]. Patient preference and insurance coverage are the two main issues hampering recruitment in randomised trials [36]; the paucity of C-ion centres is another problem in comparative trials. A single-centre trial of protons versus C-ions can only be performed in the few centres where both particles are available—at the time of writing, at HIT and MIT in Germany, CNAO in Italy, MedAustron in Austria, Shanghai Proton Heavy Ion Center in China, and HIBMC in Japan. For C-ions, one of the main questions of the trial would be whether the high LET provides an additional advantage compared to protons [37]. However, even in trials directly comparing protons and C-ions at the same total dose and dose per fraction, delivered with the same technique (e.g. pencil-beam scanning) and at the same angles, the physical dose distribution will not be identical. One of these approaches is, for example, the randomised phase-II ISAC trial at HIT, in which patients with sacral chordoma should receive a dose of 16 × 4 Gy (RBE) protons compared to 16 × 4 Gy (RBE) carbon ions [38]. If the biological treatment planning is correct, the result should be identical local tumour control in both arms.

A different approach to randomised trials is to compare the “best possible protocols” as established through phase-I/II trials. For instance, this is the approach of the HIT-1 chordoma trial [39], which compares 2 Gy (RBE) protons × 36 fractions to 3 Gy (RBE) C-ions × 21 fractions. The

fractionation scheme was selected in phase-I/II trials. The results of these trials have shown excellent long-term survival in patients treated with C-ions for chordoma and chondrosarcoma of the skull base [40].

Another "best protocol" approach with multi-centric recruitment is the French–Italian ETOILE study, for which patients have been recruited since 2016 at 20 different centres in France and randomised for carbon ions versus standard treatment with X-rays. The patients randomised in the experimental arm are all attending treatment with carbon ion beams at CNAO. Such a transnational scheme will be used for two other international randomised trials aiming to compare X-rays with C-ions for locally advanced pancreatic cancer. Treatment of pancreatic cancer with C-ions is attracting great interest thanks to the exceptional results reported by NIRS [41] [42] in a type of tumour that has high incidence and mortality. These international trials are complex but valuable opportunities to broaden access to hadron therapy and enhance the possibilities of patient recruitment: C-ion patients are thus recruited in Europe, Asia, and the USA, while the control arms, with intensity-modulated radiotherapy (IMRT) or proton beam therapy, are performed "at home". **Table 1** provides a list of some clinical trials and their details reported in 2020.

Table 1: Ongoing, foreseen, or completed randomised clinical trials comparing C-ions to either protons or photon therapy. From https://www.clinicaltrials.gov, which registers all clinical trials in the world.

Ion prostate irradiation	NCT01641185 IPI Completed (??)	Heidelberg University, Germany	II	Prostate cancer	Protons	C-ions
Comparison of proton and carbon ion radiotherapy with advanced photon radiotherapy in skull base meningiomas	NCT01795300 PINOCCHIO Not yet recruiting (80)	Heidelberg University, Germany	III	Skull base meningioma	X-ray *vs* Protons *vs*	C-ions
Ion irradiation of sacrococcygeal chordoma	NCT01811394 ISAC Recruiting (100)	Heidelberg University, Germany	II	Sacrococcygeal chordoma	Protons	C-ions
Randomized C-ions vs. IMRT for radioresistant tumors	NCT02838602 ETOILE Recruiting (250)	Lyon University Hospitals, France	III	Adenoid cystic carcinoma, chordoma and sarcomas	IMRT or protons in France	C-ions at CNAO in Italy
Sacral chordoma: surgery versus definitive radiation therapy in primary localized disease	NCT02986516 SACRO (100)	European multicentric, Italian sarcoma group	III	Sacral chordomas	Surgery	C-ions, Protons or mix Rx-P
Prospective multicenter randomized trial of carbon ion vs. conventional radiotherapy for pancreas cancer	NCT03536182 CIPHER Not yet recruiting	Toshiba and UT South-western, Dallas, TX	III	Locally advanced pancreatic cancer	X-rays*	C-ions*
Carbon ion re-radiotherapy in patients with recurrent or progressive locally advanced headand-neck cancer	NCT04185974 CARE Not yet recruiting	Heidelberg University, Germany	II	Recurrent H&N cancers	X-rays	C-ions
Neoadjuvant irradiation of retroperitoneal soft tissue sarcoma with ions	NCT04219202 Retro-Ion Recruiting	Heidelberg University, Germany	II	Retroperitoneal soft tissue sarcoma	Protons	C-ions
Prospective trial comparing carbon ions to IMRT in pancreatic cancer	BAA-N01CM51007- 51 Not yet recruiting	NCI, USA	I/III	Locally advanced pancreatic cancer	X-rays*	C-ions*

* Combined with chemotherapy
$ Boost following conventional chemoradiotherapy
£ Fractionated stereotactic photontherapy

The urge to produce clinical data and results to corroborate the strong physical and biological case for ion beam therapy is increasing. This calls for a dedicated RI that, based on accumulated experience, could implement much-needed carefully designed clinical trials.

In 2020, two review articles were published, one by European [43] and one by American [44] radiation oncologists. The latter ends with the following sentences "Given the promising early clinical data as well as the advantages of heavy ion therapy, our institution [Mayo Clinic] recently announced

the intent to construct a heavy ion facility in Jacksonville, Florida." The construction of this facility is in full swing at the time of writing.

2.2.2 Paediatric patients

Typically, protons have been preferred to C-ion therapy for the treatment of paediatric patients. The concern here stems from the risk of late effects, including second cancers, that C-ions might induce in the developing tissues of children. However, this hypothesis is not really supported by data. As shown in **Fig. 21**, the toxicities observed at HIT in paediatric/adolescent patients are similar for protons and C-ions [45].

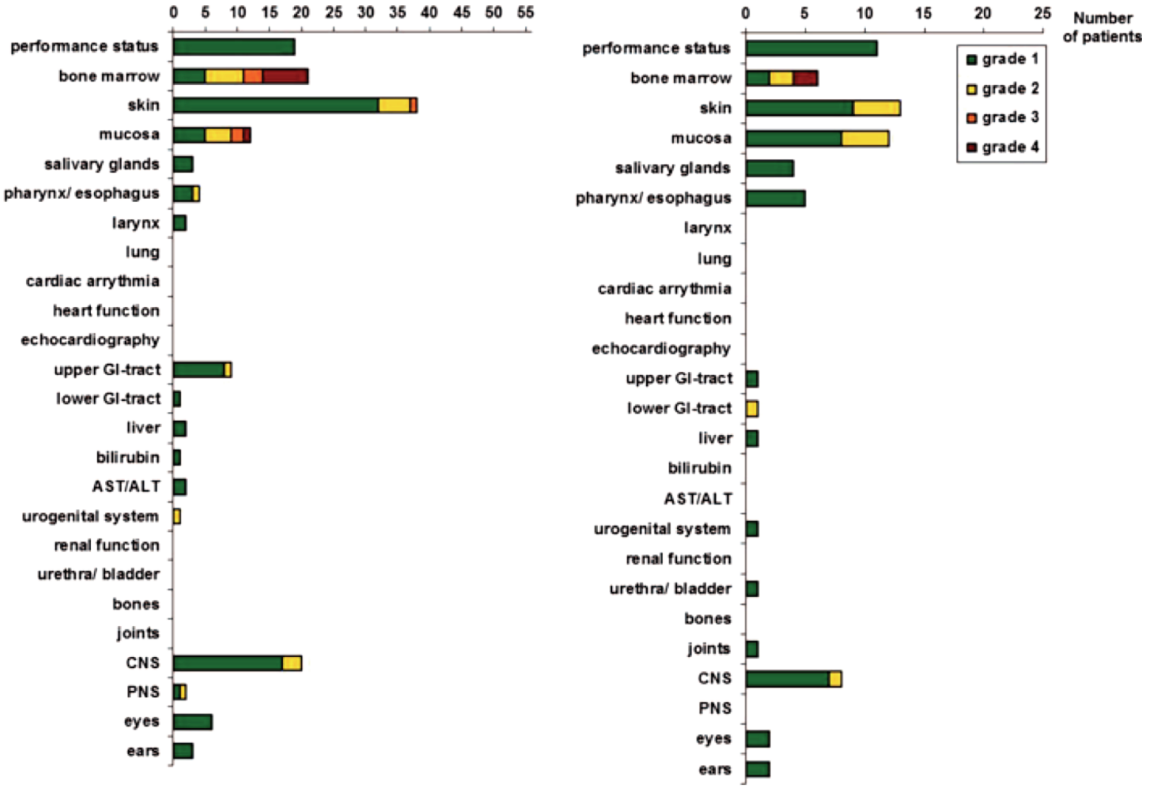

Fig. 21: Acute toxicities induced by protons (left) and C-ions (right). A total of 83 paediatric patients (range 1–21 years, median age 14 years) were treated at HIT in Heidelberg for different tumours.

Moreover, the idea that C-ions can increase the risk of second cancers is also not supported by the radiobiological rationale and by epidemiological data. From a radiobiological point of view, it should be pointed out that exposure to C-ions notably reduces the volume of normal tissue irradiated, similar to treatment with protons, and this ultimately reduces the risk of second cancers. A comparison of second-cancer risks that result from using protons or advanced X-ray treatment modalities is shown in **Fig. 22** [46]. Despite the fact that such advanced X-ray treatments use radiation beams shaped to conform to the target volume in the best possible way, protons—and similarly C-ions—still deliver much lower doses to healthy tissues due to their physical properties, which yield the Bragg peak.

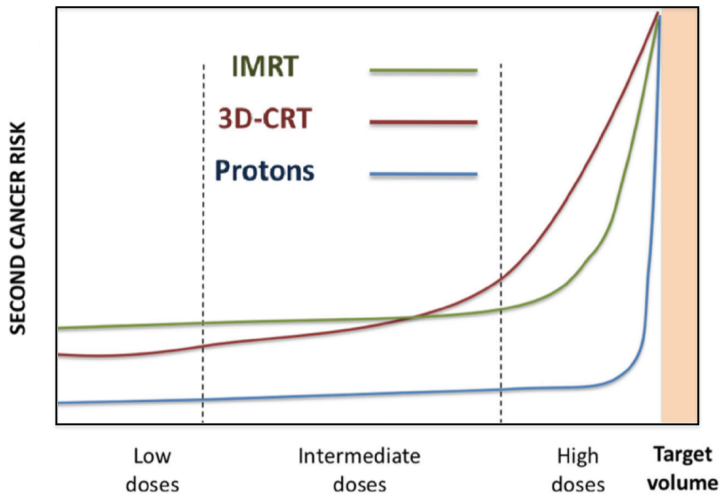

Fig. 22: Comparison of second-cancer risks using advanced X-ray treatment techniques such as IMRT (green curve), 3D conformal radiation therapy (red curve), or protons (blue curve).

It has been argued that C-ions can be more problematic than protons regarding "leakage dose" due to nuclear fragmentation and the production of neutrons that can irradiate out-of-field organs. However, experiments in phantoms have clearly shown that the opposite is true when pencil-beam scanning is used (**Fig. 23**). In fact, in pencil-beam scanning, fewer particles are used with C-ions than with protons to produce the same dose [47].

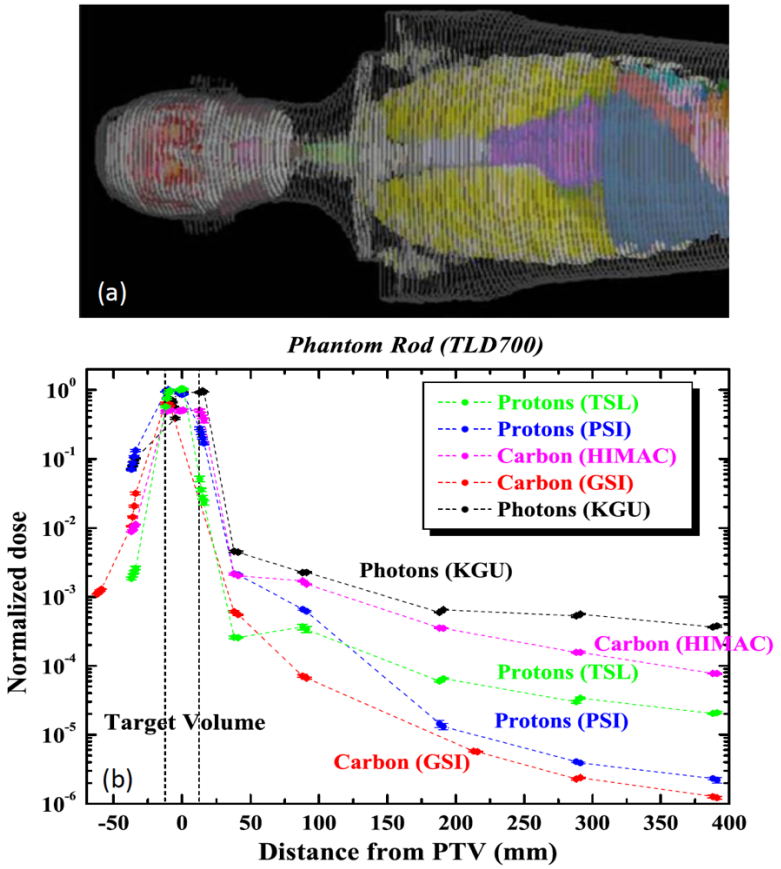

Fig. 23: Measurements of leakage dose in an anthropomorphic phantom (top) irradiated with different radiation qualities. The plot (bottom) compares X-rays 25 MV (KGU, Frankfurt), scattered protons (TSL, Uppsala), or C-ions (HIMAC, Chiba) with pencil-beam scanning protons (PSI, Villigen) or C-ions (GSI, Darmstadt) at different distances from the planning target volume (PTV). The treatment plan simulated a brain tumour, and the dose is measured all over the body.

The distal dose with C-ions is indeed so low that HIT is currently treating all women in Germany who must receive radiotherapy during pregnancy with C-ions, as eligible choice over X-rays, which would cause a much higher uterine dose (**Fig. 24**).

Fig. 24: Foetus dosimetry during radiotherapy of a pregnant woman with C-ions at HIT.

Apart from physics and biology, NIRS has recently published epidemiological data supporting the argument that C-ions induce less second-cancer risk than conventional X-rays. The data presented in **Fig. 25** show the cumulative incidence of second cancers in patients with prostate cancer treated with C-ion beams and compared with surgery and X-ray [26] treatments.

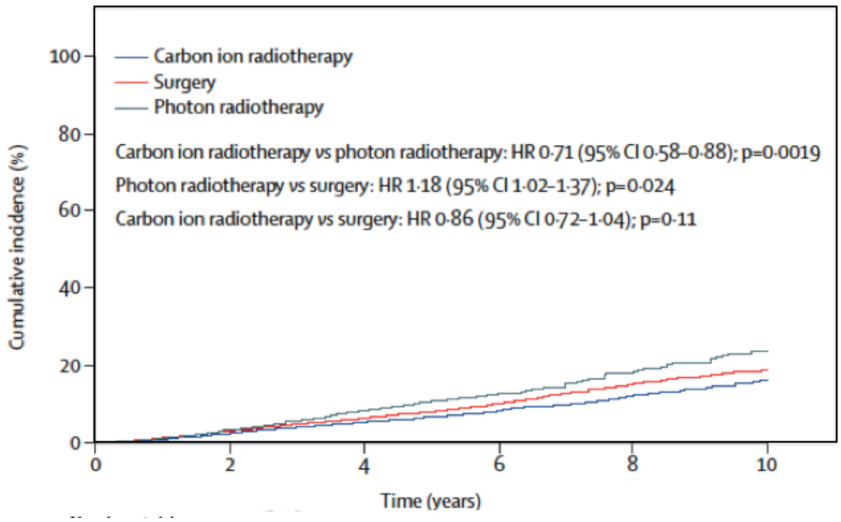

Fig. 25: Cumulative incidence of second cancers in patients with prostate cancer in Japan after three different treatments [25].

The hazard ratios show that C-ions have a significant advantage over X-rays in terms of second-cancer risk, and there is even a visible, yet non-significant, reduction compared to surgery. The follow-up of the patients was limited to 10 years, but the preliminary data are very encouraging and show that the risk of second cancers is reduced using C-ions; therefore, paediatric patients can be safely treated with heavy ions as they are already with protons. Based on such results, a next-generation facility with advanced equipment would be ideally suited to establishing a sound paediatric irradiation programme with C-ions, thus supporting much needed future studies.

While the need for an advanced research facility is clear on the basis of the open questions at the time of writing, it is also clear that the potentially interesting research topics are not limited to these. Such facilities can typically take ten years to come into operation. A next-generation advanced facility such as that proposed should be adequately equipped to adapt to and tackle emerging research topics.

In addition, clinical activities should be adapted to the scheme of devoting 50% of weekday daytimes, along with nights and weekends, to non-clinical research, as described in Section 1.1.2. This fundamental choice will ultimately limit the number of patients that can be treated. According to a conservative estimate, the number of patients that can be treated full time in a room is 250 per year. Therefore, for the three rooms of the proposed facility, one can safely estimate that 375 patients/year can be irradiated after reaching routine operation, which is expected after three years of setting up.

When the proposed facility is almost ready, the medical staff of the RI, in discussion with collaborating radiation oncologists, may define the clinical programme considering the status of the hadron therapy field, the research ongoing in the other centres, their competences and interests and, last but not least, the capacity for treatment of patients. To give as complete a picture as possible, two different approaches are described here:

(i) the rest of this section describes a clinical programme that starts from the present status of the epidemiology and lists the proton and ion indications of the highest priority;

(ii) the next section, Section 2.3, discusses the present research challenges in hadron therapy that could be the focus of the research programme of future facilities.

Additionally, the use of ions other than protons and C-ions is discussed in Section 2.4.

2.2.3 Types of tumour to be treated and their epidemiology

Table 2 presents information based on European preliminary epidemiological studies performed on data from the Italian and Austrian carbon therapy projects and from a French preliminary study. This made it possible to establish a census of priority cases for this type of therapy [48]. In the future, the epidemiology will have to be corrected for the age distribution of the regional population.

Table 2: Proton therapy and carbon ion therapy indications of the highest priority.

Types of tumour eligible with highest priority for proton therapy	Types of tumours eligible with highest priority for ion therapy (carbon)
Adults' skull-base tumours. Adults' unresectable or relapsing meningioma. Other rare adults' central nervous system tumours. Childs' central nervous system tumours. Any other child's solid tumours.	Adenoidcystic carcinomas of salivary glands, including head and neck, thorax, and sinus adenocarcinomas. Mucinous melanomas of head and neck, chordomas and chondrosarcomas of skull base and spine. Soft-tissue sarcomas of low and medium grade, unresectable or partially resectable without threatening metastasis. Non-small cell lung carcinomas, of small and medium size (N0, M0) unsuitable for surgery. Pelvic local relapses of adenocarcinomas, M0 and previously irradiated by X-rays. Hepatocarcinomas unique and of large size.
Total: about 80 cases/year for 10 million inhabitants	**Total: about 200 cases/year for 10 million inhabitants**

The cases eligible for hadron therapy account for about 10% of all radiotherapy patients, amounting to about 25,000 patients per 10 million inhabitants. About 1% of this 10% are in the very first level of priority, as listed in **Table 2**.

Regarding projections for the proposed facility, the following considerations are taken into account for the case of SEEIIST. The entire South East Europe region covers about 40 million inhabitants, and at present, there is no medical treatment facility using either protons or heavier ions in the region. Based on the estimated 375 patients that can be treated per year in three rooms during 50% of daytime periods within the week, reaching routine operation after three years of activity, SEEIIST is expected to be able to treat about one third of the theoretical needs of the South East European region populations regarding medical cases of highest priority for ion therapy as listed in **Table 2**. Considering

the current difficulties of recruitment and the occurrence of deterrent comorbidities, this is a very high potential, far above any single large European country.

In **Table 2** (which shows the highest priorities), the hypotheses are: for proton therapy, a significant reduction of toxicity and, for C-ion therapy, a gain of 20% to 25% of tumour-progression-free survival, increasing the success rate from circa 50% to above 75%. The second-priority indications are shown in **Table 3**. For the ion therapy cases listed in **Table 3**, the approach is essentially based on the identification of tumours that are either anatomically difficult to treat with X-rays and/or are very radioresistant.

Table 3: Indications of secondary priority for heavy ion therapy.

Sarcomas after definitive R1 resection (+ children). Lung carcinomas of medium size unsuitable for surgery. Prostate adenocarcinomas, locally aggressive. Head and neck locally advanced squamous cell carcinomas. High-grade gliomas (+ children). Gastrointestinal tumours, highly radioresistant or anatomically difficult (some pancreatic tumours, pelvic tumours, etc.). Skull-base meningiomas, unresectable. etc.
Total: > 500 cases/year for 10 million inhabitants

Concerning proton therapy, the scope of the application is less well defined because it depends on three factors: (i) the level of quality of the X-ray offer (for tumours with difficult anatomical localisation); (ii) the existence or not of an offer of ion treatments for radioresistant tumours; and (iii) the economic resources that can be allocated to a therapeutic optimisation, for which proton therapy is fundamental. Taking these parameters into account, the demand for proton therapy can range from one- to three- or even four-fold compared to the demand for heavier ions. Thus, one can estimate about 200 to 800 cases of first- and second-priority proton therapy for 10 million inhabitants per year, considering almost all the children to be treated for curative purposes.

If these needs are met by commercial proton therapy facilities in the region where the next-generation ion facility will be built, the focus of the future facility will then be on priority treatments with carbon and other ions, such as helium.

In general, it can be emphasised that, for most of the cases regarding rare tumours, the recruitment process to obtain a particle therapy decision requires, in the first instance, a healthcare system that is efficient and able to handle all types of cancers and to cover the entire population in an equitable manner. Negotiations with the healthcare system and insurance policies is a concern, and this is one of the main challenges that any future ion facility has to address and handle.

Thus, a clinical network of oncology departments of hospitals should be organised to handle cases within the geographical area covered by the future facility. This network is expected to organise the identification of eligible cases, the systematic and traceable discussion of these cases by a collegial and multidisciplinary centralised tumour board, and to apply the same selection criteria in all participating centres, employing efficient communication means. This work would have to be done downstream of the local multidisciplinary tumour board meetings, which would have the role of proposing a radiotherapy orientation for the eligible cases. Definitive eligibility would be devoted to the multidisciplinary centralised tumour board. The clinical network would also be in charge of multi-centre clinical studies.

2.2.4 Baseline clinical research

As mentioned above, the rising offer of ion therapy around the world enhances the need for a definitive recognition of this therapy by health-insurance schemes, and thus the need for a quantitative demonstration of a strong actual medical benefit.

In reality, the increasing development of particle therapy in Europe makes the establishment of multi-centre prospective clinical studies possible. It is thus foreseeable that the proposed new facility could play an important role in such projects, taking a leading role in multi-centre clinical studies in particular. As part of a dynamic network of similar institutions in Europe, it is expected to actively contribute to clinical research programmes. Furthermore, it is envisaged that it will itself become a driving force to make new proposals and to be the sponsor of additional original clinical trials.

It could then be assumed that the acceptance of a patient to be definitively eligible for a hadron therapy, paid for by health insurance, should be conditional on his/her inclusion in a trial that would correspond to his/her type of tumour, or, at least, his/her inclusion in a follow-up cohort. This principle includes randomised comparative studies comparing hadron therapy to X-ray therapy, which would require close collaboration with all the referring centres.

This principle being laid down, it must be recognised that, for paediatrics in particular, no comparative clinical studies have yet been carried out, and many indications of proton therapy in paediatrics are considered, by many, to be an accepted standard. The additional advantages of carbon ion therapy, as discussed in Section 2.2.2, deserve long-term research activities.

In adult situations, even for indications considered to have been validated in proton therapy, the question of the comparison of carbon therapy versus proton therapy arises. As a result, any adult receiving an ion therapy should be able to participate in a prospective clinical research protocol, either interventional or observational.

However, it will not be possible to solve all issues by prospective comparative randomised trials; they are needed to check and measure specific highly critical conditions, but many more questions need to be answered without resorting to unfeasible studies. Thus, radiation oncologists propose relying on modelling of the medium- and long-term effects as well as the risk of second cancers. Works in this direction have been carried out since the 1980s, but an acceleration of these developments has been prompted by societal demand for the most efficient allocation of medical resources.

The possibility of predicting, for each patient, the effect of available treatments also makes it possible to optimise the costs. Thus, the field of model-based medicine, in the service of personalising therapeutic choices and optimising the usefulness of treatments, is the basis for organisations aiming to develop hadron therapy in Europe for years to come, in the framework of the European Society for Radiotherapy and Oncology (ESTRO) and of the European Organisation for Research and Treatment of Cancer (EORTC). In this sense, the Dutch and Danish projects are exemplary [49].

Clinical research topics are extremely diversified, and different approaches can be adopted:

(i) first of all, ion therapy still needs to prove its medical utility and economic efficiency through cautious medico-economic studies, despite its increased ability to cure difficult-case patients; this should be a part of any comparative study;

(ii) second, because of its proven tolerance and reduced invasiveness, ion therapy could clearly demonstrate its ability to advantageously cure some diseases that are currently largely treated by difficult, expensive, and painful surgical or invasive procedures, including hepatic tumours, pancreatic cancers, lung tumours, sacral chordomas, etc., and even benign conditions such as brain ablative procedures and heart arrhythmias;

(iii) third, ion therapy has the potential to pioneer new approaches in radiation oncology, renewing concepts of radiotherapy, as detailed in the next two sections.

2.3 Research challenges in carbon ion therapy

As underlined in the previous section, despite the fact that a large number of patients have been treated worldwide with C-ions (more than 57,000 by 2023), the therapy is still expected to prove its advantages based on results of randomised trials, and it is, generally, still considered as not being an established “standard”. The benefits are potentially enormous, but they remain largely unexploited. The paucity of facilities makes large clinical trials difficult, and many issues require more pre-clinical research.

Examples of today's "hot" topics in particle therapy research, where the proposed facility could make an impact, are provided below.

2.3.1 Hypofractionation

Thanks to tremendous improvements in IGRT, there is a tendency to reduce the number of fractions and increase the dose per fraction ("hypofractionation"). The advantages of hypofractionation for both the patient and for costs are enormous. X-ray stereotactic body radiation therapy (SBRT) and hadron therapy are both pushing hypofractionation towards the range of 1–3 fractions (oligofractionation) with a very high dose per fraction (up to 25–30 Gy). For non-small cell lung cancer (NSCLC) and oligometastases, SBRT has proven high rates of control, durable local control, and minimal normal-tissue complications. At very high doses, vascular injury, i.e. damage to the endothelial cells supplying the cancer tissue with oxygen and nutrients, may become a dominant pathway for tumour suppression. Damage to the tumour stroma at high doses was originally demonstrated in fibrosarcoma and melanoma grown in genetically modified mice, where vascular endothelial cell apoptosis was shown above 10 Gy per fraction [50]. The ceramide pathway orchestrated by acid sphingomyelinase is a major pathway for the apoptotic response. In later clinical work involving the use of single-fraction high-dose spinal SBRT, investigators from the Memorial Sloan Kettering Cancer Centre (MSKCC, NY, USA) recorded pro-necrotic response after doses in the range 18–24 Gy [51], a radiographic change consistent with a devascularising effect.

Even though the engagement of the vascular component in the radiation response can be crucial at very high doses, it should be underlined that according to the conventional linear-quadratic model used in fractionated radiotherapy, hypofractionation leads to very high biologically effective doses (BEDs). This was not possible in the past because of the damage that would be caused to the normal tissue, but it can now be spared, at least for parallel organs, with modern image-guided techniques. In NSCLC, BED correlates with the TCP over a wide range of fractionated conformal radiotherapy and SBRT regimes. The question of whether oligofractionation can only be justified by the improved physical dose distribution in IGRT and consequently very high BED, or whether it requires a different radiobiological mechanism involving vascular damage and possibly reperfusion, therefore remains open.

The high conformity granted by the Bragg peak makes charged particle therapy ideal for radiosurgery. Particle radiobiology research at high doses is needed to support and guide oligofractionation in hadron therapy. Experiments in 3D cultures of human endothelial cells or lung cancer cells injected with basement membrane matrix into nude mice showed reduced angiogenesis and vasculogenesis capability after exposure to high-energy charged particles, suggesting that the vascular damage may be particularly effective with protons or heavier ions [52].

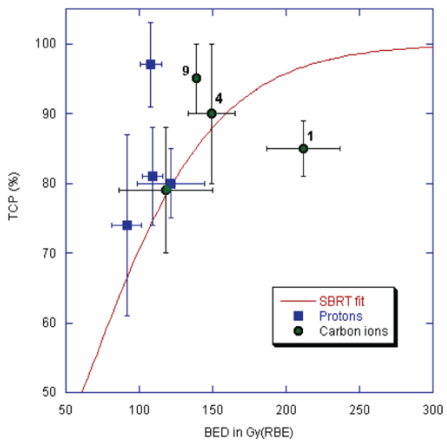

Fig. 26: Tumour control probability (TCP) versus biological effective dose (BED) for different stereotactic body radiation therapy (SBRT) and hadron therapy trials for non-small cell lung cancer (NSCLC). The red curve represents the fit to the X-ray SBRT data using the standard linear-quadratic model. Data points are calculated

from published trials with protons or C-ions. The number of fractions is shown next to the data points for oligofractionation ($n < 5$) trials.

Hypofractionation with protons and C-ions is underway for NSCLC in several centres. Published TCP data for C-ion therapy in NSCLC are plotted in **Fig. 26**, along with the curve derived from X-ray SBRT trials [53]. C-ion TCP values are generally consistent with those for X-ray SBRT TCP. One major deviation is observed in the single-fraction treatment at NIRS in Japan, which corresponds to BED > 200 Gy (RBE) [54]. In the Japanese treatment plan, RBE is assumed to be independent of the dose per fraction; this can lead to overestimations at high doses per fraction, up to a factor of two.

2.3.2 Hypoxia

A potential advantage of hadron therapy in hypofractionation is the reduced oxygen-enhancement ratio (OER) obtained using high-LET radiation [55]. Hypoxia is one of the main factors causing radioresistance and thus reducing local control of solid tumours. Therefore, one of the main reasons for fractionation in radiotherapy is the possibility of re-oxygenation of the hypoxic areas. Re-oxygenation will be reduced in hypofractionation and finally lost in single-fraction/high-dose radiosurgery. Combinations with hypoxic sensitisers have been proposed for SBRT. Due to the reduction of the OER using ions, carbon therapy may be an alternative.

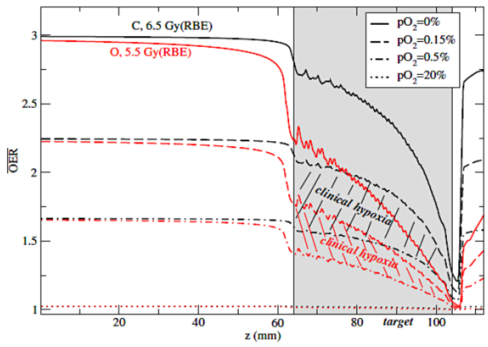

Fig. 27: Comparison of the computed oxygen-enhancement ratio (OER) along a spread-out Bragg peak (SOBP) for carbon (black curves) and oxygen (red curves) at different levels of partial O_2 pressure. The hatched areas represent the clinically interesting regions for hypoxia ($0.15\% < pO_2 < 0.5\%$). The indicated doses are prescribed RBE-weighted doses in the target to achieve isosurvival.

Targeting specific hypoxic regions can be achieved with dose- or LET-painting strategies. For oligofractionation or single-fraction/high-dose treatments, the use of ions heavier than carbon (such as ^{16}O) may be beneficial because with these ions, the OER can be further reduced in the clinically relevant hypoxia region (**Fig. 27**).

2.3.3 Combined treatments

Even though local control is generally very high with carbon ion therapy, in most malignancy cases, radiotherapy must be combined with systemic therapies to control metastasis and increase survival. Combined radio- and chemotherapy protocols are already used in many cancers, such as glioblastoma multiforme (GBM) or pancreatic cancer. However, very few radiobiology studies specifically address the potential synergistic interactions of drugs and ion irradiations. In-vitro experiments on GBM have provided useful indications on the combination of different drugs with C-ions.

Even more important is the combination of particle therapy with immunotherapy, which is rapidly gaining traction in clinical settings, with high expectations for cancer cure. Radiation induces both immune-stimulating and immune-suppressive pathways, depending on the cell death pathway. While immunotherapy can block the immune-suppressive pathways, ions can induce different cell death pathways, eliciting a more generalised immune response than photons.

This hypothesis is supported by the strong bystander effect associated with high-LET particles and by pre-clinical results with C-ions in animal models [56]. At the same time, the physical

characteristics of hadrons can support the immunogenicity of radiotherapy. In fact, an effective immune response must be sustained by a sufficient number of active effector and memory T-cells. However, standard fractionated radiotherapy notoriously induces lasting lymphopenia because of the inevitable exposure of circulating blood during the treatment and the inclusion of active bone marrow, lymph nodes, and spleen within relevant dose volumes. The reduced integral dose associated with hadron therapy will spare more T-cells, thus favouring an immune response. This has been shown in measurements of chromosomal aberrations in the peripheral blood lymphocytes of patients during a radiotherapy course [57].

A decrease in the fraction of cells carrying chromosomal aberrations was observed in patients with uterus or prostate cancer treated with C-ions compared to X-rays. Lymphopenia is reduced using protons or C-ions compared to X-ray radiotherapy (**Fig. 28**) [58]. Interestingly, a retrospective comparison of the patients treated at the HIBMC in Japan with protons or C-ions for head and neck tumours found similar results for local control but a higher survival rate in the patients treated with carbon ions (**Fig. 20**).

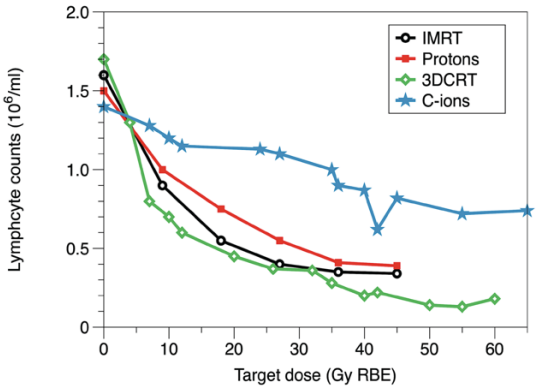

Fig. 28: Median values of lymphocyte count in patients with oesophageal cancer during the course of radiotherapy. Lymphopenia is associated with a poor prognosis in oesophageal cancer.

Specific trials to address the combination of hadron therapy and immunotherapy will certainly be performed and may lead to a breakthrough in combined treatment protocols using immunotherapy. This emerging field opens a broad research landscape for an intense clinical research programme for which the support of a next-generation facility could make an important impact.

2.3.4 Radiogenomics

The ultimate goal of radiogenomics is to develop a genetic-risk-profile individualisation for radiation dose prescriptions to optimise tumour control while minimising normal tissue damage. Genome-wide association studies have already been successful in finding novel genetic variants with a high risk of developing some common diseases, for instance breast cancer. Radiogenomics uses a similar approach to predict the sensitivity of normal and cancer tissues to radiation.

2.3.4.1 Normal tissues

Radiogenomics is extremely attractive for assessment of the normal tissue response of patients, as long as the genetic component plays a major role in determining radiosensitivity. This is clearly the case for those syndromes—such as ataxia-telangiectasia (AT) or Nijmegen breakage syndrome (NBS)—in which germline mutations of DNA repair genes induce extreme radiosensitivity. These diseases are nonetheless rare, confined to a limited number of families, phenotypically obvious, and are certainly not responsible for the observed variability in radiotherapy response. It is interesting to note that while AT patients are homozygous for mutation in the ATM protein, around 3% of the population is heterozygous for ATM and a similar fraction is hypersensitive in radiotherapy trials. ATM haploinsufficiency results in increased radiosensitivity in mice, thus suggesting that this subgroup may

be more at risk of side effects in radiotherapy and of radiation-induced cancer [59]. ATM is one of the candidate genes to be screened as a potential biomarker of radiation response.

Radiogenomics has used the candidate-gene approach to look for variations in many other genes involved in radiation response—e.g. those in the pathways of DNA repair (BRCA1/2), cytokine production, scavenging of free radicals (SOD2), and so forth. Genetic variations include single-nucleotide polymorphism (SNP), copy-number variations, and other epigenetic modifications. Unfortunately, although several studies have initially reported associations between radiation toxicity and SNP, a prospective study aimed at validating this failed to detect any of the previously reported associations, suggesting that SNP may be irrelevant for individual sensitivity.

Very few studies deal with radiation quality in radiogenomics. Haploinsufficiency for ATM results in accelerated cataractogenesis in mice exposed to both X-rays and heavy ions, and the RBE is higher for heterozygotes compared to wild type [60]. In a recent microarray hybridisation analysis of irradiated normal human bronchial epithelial cells, it was found that the great majority of genes with modified expression were uniquely associated with one radiation quality (**Fig. 29**) [61]. Another important parameter was the time after irradiation (0–24 h), whereas the dose (0.5–3.0 Gy) was not a significant parameter. A new next-generation facility with expert medical staff interested in the personalisation of radiotherapy treatments could greatly contribute to this basically uncharted domain.

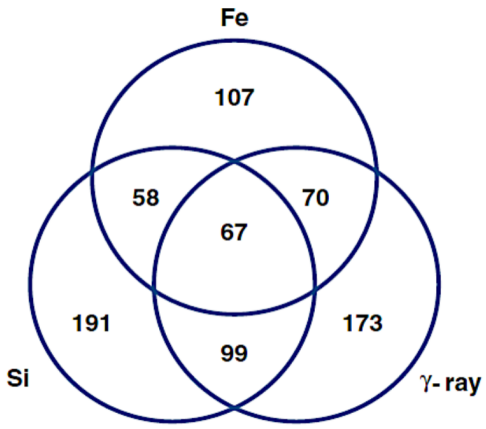

Fig. 29: Differentially expressed genes in human bronchial epithelial cells exposed to X-rays or heavy ions. This Venn diagram shows the numbers of genes, either specific to—or overlapping with—different radiation types. (Courtesy of Michael D. Story, UT Southwestern.)

2.3.4.2 Tumour tissues

The integration of molecular data with local-control data can allow the generation of biomarker signatures that predict the response of tumours to therapy. This method has been applied to in-vitro survival curves of different human tumour cell lines. Microarray profiling identified 22 genes that are differentially expressed in radiosensitive cancer cells and 18 genes associated with resistant cell lines [62]. Using a molecular regulatory network model based on mRNA expression profiles, it has been possible to identify ten hubs of interactions associated with radiosensitivity [63]. It is not clear whether these patterns can be used for all cancers or whether they are tissue specific. Individual NSCLC patients' responses to chemotherapy are highly variable [64], and similar variability is observed when irradiating NSCLC cell lines. Molecular markers, including epidermal growth factor receptor, K-ras, vascular endothelial growth factor, mammalian target of rapamycin, and anaplastic lymphoma kinase, have been proposed as potential biomarkers for the response of NSCLC to ionising radiation. For head-and-neck squamous cell carcinoma, a recent study showed that Ku80 overexpression was an independent predictor for both local recurrence and mortality following radiotherapy [65]. These results are easy to interpret, Ku80 being a key molecule for DNA DSB repair.

The variance in radiosensitivity, which is associated with the genetic background, is reduced when cells are exposed to densely ionising radiation. The interindividual variability in radiosensitivity can be assessed with organotypic tissue slices from human tumours. A recent study found

interindividual variability for GBM slices treated with temozolomide, and a smaller variability was found after C-ion irradiation [66]. The RBE decreases for cells with high α/β ratios (quantified by the so-called "α/β ratio", measured in Gy) (see also Section 2.4), i.e. by decreasing intrinsic radioresistance, and it eventually reaches unity for very radiosensitive cell lines. For this reason, high-LET heavy ions are preferentially used for radioresistant tumours. This is also a very attractive feature for targeting specific resistant sub-volumes in a tumour, such as the cancer stem cell niche. Expression of molecular biomarkers of radioresistance should, therefore, represent an indication for hadron therapy.

Radiogenomics in tumour tissues can be used for synthetic lethal genetic screening. Two genes are considered synthetic lethal if the mutation of either one alone is compatible with cell viability, but mutation of both leads to cell death. Therefore, targeting a gene that is synthetic lethal to a cancer-relevant mutation should kill only cancer cells and spare normal cells. Synthetic lethality thus provides a conceptual framework for the development of cancer-specific cytotoxic agents and can be extended to combined therapies that target combinations of genes conferring radioresistance to cancers.

This is just one example of current activities in radiogenomics, which is another emerging topic of interest in the radiation oncology community for which targeted research activities at a next-generation facility could support much needed progress.

2.4 Therapy with other ions

As previously discussed, hadron therapy centres are currently using only either protons or carbon ions. Several other ions have been used in the past (especially at LBL), and the use of such ions is once again under consideration. The idea of finding the "optimal particle" or the "magic bullet" for curing cancer is, however, unsound. All ions share the same physics described in the previous sections, and the radiobiology of several particles has been studied for decades. Therefore, no major breakthrough can be expected in using particles with $1 < Z < 6$. Furthermore, very heavy ions with Z well above 6 cannot have useful applications for deep tumours. Fragmentation drastically modifies the Bragg curve, with a strong increase of the dose in the entrance channel, meaning that they are more similar to photons than protons: there is a small Bragg peak caused by the few residual primary ions and a long fragment tail. Moreover, the high LET of heavy ions in the entrance channel raises concerns for normal-tissue toxicity. The question, then, is whether it is worth exploring ions other than protons and C-ions.

The rationale for using other ions is again a combination of physics and biology [67]. From **Fig. 14**, it is clear that helium ions have much smaller lateral scattering than protons, and they are thus expected to provide sharper dose gradients and better treatment plans, as is indeed shown in **Fig. 30** for a skull-base chordoma. Helium, therefore, presents a very attractive alternative to protons.

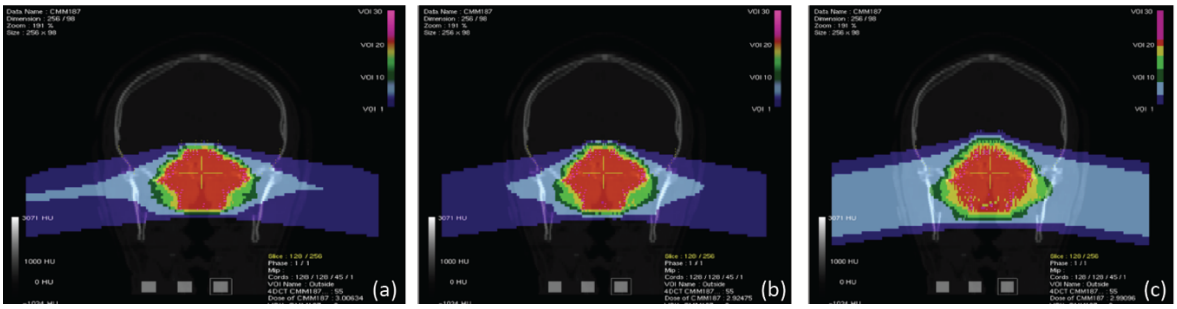

Fig. 30: Treatment plan for a chordoma of the skull base for protons, helium, or carbon ions. The plans are calculated with TRiP98/LEM assuming α/β = 2 Gy for both late toxicity in the brain and the tumour target.

The improved dose distributions, with limited fragmentation, would make helium ions the preferred choice for tumours close to OARs, where sharp gradients are needed, or for small targets in non-cancer diseases, such as in future treatments for cardiac arrhythmias. As noted in Section 2.2.2, C-ions have as yet had very limited use with paediatric patients, mostly because of the concern regarding possible second cancers caused by the high-LET exposure. These concerns would not apply to helium, which has low LET in the entrance channel, sharper dose gradients, and, possibly, an increased RBE in the SOBP, which would make it more effective for radioresistant tumours. Over 2000 patients were

treated with helium at Berkeley, and its clinical use is therefore considered to have already been validated. The commissioning of helium ion therapy and the first patient treatment with active beam delivery at HIT was reported in [68], which reached the following summary conclusions: "Helium ion beam therapy has been successfully commissioned and introduced into clinical use. Through comprehensive validation of the absorbed and RBE-weighted dose predictions of the RayStation TPS, the first clinical TPS for helium ion therapy using raster-scanned delivery was employed to plan the first helium patient treatment at HIT."

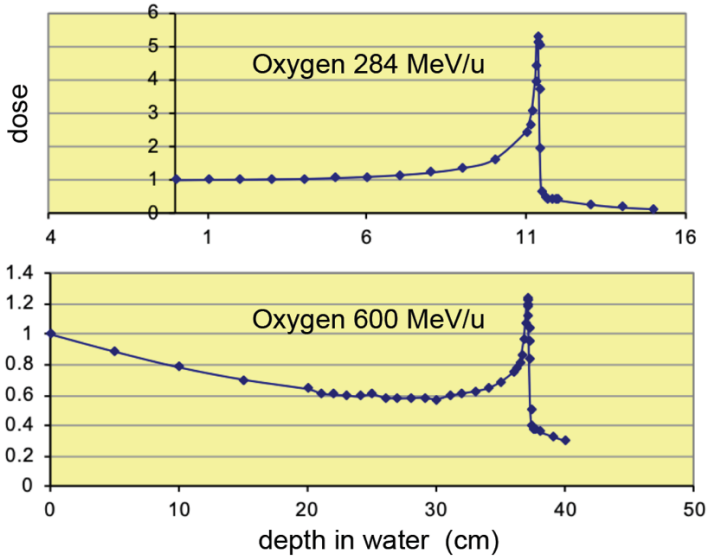

Fig. 31: Measured Bragg curves for oxygen ions of 284 and 600 MeV/n in high-density (0.97 g/cm^3) polyethylene. (Courtesy of Adam Rusek, BNL, USA.)

Oxygen would be even better than carbon in terms of lateral scattering, but it would undergo more fragmentation. At high energy, inelastic nuclear interactions will significantly reduce the entrance dose (**Fig. 31**). However, the dose-averaged LET on the SOBP will be higher for ^{16}O than for ^{12}C, and this will cause a significant reduction of the OER. The rationale for using ^{16}O is, therefore, based on the reduced OER, and thus on the possibility of overcoming the resistance of very hypoxic tumours, or to improve effectiveness in hypofractionation, where re-oxygenation is reduced or even absent for high-dose single-fraction treatments.

The choice of carbon ions was mostly based on the plateau-to-peak ratio. Comparing different ions, the results will depend on the beam geometry, RBE model, and sensitivity of the tumour and the normal tissue. In **Fig. 32a**, a (25 × 25 × 25) mm^3 tumour target is centred in an irradiation volume of 16-cm length and irradiated with four different beams. Two cases are compared:

Case (b): equal sensitivity of tumour and normal tissues with α/β (target) = α/β (normal tissue) = 2 Gy,

Case (c) *more radiosensitive target* with α/β (target) = 10 Gy and α/β (normal tissue) = 2 Gy.

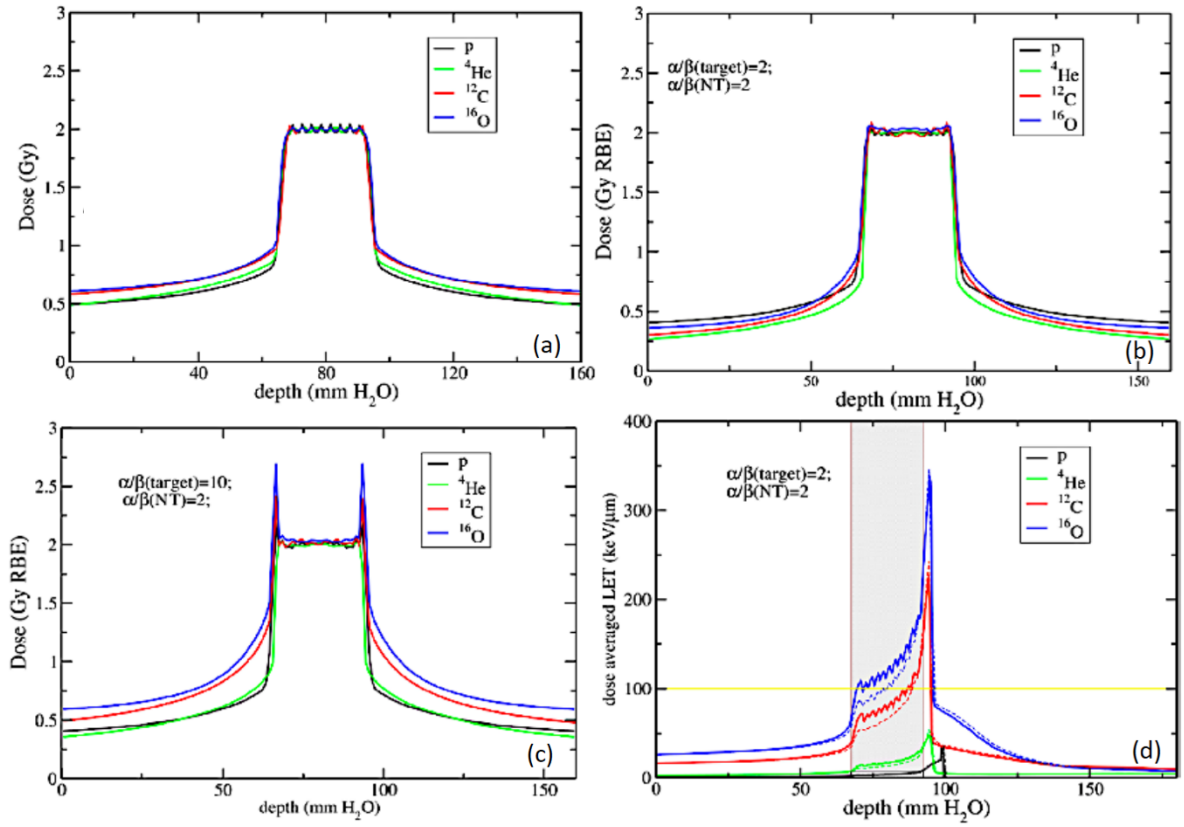

Fig. 32: Double opposed field irradiation of an idealised geometry simulating a typical head-and-neck cancer case. (a) Physical dose optimisation. RBE-weighted dose optimisation for different sensitivity scenarios: (b) the two tissues have the same sensitivity and (c) the tumour tissue is more radiosensitive than the normal tissue. (d) The dose-averaged LET for a single beam is shown for the physical (dotted lines) and biological (solid lines) dose optimisation.

In **Fig. 32a**, the physical doses released by the different charged particles are compared for the delivery of 2-Gy homogeneous dose to the target. In this case, we notice that, for the same dose to the target, a higher dose is released to the surrounding normal tissues by carbon and oxygen compared to protons and helium. Biological optimisation was also performed for the two configurations of target and normal tissues described above.

In **Fig. 32b** (in which the same radiosensitivity is assumed for both tumour and normal tissue), it can be seen that the optimal sparing of normal tissues is obtained with helium ions. Protons release the highest biological dose in the entrance channel, while in the region proximal to the target, the carbon and oxygen curves intersect with the proton profile, resulting in a higher biological dose. The situation changes quite drastically when considering a radiosensitive tumour (**Fig. 32c**). In this case, similar results are obtained with protons and helium, showing the highest peak-to-plateau ratio. In contrast, a clearly higher dose is released to normal tissues by carbon and oxygen. Finally, **Fig. 32d** shows the dose-averaged LET values for single beams (solid lines) compared to those arising from a physical dose optimisation (dotted lines). For oxygen, the LET along the SOBP is > 100 keV/μm, and at this value, the OER is expected to drop to 1.

These results suggest that both the physics of the different ion beams and biological aspects strongly influence the resulting dose profiles. Therefore, the choice of the optimal ion depends on the specific tumour configuration. This is why there is no “magic bullet”; nonetheless, depending on the tumour, some particles can do better than others. Multi-ion optimisation in the treatment planning is feasible and can lead to specific improvements. This justifies the current efforts to implement the use of helium and oxygen ions at HIT in Heidelberg and similar plans at CNAO and MedAustron.

Therefore, a next-generation facility should provide the possibility of using multiple ions in tumour treatments, as this is expected to become the focus of research on both animal and human

patients. Furthermore, in-vitro radiobiology experiments, as discussed in the next section, may also play a crucial role in advancing this field. Indeed, a future facility equipped with multi-ion sources and the ability to accelerate many different ions opens up enormous possibilities for such research activities.

2.5 Radiobiology programme

2.5.1 General framework

To make full use of the beneficial radiobiological properties of ion beams, the research effort aims to provide enhanced knowledge of tumour resistance mechanisms and develop methods to identify them, at the time of the diagnosis, to help clinicians in their decision-making regarding treatment. This need is widely recognised in the community, and many research programmes are ongoing in clinical and research centres. Such research efforts are coordinated within the IBC (see Section 1.1.3) and will provide unique opportunities related to the high intensity that the accelerator can reach. A future facility such as SEEIIST would naturally be an integral part of these efforts.

2.5.2 In-vitro and in-vivo radiobiology: Open problems

The radiobiological background for hadron therapy is described in Sections 2.1, 2.5, and 2.6. While establishing the physical properties of these radiations has been the aim of intense research, less focus has been put on the actual biological responses to cell irradiation.

The radiobiological response to hadron radiations is, at many levels, different from that to photon radiation. Data for determining clinically relevant RBE values are of great importance; however, it should also be emphasised that the biological effects of particle radiation are not simply a matter of dose–effect relationships that can be adjusted with an RBE factor for all endpoints. Instead, they reflect fundamentally different biological mechanisms. To fully exploit the advantages of hadron therapy, there is a range of unresolved radiobiological questions that must be answered, and there is a need for more experimental in-vitro and in-vivo radiobiological data to support and elaborate on the existing knowledge.

Indeed, research in this field is of the utmost importance to further exploit the benefits of hadron therapy, as is capitalising on the experience of the clinical facilities already in operation. While it is difficult to envisage which research topics might be of highest interest at the time when beams would become available in the experimental hall of a new facility, some of the most important topics are as follows:

(i) An increased proton RBE at the end of the particle range is clearly visible in in-vitro studies, but in clinical settings, this seems to play a less pronounced role. Therefore, the debate is ongoing as to whether the increased RBE at the distal edge of a treatment field needs to be considered in treatment planning for proton therapy. To close the gap between in-vitro and clinical studies, in-vivo studies are indispensable for gaining a better understanding of the above-mentioned discrepancies.

(ii) Due to the better conformality of the dose, partial volume effects might play a more important role in ion beam therapy; because small volumes are typically involved, these might counteract the locally increased effectiveness. This interplay between partial volume and RBE effects also requires in-vivo studies, as partial volume effects cannot be mimicked by in-vitro systems.

(iii) There is increasing evidence that radiation treatment, in combination with stimulation of the immune system, might further increase the effectiveness of the treatment. Furthermore, modulation of the repair capacity, in combination with radiotherapy, might be beneficial. Systematic studies on all such types of combination treatments are required.

(iv) Stem cells are at the origin of normal tissue regeneration and also represent the major players for the regrowth of tumours after radiotherapy. Gaining a better understanding of the

peculiar properties of stem cells with respect to radiosensitivity, repair, and regeneration capacity is of high importance for the improvement of any radiation treatment modality.

(v) Drugs, nanoparticles, and other agents can modify the radiation response and thus the bio-effectiveness of radiotherapy. There are many open avenues because only a small fraction of the possible choices has been experimentally studied.

(vi) Cell migration represents one of the key processes leading to metastases. The problems to be tackled are how far radiation can either enhance or reduce the ability of cells to migrate and affect the occurrence of metastases, and whether there are differences, in that respect, between sparsely and densely ionising radiation.

(vii) Treatment planning for ion beam therapy requires the use of biophysical models. Although extensive experimental data are already available, discrimination between different models needs to be optimised using experimental conditions that are particularly sensitive to model differences; consequently, additional experimental data are often necessary.

(viii) As conformity of the treatment is much better with ion beam irradiation, and it also simultaneously reduces the volume of the irradiated normal surrounding tissue and/or the received dose (thus reducing normal-tissue complications), other factors, such as the probability of inducing second cancers, will become important when choosing the optimal treatment modality.

Considering other research directions, such as radiation protection or more fundamental studies to elucidate the mechanisms of radiation action, there is also a plethora of further topics that a future facility could tackle to contribute to advancements of the field [69]:

(i) FLASH, i.e. treatment with very high dose rates, promises a revolution in radiotherapy, both for medical physics (ultrashort treatments, reduced impact of moving organs) and for radiobiology (apparent sparing of the normal tissue without decreasing tumour radiosensitivity).

(ii) Mini-beam, also known as microbeam or spatially fractionated radiotherapy, exploits the ability of the tissue to regenerate when the volumes are irradiated with a grid pattern.

(iii) Radioactive ion beams [70] are ideal for simultaneous treatment and beam visualisation (theragnostics).

All these activities require high intensities, as shown in **Fig. 33**. Therefore, these research topics, which are and will continue to be studied in existing facilities including FAIR, are particularly suited to a next-generation facility, because both pre-clinical and translational/clinical tests will be possible in the same facility. The potential of these new modalities is enormous, and the proposed facility will be in an ideal position to test their potential and translation in clinical settings.

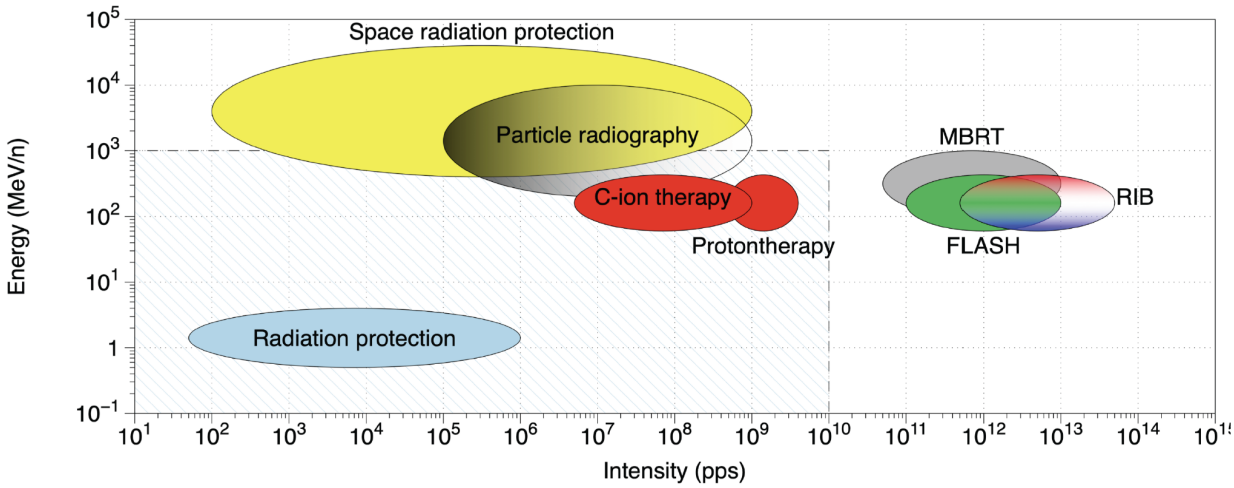

Fig. 33: Biomedical applications at new accelerators. The shaded rectangle includes the (energy/intensity) region covered by particle accelerators. MBRT = mini-beam radiotherapy; FLASH = ultra-high-dose-rate therapy; RIB = radioactive ion beams for therapy and beam visualisation.

As far as the topic of radioactive ions beams is concerned, the potential isotopes and their production mechanisms are listed in Table 4.

Table 4: Positron-emitting radioisotopes that can be used as projectiles in theragnostics (from [70]).

Target	Nuclear reaction channels	β^+ isotopes	Half-life
C	$^{12}C(p,pn)^{11}C$, $^{12}C(p,p2n)^{10}C$	^{10}C, ^{11}C	19.29 s, 20.33 m
N	$^{14}N(p,2p2n)^{11}C$, $^{14}N(p,pn)^{13}N$, $^{14}N(p,n)^{14}O$,	^{13}N	9.96 m
O	$^{16}O(p,pn)^{15}O$, $^{16}O(p,3p3n)^{11}C$, $^{16}O(p,2p2n)^{13}N$, $^{16}O(p,p2n)^{14}O$, $^{16}O(p,3p4n)^{10}C$	^{14}O, ^{15}O	70.61 s, 122.24 s
P	$^{31}P(p,pn)^{30}P$	^{30}P	2.50 m
Ca	$^{40}Ca(p,2pn)^{38}K$	^{38}K	7.64 m

2.5.3 Equipment for the radiobiology programme

The beam delivery for the experimental hall for radiobiology experiments must have the same flexibility as for the patient treatment rooms; i.e. it must be equipped with two fully active 3D raster scan systems and corresponding monitoring systems. For some experiments, broad beam irradiation can be used. The minimum field size for radiobiology experiments is (10 × 10) cm^2, so the delivery system is simpler than those used for radiotherapy.

Reducing the redundant system layout, i.e. using only one position-sensitive and one intensity-sensitive monitor chamber, could reduce the costs, in particular for the first experiments. Initially attractive solutions could consist of a hybrid system combining an active lateral 2D-scanning system with a range shifter that allows scanning the beam in depth. This solution requires only a few pre-set mono-energetic beams to be prepared for the experimental area.

As passive depth scanning produces a slightly higher contribution of fragments in the beam, the level of accuracy and comparability to the fully active 3D beam delivery should be carefully investigated. Comparisons between the passive system at HIMAC with the active system at GSI, however, have revealed that the differences are marginal if other conditions—in particular the width and depth of the SOBP—are identical. For standard irradiation with a comparably small SOBP, simpler solutions can be implemented using 3D ridge filters that allow for substantial reductions in irradiation times, thus increasing sample throughput.

Application of simple rectangular fields with mono-energetic beams does not require the use of a complex TPS; the control system can thus use a simplified version of the typical patient-like delivery procedures based on a separate simple, robust, and fast software module for this task. For the more

patient-like biological experiments, however, the full chain should also be available, starting with the plan generation using an experimentally oriented TPS procedure with its software.

A consequence of the usually high-energy beam and sophisticated beam delivery systems is flexibility with respect to sample types and target geometries. Most experiments can be performed using standard culture flasks (12.5, 25, or 75 cm^2). Furthermore, phantoms can be used, in which biological samples are spatially distributed, or any other more complex geometry, by exploiting the capabilities of the scanning beam delivery system.

For standard experiments, a robust sample handling system is needed that allows for high-throughput experiments that make optimal use of the available beam time, with limitations primarily due to the irradiation time per sample. Simple moving belts have been helpful, e.g. at the GSI facilities, where up to 10–15 samples can be placed in a row and irradiated sequentially without the need for access to the treatment room.

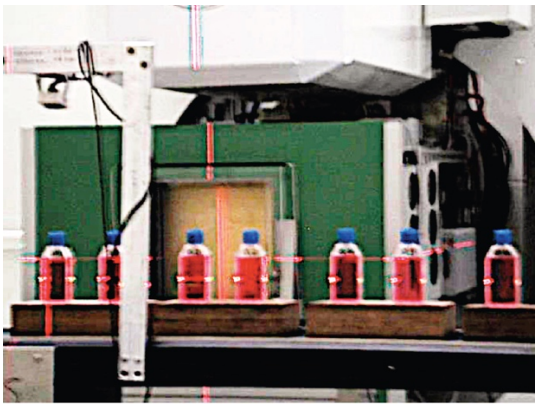

Fig. 34: Conveyor belt system used at GSI.

2.6 Animal programme

2.6.1 General framework

As mentioned in the previous section, in hadron therapy, there is a surprising lack of data from in-vivo experiments; in other treatment modalities, these have been regarded as a necessary link between the hypotheses generated by in-vitro experiments and patient treatments. Cell experiments give good indications of the various effects, but in reality, in vivo, there are many interacting biological functions, which is impossible to mimic in vitro.

To be able to comply with the issues of a different radiobiology and a varying RBE, it is crucial to undertake experimental biological studies to determine the extent and magnitude of these effects. As a necessary next step from in-vitro studies, in-vivo studies enable simulation of clinical treatments in animal models and give essential information to determine the optimal radiation modality to protect normal tissues and to optimise the anti-tumour effects.

By adhering to the concept of dedicating 50% of weekday time along with nights and weekends to research, a next-generation facility would have the possibility of devoting ample time to such studies, employing a variety of in-vivo models; this would make such a facility unique in the global landscape.

2.6.2 Research challenges in animal studies

The list of open problems in particle radiobiology raised above should be addressed in systematic, large-scale in-vivo setups using relevant ions. This should include simulation of clinical treatment with fractionation as well as different positions in the beam. The effects of these factors on tumour response, as well as the differential effects of the previously mentioned treatment modalities (e.g. FLASH, mini-beam radiotherapy, combination with immunotherapy, etc.), need to be studied. A panel of tumour models with a range of different radiobiological properties [71], e.g. intrinsic radiosensitivities, hypoxic fractions, levels of stem cells, immunogenicity, etc., should be used to elucidate these effects.

There are different factors to consider when choosing tumour models. For particular research questions, patient-derived xenograft models are preferred, as these are expected to be reflective of the original complex tumour biology. Therefore, they could better predict the clinical usability and the clinical translation of a treatment [72]. However, for any xenograft model, the host used must be immunocompromised to prevent transplant rejection, which means that the interaction with the immune system is disregarded in these studies. In this regard, the use of so-called humanised mice, which are engrafted with human hematopoietic stem cells, can enable the interactions between the immune system and the radiobiological effects [73]. The use of syngeneic tumour models—tumour tissues derived from the same genetic background as the host—are also relevant in radiobiology studies, as an intact immune system is retained.

Relevant normal-tissue models should include functional and tissue endpoints, representing both early and late radiation-induced reactions. The following is a non-exhaustive list of in-vivo models that can be included:

(i) assays for acute skin reactions [74] and radiation-induced fibrosis [75] (**Fig. 35**);

(ii) models of neurological damage of the spinal cord, central nervous system, peripheral nerves, optic nerve, etc. [76];

(iii) lung injury [77];

(iv) urinary bladder function [78];

(v) cartilage tolerance;

(vi) cognitive assays, such as novel object recognition (NOR) and novel object location (NOL) [79].

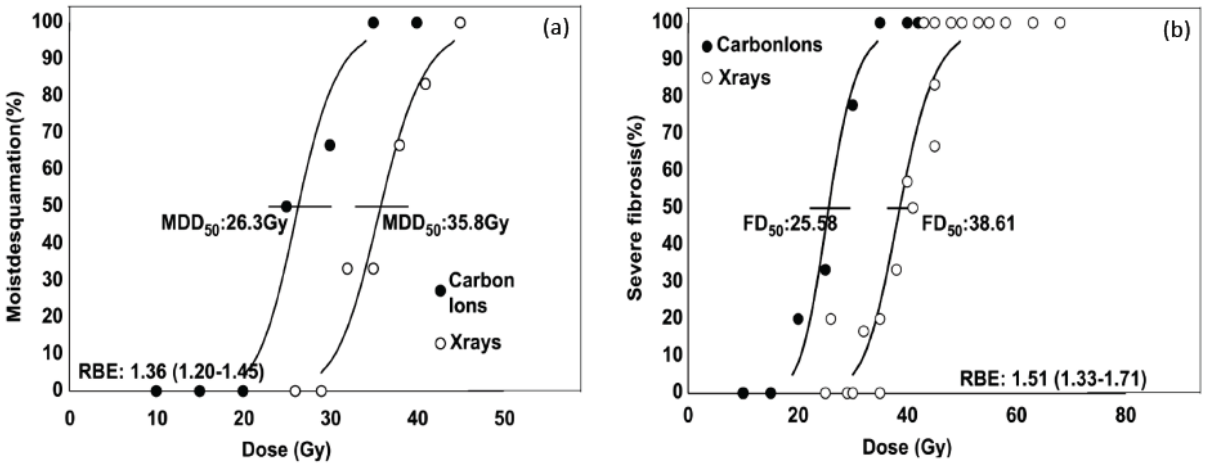

Fig. 35: Examples of in-vivo data on early and late radiation-induced reactions: (a) acute skin reaction (moist desquamation of irradiated areas of the skin); and (b) radiation-induced fibrosis, a late reaction of tissue to radiation [80].

As animal models are not trivial to set up in a facility, an animal study programme could be partly based on researchers from other institutions at which animal models have already been implemented, refined, and optimised. Projects would use animals that stay temporarily at the facility for irradiation and are then returned to the home institutions for follow up, as this can be a very long process; for late reactions, the time dedicated to observing the animals can be up to several months or even years.

2.6.3 The programme

To conduct the experiments, an *in-house animal facility* should be established for permanent housing of small rodents. Larger animals might be treated in collaboration with an *external academic veterinary department*. This long-term activity could provide data for the development of biological models and

their implementation in human TPSs, in collaboration with the other European institutions. Such high-quality pre-clinical research is necessary to secure solid foundations for clinical research.

2.6.4 Equipment for the animal experiments programme

An example of a small-scale, yet complete and self-sufficient, animal facility for small rodents is shown in **Fig. 36**. The proposed RI should feature an animal facility located in a building close to the experimental areas and similar to the one shown in this figure. In addition, a cleaning room for washing equipment, as well as a laboratory, should be available to the internal and external scientists performing their experiments at the facility. The facility should be equipped with at least one laminar flow hood for animal handling.

It has to be considered that there are legal requirements for the building specifications for an animal facility, e.g. regarding the noise level, ventilation, and temperature. Therefore, the facility for housing of experimental animals needs to be approved and controlled by the local authorities. In addition, any auxiliary facilities for housing and treatment of animals must comply with EU regulations.

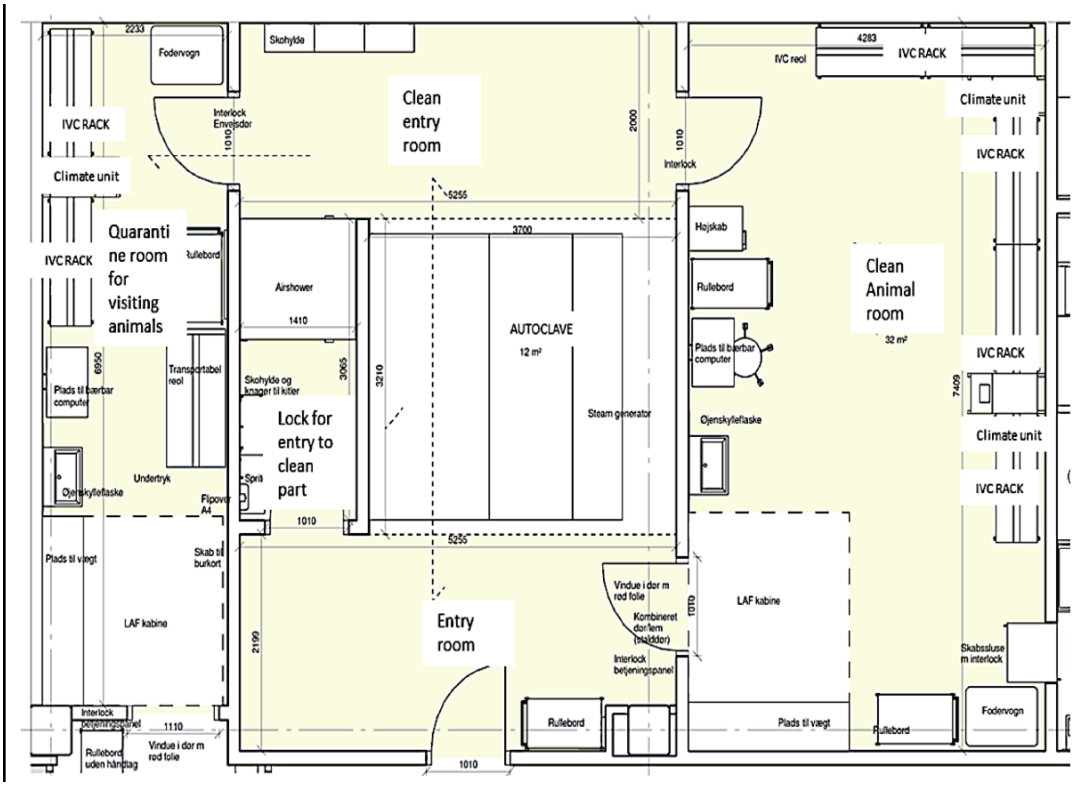

Fig. 36: Schematic of the animal facility for small rodents at the department of experimental clinical oncology, Aarhus University Hospital.

Visiting scientists are expected to bring their own equipment, and sometimes animals. Therefore, the animal facility should have devoted cabinets for small rodents, and even large animals, with all the necessary connected services. There should be access to a range of general laboratory equipment; this could be done in connection with the in-vitro facility. It is necessary to have an isolated section that can serve as the quarantine room for a temporary medical physics programme, its equipment, and for housing of animals to ensure that there is no risk of contamination between visiting and in-house animals.

The animal facility and these laboratories should be built in close proximity to the experimental beam room to avoid long transport times between animal preparation and animal treatment. One possibility would be to place the animal facility in a basement with a direct connection to the experimental beam room to avoid patient areas being exposed to allergens.

Larger animals, including dogs with natural tumours, could be brought to the site only when needed, and the follow-up would then be conducted in an external facility or facilities, possibly in the framework of a *veterinary network*.

2.6.5 Studies on large animals

Most pre-clinical studies in radiotherapy use rodent models. The use of large animals is highly problematic because of the associated high costs, maintenance difficulties, ethical considerations, and lack of well-defined tumour models and genetically editable systems. However, large animals are irreplaceable for examining new applications of particle therapy in non-cancerous diseases such as cardiac arrhythmia (**Fig. 37**) [81].

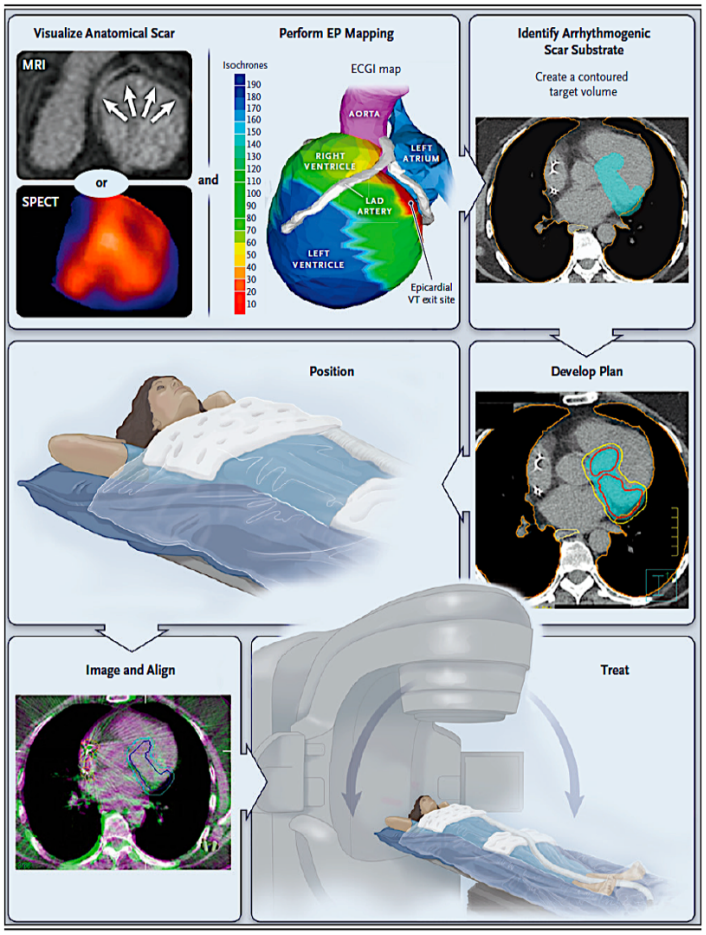

Fig. 37: Workflow for non-invasive, electrophysiology-guided stereotactic body radiotherapy (SBRT) ablation of ventricular targets in arrhythmia patients using X-rays.

Among the many arrhythmias, ventricular fibrillation is a preferred target because it is a deadly disease that can only be treated with catheter ablation. Recent studies have shown that SBRT can be an effective alternative strategy to treat ventricular fibrillation. This paves the way to applications of radiotherapy in cardiology, with the advantage of providing a non-invasive treatment that can be repeated. However, SBRT produces a large dose bath that can be reduced using charged particles (**Fig. 8**), thus reducing side effects and allowing dose escalation for better conformality. A pilot study in a swine model at GSI has demonstrated the feasibility of this approach using C-ions (**Fig. 38** and **Fig. 39**) [82]; this was later confirmed at the Mayo Clinic using protons, and the first human patient was treated with protons at CNAO in December 2019 [83].

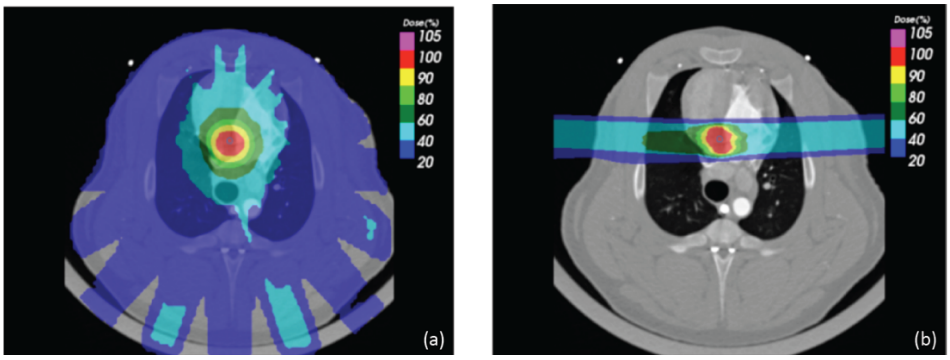

Fig. 38: Comparison of treatment planning with SBRT (left) and C-ions (right) for ventricular ablation in a swine.

Access to pigs would allow the development of new strategies for treatment of heart diseases using charged particles. Farm pigs are commonly used in cardiology because they have heart structures similar to those of humans. Therefore, establishing a pig farm in collaboration with regional veterinary departments and cardiology departments at nearby universities would be beneficial for the future proposed facility.

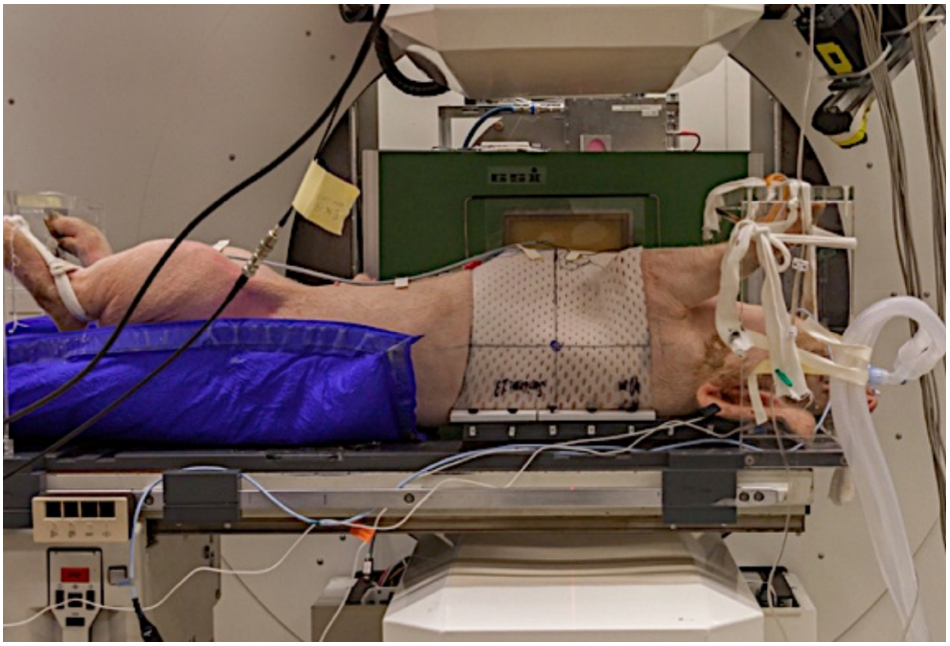

Fig. 39: Treatment of a swine for atrial fibrillation at GSI. The animal is anesthetised, maintained in forced ventilation, and blocked using thermal mask immobilisation. Beam delivery is checked using a positron emission tomography (PET) camera.

Pigs are not the only large animals that can be used in research. A second very interesting and unique possibility is using pet patients, i.e. to open the facility to treatments of sick dogs and cats. Several radiotherapy units offer this possibility, the most advanced being the one at Colorado State University (CSU) in the USA (**Fig. 40**). Both oncological and non-oncological diseases could be treated with particles in the framework of comparative veterinary trials.

Veterinary trials have the potential to address many questions raised in the clinical community and should be tackled by randomised trials. Offering free or low-cost treatment to pets could pave the way to several trials, and it could attract veterinary clinics from all over Europe to treat sick pets. The results of such clinical trials have high translational potential for humans, as demonstrated by the CSU experience.

Fig. 40: Irradiation of a dog patient in the CSU veterinary clinic.

2.7 Medical physics programme

2.7.1 General framework

From a medical physics point of view, the success of tumour treatment depends on the quality of every element within a chain, starting with the imaging modalities (prior, during, and after the irradiation), treatment planning, dose verification, patient positioning, dose delivery, monitoring during the irradiation, and potential feedback to the dose delivery system. As a consequence, the push towards increasingly accurate and patient-tailored hadron therapies has greatly contributed—and will continue to contribute—to the development of all these areas of medical physics.

Major progress has been made in conventional radiotherapy over the last two decades. Highly integrated systems are available from industrial vendors that combine the irradiation functionality with volumetric imaging during the treatment process. The treatment can be adapted to slow (anatomical) or fast (organ movement) changes. The latest innovation—the combination of MRI tomography with an electron linac—has now reached radio-oncology departments.

Even though the amount of knowledge accumulated is impressive, with increasing numbers of patients worldwide being treated with carbon ions, many areas would benefit enormously from further research and development. Other areas are almost uncharted, in particular since the medical community is moving towards the use of ions other than carbon, such as helium and/or combinations of ions [84] [85].

To fully realise the potential of ion beam therapy, a broad medical physics R&D programme can be established. Such a programme will be more effective if it is conducted in close cooperation with clinical teams and strong biophysics modelling groups; this is a recommendation that can be implemented by the proposed next-generation facility.

2.7.2 The programme

2.7.2.1 Beam characterisation

The introduction of new ion species requires a comprehensive and very accurate beam characterisation [86]. These measurements are used to tune Monte Carlo transport codes that are employed to generate libraries of base data for both clinical and research treatment planning platforms:

(i) For every new ion species, stopping power and range measurements will be performed in adjustable water columns to tune and benchmark the transport code.

(ii) The production of projectile fragments heavily impacts the characteristics of the Bragg peak and the radiobiological properties. Therefore, the underlying cross

sections will be determined by elaborate measurements, e.g. by using time-of-flight telescopes [87] or semiconductor pixel detectors such as Medipix.

(iii) The quality of the planned dose distribution depends critically on the preciseness in the description of the evolution of the beam-spot size along the trajectory, including every element (vacuum window, detectors, shaped range shifters, and the tissue itself). Dual or even triple Gaussian functions will be fitted to the results of the scattering measurements to generate the base data for the TPSs.

The results will be implemented in a Monte Carlo-based transport code, such as FLUKA [88], to support both clinical treatment planning and the various research programmes.

2.7.2.2 Dose delivery

Typically, the dose is delivered using active beam scanning systems; i.e. the target volume is subdivided into thousands of tiny voxels, and focused pencil beams are guided into these voxels by changing the beam energy and employing fast magnetic deflection. Each spot is irradiated for some milliseconds, and detectors monitor the beam properties during the scanning process. The dose delivery time per field for a brain tumour is of the order of 100 s, which is perfectly fine for static targets and standard dose fractionation. Target volumes that are influenced by the breathing cycle or the heart action show significant motion at a much shorter time scale, and they cannot safely be treated using this approach. As a non-optimal compromise, the dose delivery is gated based on real-time monitoring of the patient's surface movement or simple strain gauges. Ideally, the dose delivery should be much faster than the target motion so that the target appears to be quasi-static. The development of an ultrafast beam delivery system, including the scanning system and the beam monitoring system, is a highly attractive research goal. This approach may be combined with short phases of breath holding and supported by surface monitoring. Here, a new generation of scanning systems needs to be developed, along with much faster position-sensitive detectors.

Standard fraction schemes use daily doses of about 2 Gy at a dose rate of about 10 mGy/s. It is an open question whether a dramatic increase in dose rate, such as FLASH irradiation (> 50 Gy/s), leads to better sparing of healthy tissue. This effect can be demonstrated for electrons; however, in the field of ion beam therapy, a number of research groups have presented inconsistent data for a variety of parameters. Certainly, FLASH is a relevant research topic to pursue in a future facility and the dose delivery system and the monitors in front of the target need to cope with these very high dose rates.

Radiosurgery with ion beams is a promising modality for small targets such as arterio-venous malformations or cardiac ablations. A dedicated micro-beam scanning system with a dedicated nozzle will be used to conduct a broad experimental programme.

2.7.2.3 Imaging modalities, motion management, and quality assurance

To increase the quality of ion beam therapy, reducing range uncertainties by applying ion beam tomography is a promising approach. Here, helium is better suited than proton tomography due to its reduced multiple scattering [89]. One task is to measure, with high accuracy, the stopping power of living tissues using new imaging modalities such as proton or helium radiography (tomography).

The development of new beam monitors for detecting—during and after treatment, with millimetre accuracy—the position where the ion beam stops in the patient's body, to assess the accuracy of dose deposition in real time, is another important research area. Due to the underlying interaction processes, the deposition of the projectiles in the irradiated volume is a source of prompt gamma radiation. Prototypes of such gamma cameras are under test at some ion beam therapy centres, and the method shall be further studied.

In earlier days, positron emission tomography (PET) isotopes originating from fragmentations were registered using in-beam PET scanners [90] or PET scanners located close to the irradiation rooms. The range distributions of the projectiles were calculated but, due to wash-out phenomena driven by

blood circulation, reliable dose verification could not be achieved. However, with the ongoing dramatic increases in computing power and the fast-growing expertise in the field of machine/deep learning, the limitations of PET, such as its lack of promptness, may be overcome. The first experiments to detect shockwaves released by positioning the Bragg peak inside a phantom have shown the potential of this approach [91].

By tracking the movement of regions of interest (the tumour or OARs), the quality and safety of this treatment modality can be improved. Again, ultrasound scanners may be used, and the introduction of in-beam MRI systems will generate precious real-time and volumetric information. These activities can pave the way to adaptive treatments. Indeed, the management of moving organs is a challenge, and it must be an important component of the research programme of future facilities such as that proposed.

2.7.3 Biophysical modelling

Modelling and predicting the biophysical processes elicited from particle beam interactions within the human body must be performed at both the macroscopic and microscopic scales to further exploit ion beam therapy. Advanced computational methods could be introduced into both the clinical environment and the pre-clinical research programme. The use of concomitant and foresighted modelling is expected to improve the accuracy of the clinical TPSs used daily by clinicians and support their validation, commissioning, and routine clinical use against dosimetry and in-vitro biological measurements. Monte Carlo [92] [93] and analytical simulation codes [94] [95] will be used to investigate data from large patient cohorts or radiobiological studies [96] and develop improved treatment protocols [97] [98]. Such biophysics modelling requires a very powerful computing environment, such as a GPU farm, and this should be part of the equipment located at the future facility or at its collaborating partners.

2.7.4 Equipment for the medical physics programmes

The biophysical experiments can be performed in the proposed facility's experimental hall at the end of dedicated transport lines. At least one of these horizontal lines should be equipped with the standard nozzle and the field size of the scanning beam delivery used for the patient treatments. This "standard" irradiation facility can be used to run physics experiments such as those seeking to develop and qualify new detector concepts, test motion monitoring devices, or examine in-vitro and in-vivo programmes.

Another horizontal beamline can be used for experiments requiring non-standard beam and/or irradiation parameters. This nozzle would offer multiple iso-centres and can be equipped with experiment-specific beam monitors that can handle very low as well as very high beam intensities. The setup could be adapted to the requirements of individual experiments, for example:

- 3D mini-ridges [99] for advanced passive beam spreading (FLASH, moving organ studies);
- time-of-flight-telescopes for fragmentation studies;
- mini-beam configurations for radiosurgery studies or fan-type irradiations.

At a later stage, based on the experience gained, the potentialities of the proposed facility can be widened; room could be reserved for additional beamlines. These experiments will greatly benefit from the fact that a significant portion of the daily schedule is dedicated to research activities as a core concept of the proposed facility.

2.8 Materials science programme

Over several decades, ion beam facilities that were originally conceived and developed for nuclear physics research have impacted numerous other fields, including materials science, condensed matter physics, geosciences, mineralogy, environmental physics, and biomedical sciences. The numbers of applications in both basic research and industrial technology are still continuously growing. Ion beams are used in fabrication processes involving implantation and doping, surface modifications, and nanostructuring. They also offer great possibilities for ion beam analysis (IBA), which is typically based on beams of energies up to several MeV. IBA techniques can be used to probe the elemental

compositions of solids and obtain high-resolution depth profiles in surface layers. Thanks to novel accelerator technology, instrumentation, and high-performance computing, IBA methods are highly sensitive and non-destructive, thus allowing the analysis of delicate samples, including precious artefacts and archaeological, forensic, or biological objects. Hundreds of IBA laboratories currently exist around the world, serving both basic research and industrial applications.

Progress in nuclear and particle physics eventually resulted in the building of larger accelerators of ever-increasing energy. The advent of new high-energy facilities also opened new opportunities for application-oriented activities, with ions of several hundreds of MeV kinetic energy and above. This has sparked research across various disciplines, a field now known as research with *swift heavy ions*. Given their high velocity, swift heavy ions deposit enormous energy densities into the electronic subsystems of solids, driving the local atomic structure far from equilibrium. Depending on the class of materials, this results in a rapid phase transition and complex structural modifications along the trajectory of each individual ion. The resulting cylindrical damage trails have a diameter of only few nanometres but are very long: depending on the energy, from a few tens of micrometres up to millimetres. These so-called "ion tracks" represent nanostructures of high aspect ratio and are mainly created in insulating materials. Combining chemical etching of ion tracks, electrochemical deposition, and surface modification techniques offers the potential to synthesise tailored nanostructures and exploit size-dependent physical, chemical, and biological properties of materials at the nanoscale. Thanks to the enormous flexibility of the technique, innovative applications of nanowires, nanotubes, and nanochannels are under investigation. Examples are shown in **Fig. 41** [100].

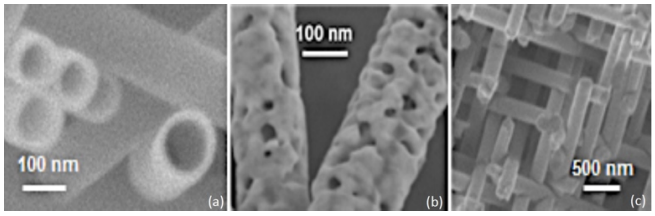

Fig. 41: Novel ion-track technology allows the fabrication of nanostructures with designed diameter, length, shape, and composition. Examples are: (a) nanotubes; (b) porous gold wires; and (c) nanowire networks [98].

The implementation of nanopores or nanowires in microsystems is still at an early stage, but promising perspectives have been demonstrated for more complex devices with novel capabilities, including sensors, nanofluidic systems, nanoreactors, and extremely small and compact analysis systems. It should also be mentioned that ion-track membranes are currently being produced commercially. Several small companies pay for beam time at accelerator facilities (e.g. at Caen, Louvain-la-Neuve, Dubna, Lanzhou, Jyväskylä, and Brookhaven) and produce and process huge quantities of track-etched membranes for a broad variety of applications.

In addition to using swift heavy ions as structuring tools, the destructive power of ion beams is also being intensively studied by a large community. Basic phenomena of ion–solid interaction processes are still not completely understood, and available model descriptions are incomplete. When swift heavy ions enter a solid, the system undergoes ultrafast electronic excitations (10^{-17} to 10^{-13} s), finally leading to atomic motion, amorphisation, and/or defect formation (10^{-14} to 10^{-10} s). Concomitant effects include the emission of secondary particles, local melting, shock waves, and permanent changes in material properties. Details of these non-equilibrium processes are strongly material dependent, with insulators being significantly more sensitive to damage creation than metals. From the past decade of research, a large set of data has been accumulated regarding the size and characteristics of ion tracks across a large variety of materials. However, the complex interplay between multiple length and time scales, as well as the mechanism by which the electronic excitation energy is converted into atomic motion and finally into stable structural changes, are still under debate.

Several large-scale high-energy ion accelerator facilities (such as GSI in Darmstadt, GANIL in Caen, and IMPCAS in Lanzhou) provide beamlines dedicated to materials science, where sample irradiation is combined with in-situ and/or online analysis. At the M-branch of GSI, three Universal Linear Accelerator UNILAC beamlines were established to obtain in-situ information about material

changes induced by swift heavy ions by means of X-ray diffraction and Raman, infrared, or UV-Vis spectroscopy (**Fig. 42**).

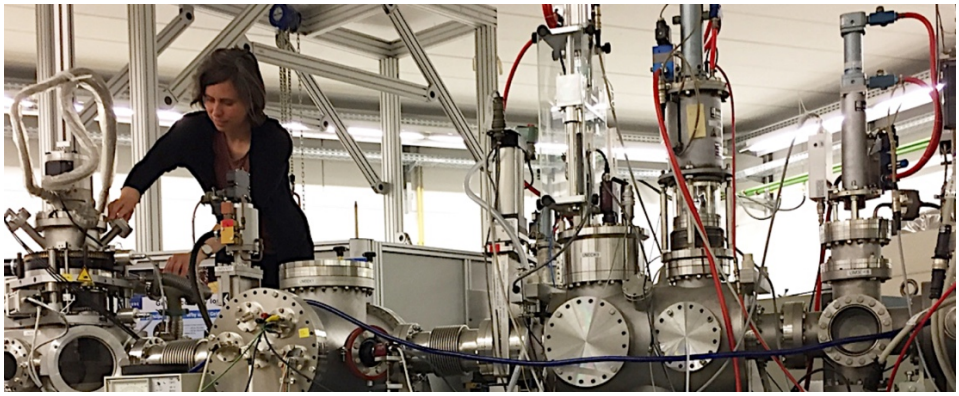

Fig. 42: In-situ methods available at the M-branch of GSI (Darmstadt) provide information about beam-induced changes by microscopic and spectroscopic means. Flexible stations for irradiations at cryogenic and elevated target temperatures are also important.

Microscopes (e.g. scanning electron and scanning probe microscopes), directly attached to the beamline, allow imaging of the topographic effects of single-ion impacts without exposing the sample to air. Another example is secondary-ion mass spectrometry for probing the composition of a given sample surface during bombardment with MeV–GeV ions.

2.8.1 Irradiation of materials under high pressure

A very promising application at new facilities is the combination of ion beams with high pressure. The principal effect of high pressure, observed in all materials, is a reduction in volume and a corresponding shortening of mean interatomic distances. Under sufficiently high pressure, every material is expected to undergo transformations into a denser structure with increased atomic packing efficiency. Often, dramatic changes in physical properties occur alongside these structural modifications. Pressure is an important tool for synthesising dense structures, including super-hard materials, novel solidified gases and liquids, and mineral-like phases that are suspected to occur deep within the Earth and other planets.

Technically, high pressures are obtained by squeezing a small sample between two gem-quality diamond anvils to pressures typically up to around 100–200 GPa. The beam energy at the new facilities is sufficiently high to penetrate through one of the anvils (of thickness in the range of several millimetres) and deposit energy in the pressurised samples (**Fig. 43**). The amount of energy is controlled by the ion species (the energy deposition increases with the mass of the projectile) and by the applied fluence.

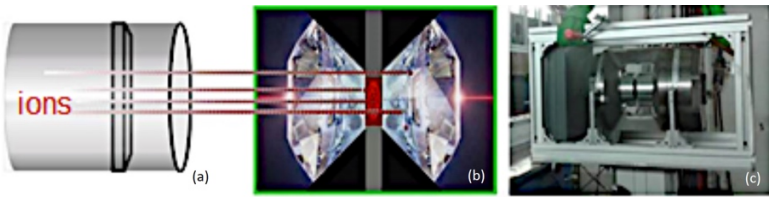

Fig. 43: (a, b) To reach the samples, the ion projectiles have to penetrate the first anvil of 2–3 mm thickness, requiring beam energies of the order of 200–300 MeV/u. (c) Paris–Edinburgh pressure cell for larger samples. (Courtesy of U.A. Glasmacher, Univ. Heidelberg.)

Diamonds, being transparent to electromagnetic radiation, provide convenient access to sample analysis, particularly by means of X-ray diffraction, as well as optical, infrared, and Raman spectroscopy. Currently, most synchrotron light sources operate dedicated beamlines for high-pressure experiments with advanced X-ray techniques.

Injecting relativistic ions through a diamond anvil several millimetres thick into a pressurised target inserts a huge amount of energy and drives the local atomic structure far from equilibrium. So

far, it has only been possible to perform a very limited number of experiments due to limited beam intensities. However, the results obtained provide clear evidence that the combination of pressure and ion beams can trigger drastic structural changes that do not occur due to the applied pressure or as a result of the ions alone. They also show that the interplay of the two extreme environments, simultaneously applied, opens unique pathways in the phase diagram that are otherwise not accessible. It was observed that, in zircon, under simultaneous pressure and ion irradiation, the high-pressure phase appeared at a lower critical pressure value than in unirradiated samples. Defects induced by the ion beam may strongly influence the phase stability when the pressure is released. After the irradiation of pressurised zirconia, the high-pressure phase was harvested; whereas, when exposed to pressure only, the material flipped back to the original structure after the pressure was released. The responses of minerals to simultaneous irradiation and pressure are completely unknown, but they may have direct implications in the field of geosciences with respect to geological formation and radioactive decay processes in the crust and upper mantle of the Earth.

2.8.2 Ionoacoustic phenomena

Due to the huge energy deposition of swift heavy ions, particularly at the Bragg maximum close to the end of the projectile range, ion beams can induce acoustic waves. Despite the large differences in energy and geometrical scale, the effect is similar to that of earthquakes, for which the analysis of seismic waves provides important information about the position and dynamic characteristics of the seismic source, as well as the otherwise inaccessible internal structure of the Earth. Ion-induced sound waves propagate over long distances and can be detected at the sample surface using conventional ultrasonic sensors. The position of the source is deduced from the measured propagation time of the waves. This technique is non-destructive and can provide real-time analysis by means of acoustic signals within a time frame of 10 ns.

Exposing solids or liquids to intense ion pulses results in an instantaneous temperature spike followed by stress and strain propagating as elastic waves of ultrasonic frequencies through the sample. Monitoring and analysing these waves at the sample surface yields information on mechanical processes and local deformations inside the bulk material such as microcracks.

The ionoacoustic method has been revisited in proton therapy, where the ionoacoustic signal promises a simple but very accurate means to measure the position of the Bragg peak during patient irradiation. In addition to this medical application, ionoacoustic particle detectors have great potential for monitoring intense bunches of light and heavy ions. The first tests were performed by exposing a water basin to short and intense bunches of U, Xe, and C ions with energies between 200 and 300 MeV/n (**Fig. 44**) [101]. The measured ion ranges were in good agreement with Geant4 simulations as well as with data from experiments conducted using an ionisation chamber behind a variable water column. The ion-acoustic energy resolution was found to be better than 1%, opening a new method for stopping-power measurements at relativistic energies.

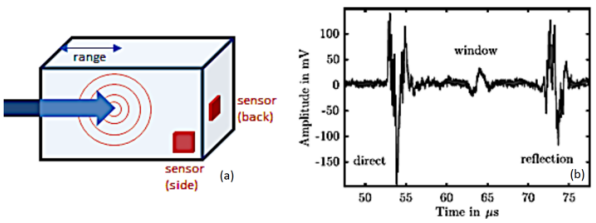

Fig. 44: (a) Scheme of ionoacoustic experiment with ion pulse coming from the left. The high energy deposition close to the Bragg maximum acts as source for the emission of an acoustic wave that is registered by two piezo sensors. (b) Acoustic wave monitored with a piezo sensor when 300 MeV/u uranium ions, accelerated by SIS18 of GSI, passing through a Kapton window, are stopped in a water basin at a depth of 14.4 mm.

The advantage of the ionoacoustic technique is the rather easy experimental setting: the information is available by means of only a few pulses, and the acoustic detectors have a huge dynamic range.

2.8.3 Radiation hardness

An important research field is the radiation hardness of materials under extreme dose conditions, and this can be addressed at the proposed future facility. This is of relevance for a variety of applications, particularly including functional materials in the next generation of high-power accelerators and in fusion and fission reactors.

Moreover, accelerators with ever-increasing beam intensity, brightness, and stored energy, such as the new FAIR facility at GSI, the European Spallation Source, or the High Luminosity Large Hadron Collider (HL-LHC) and the Future Circular Collider planned at CERN, push material requirements into more challenging grounds and unknown territories. Beam intercepting devices (e.g. collimators, production targets, beam dumps, etc.) are components exposed to extreme beam losses and high radiation doses. They have to cope with radiation damage, rapid localised heating, and transient pressure waves that propagate through the material. Changes in physical, mechanical, and thermal properties in the course of damage accumulation may severely affect their operational performance.

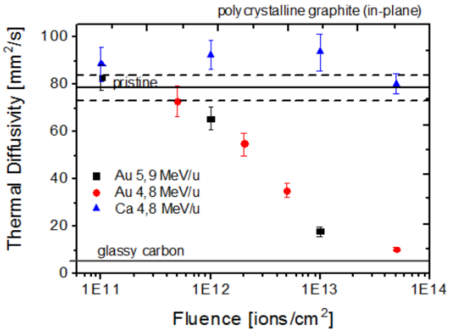

Fig. 45: Thermal diffusivity as a function of ion fluence for polycrystalline graphite samples irradiated with Au and Ca ions. Within the tested range, the thermal diffusivity degrades significantly, allowing us to predict that under these conditions, the peak operation temperature for the FAIR Super-FRS beam catchers would increase from 900 to 2500 K.

Figure 45 presents experimental results obtained at GSI on the thermal diffusivity of graphite, showing how it decreases as a function of fluence when irradiated with GeV ions [102]. Such investigations are important to estimate, for instance, the increase in the peak operation temperatures of specific components. Another example is shown in **Fig. 46**, illustrating how the accumulation of large doses can heavily affect the properties and microstructure of carbon films, used as stripper foils, mounted on a 30-mm-wide aluminium frame [103].

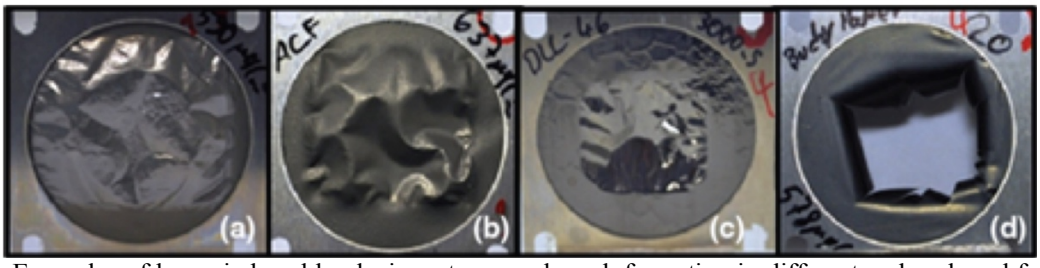

Fig. 46: Examples of beam-induced hardening, stress, and crack formation in different carbon-based foils after exposure to a pulsed beam (0.6–2.0 Hz, 0.2-ms pulse length) of 1 GeV uranium ions: (a) amorphous carbon, 10^{14} ions/cm^2; (b) arc-evaporated carbon foil, 5×10^{13} ions/cm^2; (c) diamond-like carbon, 10^{14} ions/cm^2; (d) carbon-nanotube-based foil, 10^{12} ions/cm^2.

Due to the large penetration depths of high-energy beams, homogeneously irradiated large-volume materials can be produced and tested, in situ or offline, by classical thermomechanical methods such as laser flash analysis and strain–stress measurements. An example for non-contact measurements of thermal stress waves in a sample exposed to intense ion beam pulses is shown schematically in **Fig. 47**. Such experiments provide crucial information about thermal shock resistance and allow decisions regarding whether a material is suitable for a specific application.

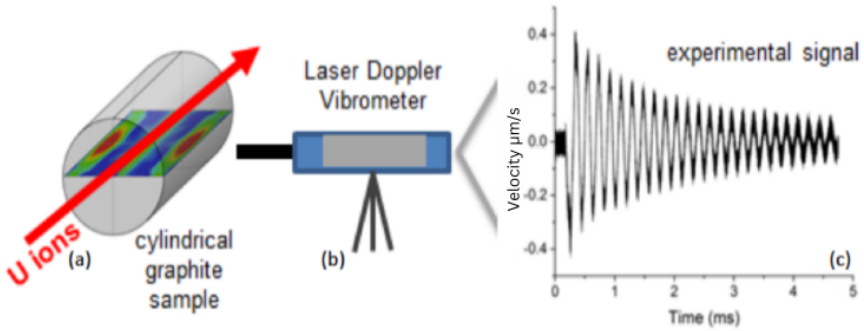

Fig. 47: Scheme of planned FAIR experiments using non-contact monitoring of thermal stress waves produced by intense ion pulses. (a, b) The laser beam from the laser doppler vibrometer is directed onto the sample surface. (c) The target velocity components along the direction of the laser beam (vibration amplitude and frequency) are extracted from the Doppler shift of the frequency of the reflected laser beam due to surface motion.

To overcome limitations of current-generation materials, it is also of great importance to develop new material solutions. Examples of advanced materials are copper–diamond–graphite and molybdenum-carbide–graphite composites; these exhibit very high thermal conductivity in comparison to graphite and are candidate materials for the primary collimators of the HL-LHC upgrade at CERN. Based on radiation tests, important feedback can be provided to the production cycle, for example, to optimise the mechanical stability in combination with radiation hardness. Shielding materials for equipment in deep-space missions are also an issue because the space environment is very hostile due to the combined action of radiation, extreme temperatures, and vacuum conditions. Synergistic effects can be a major factor for enhanced degradation and can be further tested in the future.

For systematic radiation studies on irradiated bulk materials, coordinated beam-time campaigns at different upcoming facilities will be extremely helpful because experimental results need to be accumulated under various conditions, using beams from protons to uranium, at both low and high energies and fluxes, with fluences across a broad range. In these activities, FAIR and next-generation facilities can cover complementary roles by contributing to the production of a comprehensive database that will be extremely valuable for the community. This database will also be vital for benchmarking simulations and providing reliable extrapolations on how beam-induced effects and defects correlate with macroscopic property changes under operational conditions at future high-energy and high-current facilities.

3 Preliminary technical design, organisation, and investments

3.1 Introduction

Part II of this report describes the proposed future RI, a facility conceived to pursue the goals described in Part I, namely, research studies in radiobiology, animal studies, medical physics, and materials science, together with tumour therapy. It also discusses the requirements for the selection of an appropriate site to host such a RI and quantifies the construction and running costs.

The proposed facility is conceived as an RI giving emphasis on the experimental programme, which would make it the first ion facility in Europe designed to host a rich experimental programme in addition to performing irradiation of patients. Therefore, the proposed design, shown in **Fig. 48**, incorporates two experimental beamlines in addition to the three beamlines serving the three patient treatment rooms. Clearly, ample separation between therapy rooms and experimental caves is one of the critical design constraints to avoid any undesired interference.

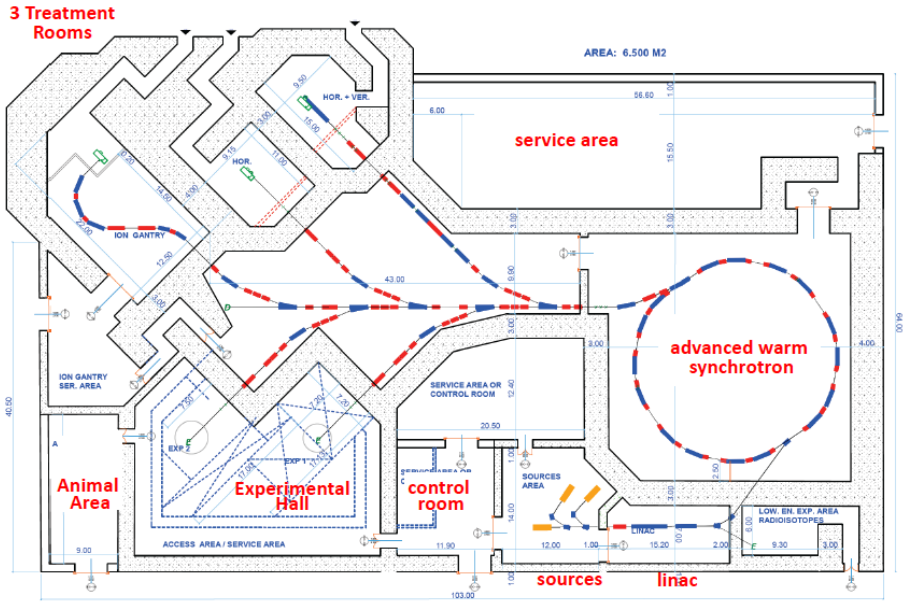

Fig. 48: Layout of the bunker of the proposed RI.

The basic layout of the synchrotron for the proposed facility follows the PIMMS design [6] [2] and is presented in Section 3.2. While following the main structure of PIMMS, the accelerator design outlined in the present proposal integrates new specific requirements for a new RI in terms of extreme beam intensity and easily adaptable injection and extraction, as presented in Section 3.4. The design of the proposed synchrotron is very flexible. An advanced synchrotron is conceived to accelerate different types of hadron beam, such as helium, carbon, oxygen, neon, or argon ions, and it is well suited to the research programmes discussed in Part I of this document and for treating tumours. Other notable differences from PIMMS are the new design for the injector linac, as introduced in Section 3.3, and the new layout of the beam transport lines, presented in Section 3.5. Moreover, the design integrates a completely new superconducting ion gantry; this is described, along with its various options, in Section 3.6. Thanks to these new features, the proposed RI can become a unique world-class facility based on the most advanced state-of-the-art technologies.

In parallel with further optimisation of this baseline, more developments are pursued in the frame of a wide European collaboration, including more advanced layouts and a novel superconducting magnet technology for the synchrotron, as discussed in Section 3.4. These R&D directions are being explored with the aim of reducing the cost and footprint of the facility by introducing beyond state-of-the-art technologies. The decision regarding which option to construct will depend on the maturity of alternatives to the baseline design at the time funding becomes available and costs can be more accurately assessed.

3.1.1 Background and methodology

A new project must be based on a reliable accelerator design, enabling construction to begin as soon as funding becomes available. For this reason, the present document describes a solution based on an advanced version of the PIMMS synchrotron design. Its feasibility and reliability are proven, and its main components can be rapidly manufactured by existing industries.

However, accelerator science and technology have made impressive progress since the development of PIMMS, as confirmed by the success of large-scale accelerator projects and by the large number of modern accelerator-based systems built worldwide for basic or applied science, for industry, and for medicine. Applying some of this progress in accelerator technology to a new generation of ion therapy and research accelerators is the goal of a study group established at CERN, the Next Ion Medical Machine Study (NIMMS)[18]. This initiative, started in 2018, seeks to progressively investigate and develop technologies that could be used in an advanced ion therapy and research facility, such as the proposed new RI, and to meet the requirements of the SEEIIST initiative. The aim of this R&D effort is to make available a portfolio of new technologies that could be progressively included in the RI baseline design as they come to maturity, replacing the corresponding PIMMS components. Depending on the final implementation schedule of a new facility, this will allow the building, at any given moment, of the most advanced accelerator that is realistically feasible with available technologies.

Considering that the accelerator represents more than 75% of the construction and operation costs of an ion therapy and research facility, the first objective of the NIMMS study is to identify technologies that would reduce the cost and footprint of the accelerator while ensuring the high reliability required by an accelerator for medicine. At the same time, the specifications for a next-generation ion therapy and research accelerator call for higher beam intensities for faster dose delivery and greater flexibility to meet the diverse needs of the research programme. This programme consists in accelerating a wide range of ions and extracting them in both slow and fast modalities. While some of the technologies developed in NIMMS address completely new approaches for producing the ion beams, three key technologies are directed at improving the synchrotron-based design, and these are described in Section 3.4 of this document.

Two Horizon 2020 European projects, Innovation Fostering in Accelerator Science and Technology (I.FAST) [104] and Heavy Ion Therapy Research Integration plus (HITRI*plus*) [105], support the design of key components, including prototypes of superconducting magnets.

3.2 Choice of the baseline design

As noted, the basic layout of the accelerator complex of the proposed facility follows the PIMMS design [6] [2], and this is described in Section 3.2.1. This study has given birth to the CNAO and MedAustron facilities, whose layouts are shown in **Fig. 49**. It has also been used as a reference for the initial design of the SEEIIST facility, proposed for construction in the South East Europe region, as described in [1]. This design is well proven, and its costs are known with a good level of confidence.

[18] https://nimms.web.cern.ch/

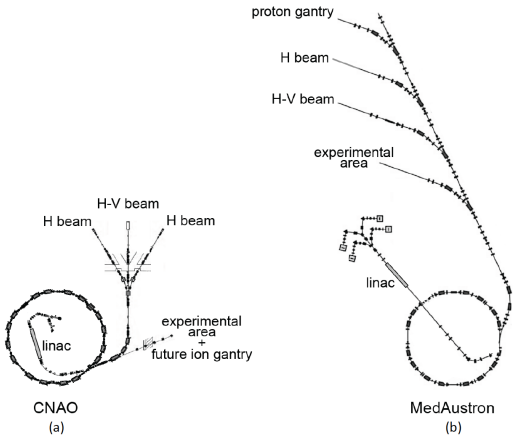

Fig. 49: The same PIMMS synchrotron design—developed during the study conducted at CERN between 1995 and 2000—has been used to construct two very different facilities: (a) CNAO and (b) MedAustron.

3.2.1 Facility layout

The layout of the bunker of the proposed facility, as could be built by SEEIIST, is presented in **Fig. 48**. **Figure 50** shows, in a simplified way, the corresponding baseline layout of the accelerator complex proposed for the new facility and its main components:

(i) three ion sources, which can provide beams for experiments and for treatment, with space to add more ion sources, if needed, for future programmes;

(ii) a linac injector;

(iii) a beamline going from the linac to a dedicated area, which could be extended and used for production of radioisotopes for medical imaging and treatment;

(iv) a medium-energy beam-transport line, which transports the selected ions to the injection point of the synchrotron;

(v) a synchrotron, which accelerates the beam to the required energy for subsequent extraction;

(vi) high-energy beam-transport (HEBT) lines, which transfer the beam either to the experimental area or to the treatment rooms, serving:

- two experimental areas;
- three treatment rooms—featuring (i) a horizontal and a vertical beamline, (ii) a horizontal beamline, and (iii) a superconducting ion gantry;
- an additional straight beamline pointing to a beam dump.

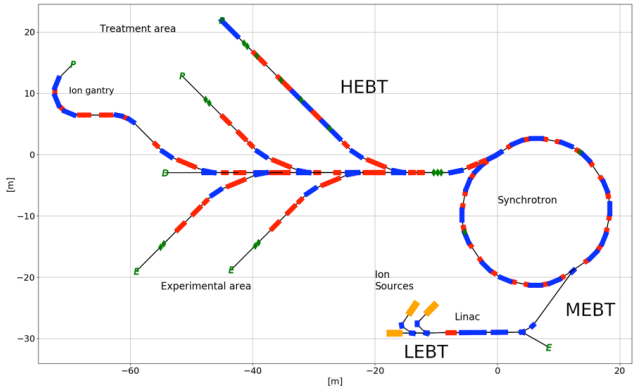

Fig. 50: Baseline layout of the accelerator system of the proposed RI.

3.2.2 Synchrotron specifications

Although the synchrotron shown in **Fig. 50** adopts the same basic layout as those shown in **Fig. 49**, its detailed design and operational features integrate the most advanced technologies. As a result, the proposed RI has the potential to become a unique facility, offering high beam intensities and a flexible beam-time structure. Its specifications are summarised in **Table 5**, where the intensity and energy range for the four intended clinical species are specified: protons, helium, carbon, and oxygen ions. In addition, the synchrotron is designed to accelerate the entire range of ions, up to argon, for research.

Table 5: Main specifications and beam characteristics of the advanced warm synchrotron.

Injection/Acceleration	**Unit**					
Particle after stripping		**p**	**$^{4}He^{2+}$**	**$^{12}C^{6+}$**	**$^{16}O^{8+}$**	**$^{36}Ar^{16+}$ (*)**
Energy	MeV/u	7				
Magnetic rigidity at injection	Tm	0.38	0.76	0.76	0.76	0.86
Extraction energy range (**)	MeV/u	60–250 (1000)	60–250 (430)	100–430	100–430	200–350
Magnetic rigidity at highest energy (for therapy)	Tm	2.42	4.85	6.62	6.62	6.62
Maximum nominal field	T	1.5				
Maximum number of particles per cycle		2.6×10^{11}	8.2×10^{10}	2×10^{10}	1.4×10^{10}	5×10^{9}
Ramp-up rate	Tm/s	< 10				
Ramp-down time of magnets	s	1				
Spill ripple, intensity ratio I_{max}/I_{mean} (average on 1 ms)		< 1.5				
Slow-extraction spill duration with multi-energy operation	s	0.1–60				
FLASH extraction (full intensity)	s	< 0.5				

(*) $^{36}Ar^{16+}$ is for research only, not for treatment.
(**) Energy range within which the beams are compliant with clinical specifications. The figures in parentheses show the higher energies possible for proton radiography and imaging, and He radiography.

The main feature of this synchrotron is its capability to store and accelerate an intensity of up to 2×10^{10} C-ions per cycle—along with equivalent intensities for all the other ions for therapy, as shown in **Table 5**—corresponding to a radiation dose of 2 Gy in a 1-litre target.

These high stored intensities allow the most advanced dose delivery techniques to be used. In particular, the ions can be either "slow extracted" using the multiple-flattops method in a single synchrotron cycle, as explained below, or "fast extracted" to reach unprecedented high dose rates for a potential future FLASH delivery [3] [4], as discussed in Section 2.7.2.2.

Synchrotron-based facilities are ideal for delivering doses by pencil beam, profiting from the relatively small beam cross section and energy spread, e.g. in comparison to cyclotrons. To reach different penetration depths, the beam energy is changed directly in the machine by programming different extraction energies. Presently, in the European facilities, for every new cycle, the beam is accelerated to a different energy flattop and then slow extracted to the patient. **Figure 51** shows a typical accelerator operation: each cycle lasts about 2 s (with the magnets reaching the maximum field each time) and the extraction flattop (in red in **Fig. 51**) can be extended to deliver a spill that varies from

0.1 s to more than 10 s. For this standard delivery method, 10^9 C-ions per cycle are enough, and European facilities are designed to accumulate and store such intensities.

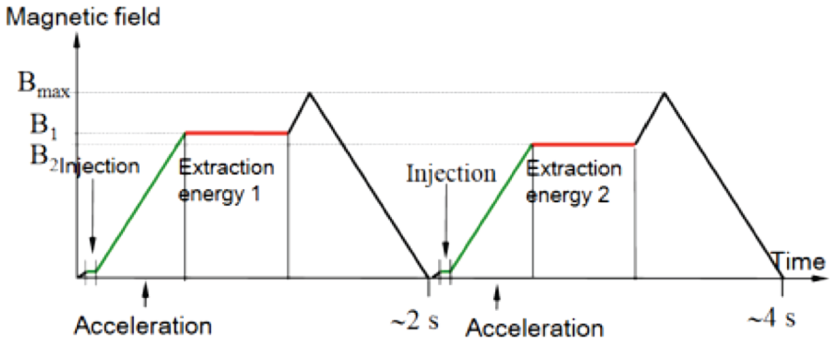

Fig. 51: Typical cycles for a synchrotron for medical use with slow extraction. For every new cycle, the beam is accelerated to a different extraction energy, corresponding to a given value of the magnetic field *B* in the main magnets. (Courtesy of P. Urschutz, MedAustron.)

The NIRS HIMAC centre in Japan developed a multiple energy extraction (MEE) method to maximise the duty cycle and, in particular, to avoid the 1–2 s waiting time between one energy flattop and the next [106]. Its operation cycle is shown in **Fig. 52**, with decreasing energy steps. This opened the way to the extraction of the beam at different energies within the same cycle, so that if enough intensity is stored in the accelerator, the entire tumour target (which normally requires 30 or more equal-energy-level "slices") can be treated without ramping the synchrotron magnetic field up and down.

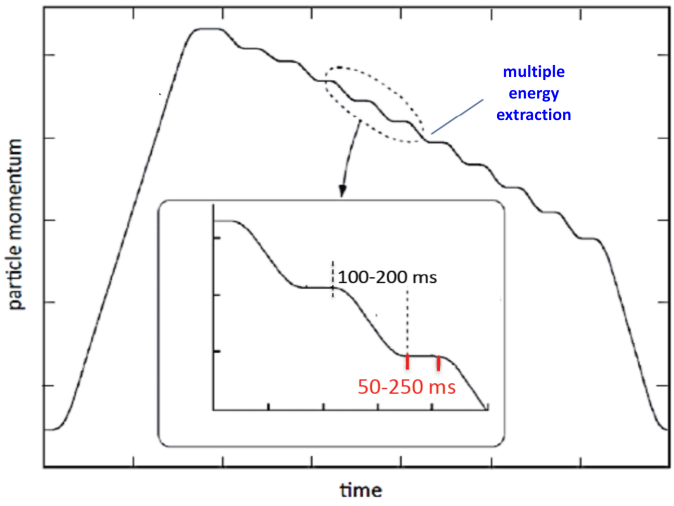

Fig. 52: Multiple-flattop operation cycle at the NIRS HIMAC centre in Japan.

The new synchrotron, by storing up to 2×10^{10} C-ions per cycle—which is more than 20 times that of today's European facilities in a circumference of about 75 m—will achieve the same record performance as the HIMAC centre, which is based on a synchrotron twice the size. This choice implies a redesign of the source and injector linac and further development of an advanced multi-turn injection scheme, which are discussed in Sections 3.2 and 3.3.

Another novelty of the synchrotron is that in addition to the slow extraction, which provides a "standard" low-intensity beam spill lasting from 0.1 s to several tens of seconds, an alternative beam pulse structure will also be available. In particular, the accelerator needs to be able to deliver the entire full-intensity beam in less than 500 ms. The studies reported in [107] assessed its feasibility. This will make it possible to apply new treatment modalities such as FLASH therapy, as discussed in Section 2.7.2.2, and extend the experimental programme.

3.3 The injector linac and sources

All the European carbon ion facilities share, with minimal differences, the same injector linac design developed between GSI and Frankfurt University in the early 2000s, as shown in **Fig. 53** [108] [109].

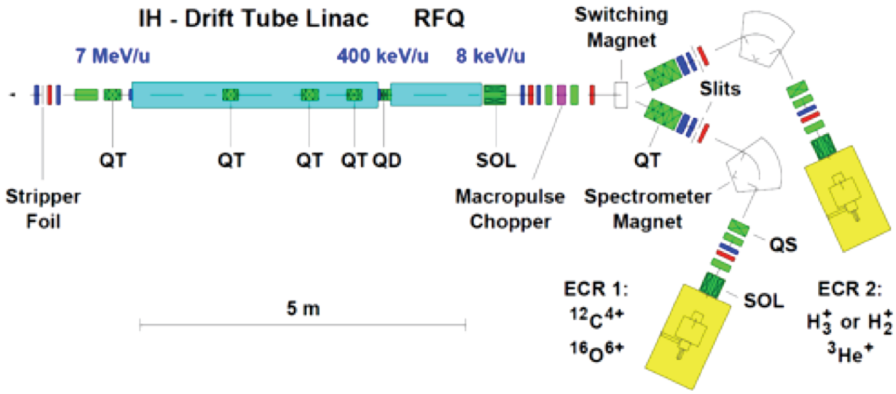

Fig. 53: European "standard" injector linac design. (Courtesy of HIT.)

The injector linac complex is composed of ion sources (two in this case), followed by a low-energy beam-transport line, a 1-m-long, four-rod radio-frequency quadrupole (RFQ) accelerator, a 4-m-long accelerator structure of the interdigital H-mode drift tube linac (IH-DTL) type and finally by a stripping foil. Both accelerating structures operate at 216 MHz and are designed to accelerate C^{4+} ions (q/m = 1/3) to 7 MeV/u, after which the remaining electrons are stripped and the beam is injected into the synchrotron [110]. The Japanese facilities use injectors at a similar frequency, 200 MHz; however, their final energy is only 4 MeV/u [111].

The linac has a low repetition rate and duty cycle (5–10 Hz with a duty cycle of only 0.1%–0.3%) and requires a peak radio-frequency (RF) power of about 1 MW, which is provided by tube-based RF amplifiers. The overall beam transmission from the ion source to the synchrotron is about 50%.

This design is compact and robust, and it can easily be reproduced for any new facility. However, its compactness has the consequence of high RF power requirements, low transmission, and high overall cost, estimated (ion sources excluded) at 22% of the cost of the full accelerator facility in the analysis reported in [1].

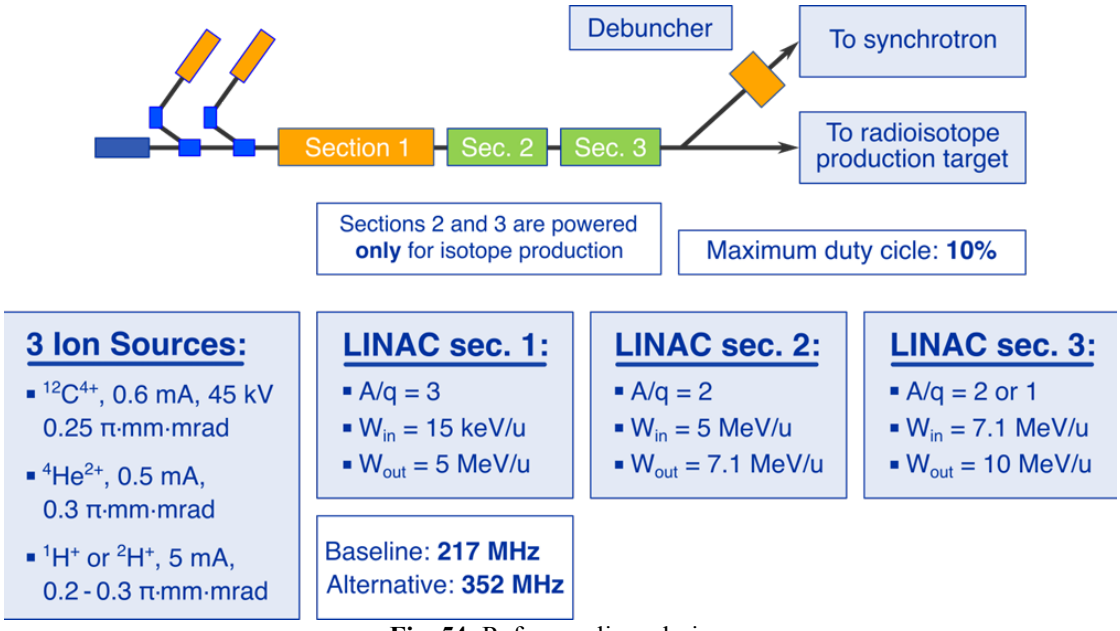

Fig. 54: Reference linac design.

To overcome these limitations, an alternative design has been developed within HITRI*plus* [105], as shown in **Fig. 54**. This is a modular configuration for optimised acceleration of three ion species—$^{12}C^{4+}$, $^{4}He^{2+}$, and protons—up to the energies required for their injection into the synchrotron—5, 7, and 10 MeV/u, respectively. An additional feature of this design is the optional operation at higher duty cycle, up to 10%, for production of radioisotopes for therapy or imaging using beam pulses that are not going to the synchrotron. The accelerating gradients to be used in this configuration will be lower than in the original design of **Fig. 53** to allow for smoother beam optics with lower beam loss and lower RF power requirements, thus reducing the cost of the RF system and paving the way for the use of more flexible and reliable solid-state power sources.

Three ion sources can be alternatively used, the first delivering $^{12}C^{4+}$ ions for the synchrotron, the second supplying $^{4}He^{2+}$ ions that can be injected into the synchrotron or used for radioisotope production, and the third producing protons that can also go to the synchrotron or to the radioisotope production target. The beams are extracted from the three sources at an energy of 15 keV/u, corresponding to a maximum of 90 keV for carbon ions. The required intensities and emittances correspond to what is achievable with the latest generation of commercial or partly commercial ion sources [112] [113].

The accelerator consists of three sections. The first section, based on an RFQ followed by an accelerating structure, is designed to accelerate ions with a charge-to-mass ratio of 1/3 up to 5 MeV/u, the optimum energy for injecting carbon ions into the synchrotron. The second and third sections are optional, in the sense that they are required to exploit the beam pre-accelerated in the first section for production of radioisotopes for imagining and therapy or for injection in the synchrotron at higher energy, and therefore higher intensity, of ions lighter than carbon. When injecting carbon, the second and third linac sections would be kept unpowered and detuned. A stripping section for the carbon beam and a debunching cavity between the linac and the synchrotron complete the injector.

The increase in construction costs required to produce linac accelerating sections capable of operating at higher duty cycle, up to about 10%, is minimal, and this would make a programme of research and therapy with radioisotopes possible in parallel with the normal operation as a synchrotron injector. For this programme, a target or a series of targets can be placed in a room in front of the linac. The output energies of the second and third sections have been defined to allow production of ^{211}At with $^{4}He^{2+}$ ions, with an optimum at 28 MeV total energy, and the production of ^{18}F and ^{11}C using 10 MeV protons for PET. More details on the radioisotope programme are given in Section 3.7.

Two alternative linac configurations have been defined within HITRI*plus* [105], one at 217 MHz, and the other at 176 MHz for the injector and 352 MHz for the rest of the linac. The 217-MHz version makes use of the same four-rod RFQ design used in the European carbon facilities. Since its output energy was fixed at 700 keV/u for optimum injection into the following structure, its length of 2.5 m is considerably greater than the 1.3 m of the RFQ design used in the European facilities. The RFQ is followed by a matching section and by an interdigital IH-DTL consisting of three cavities, transversally matched by intertank quadrupole triplets. The small energy spread of the beam at synchrotron injection is achieved by two debunchers behind IH3. The structure of the IH-DTL linac sections is presented in **Fig. 55** [114]. Beam dynamics for this configuration were analysed and optimised using the LORASR multiparticle code [115]. The main beam parameters are reported in **Table 6**.

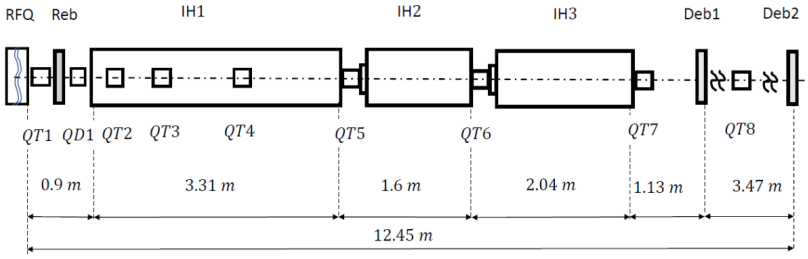

Fig. 55: Scheme of the HITRI*plus* IH-DTL.

Table 6: Main beam parameters of the HITRI*plus* IH-DTL.

Design ions	C^{4+}, α (IH1)	α, H_2^+ (IH2)	α, H_2^+ (IH3)
Operating frequency (MHz)	216.8	216.8	216.8
Input beam energy (A MeV)	0.7	5.0	7.1
Exit beam energy (A MeV)	5.0	7.1	10.0
A/q—design value	3.0, 2.0*	2.0	2.0
Beam pulse length (ms)	0.2, 1.0*	1.0	1.0
Beam repetition rate maximum (Hz)	5, 100*	100	100
Pulse currents (mA)	0.6, 5*	5	5
Input transv. norm. emittances: 95% eff., rms (mm mrad)	0.3	0.33	0.33
Exit transv. norm. emittances: 95% eff., rms (mm mrad)	0.33	0.33	0.33
Input long. norm. emittances: 95% eff., rms (A keV ns)	0.35	0.44	0.44
Exit long. norm. emittances: 95% eff., rms (A keV ns)	0.44	0.44	0.44
Exit energy spread (%) after debunching for 95% of particles	± 0.1	± 0.1	± 0.1
Simulated particle transmission (%)	99.99	99.99	99.99

*: The first number refers to $A/q = 3$ operation.

An alternative design has been developed to exploit possible advantages of a higher frequency [116]. After the ion sources, the beam is accelerated up to the energy of 700 keV/u in an RFQ at 176 MHz, with a length of 2.25 m. From the RFQ, the beam goes into a quasi-Alvarez DTL (QA-DTL) structure at 352 MHz designed for a charge-to-mass ratio of 1/3, followed by two DTL tanks of the Alvarez type at 352 MHz, designed for a charge-to-mass ratio of 1/2. The simulated beam transmission through this configuration is 100%, with transverse emittance growth of the order of 10% for carbon, and lower for lighter ions.

Table 7 presents a comparison of length and RF power for the different accelerating sections and for the two frequency sets, and **Fig. 56** compares the cross sections of the two main accelerating structures, IH1 and QA-DTL.

Table 7: Length and RF power of the linac accelerating sections for two frequency sets.

Structure		217 MHz	176/352 MHz	
RFQ	Length	2.5	2.25	m
	RF power	280	200	kW
IH1 / QA-DTL	Length	3.45	5.1	m
	RF power	350	630	kW
IH2 / DTL1	Length	1.25	1.5	m
	RF power	270	200	kW
IH3 / DTL2 (q/m = 1/2)	Length	1.68	2.3	m
	RF power	440	320	kW
TOTAL	Length	8.9	11.1	m
	RF power	1340	1350	kW

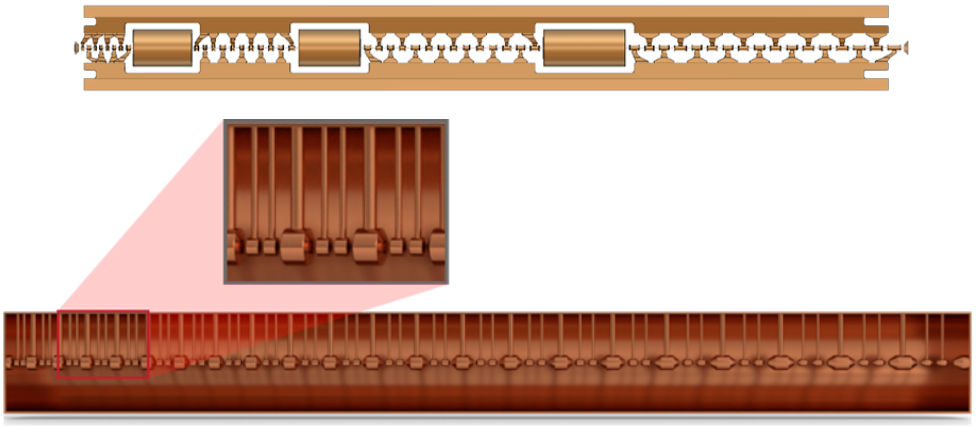

Fig. 56: Transverse cuts of the structures of IH1 (top) and QA-DTL (bottom) for C^{4+}.

The total required RF power is approximately the same for both linac configurations, with the 217 MHz version being 2 m shorter. While a more detailed analysis, including the RF sources, would be needed for an accurate cost comparison of the two options, it is clear that the IH solution has the advantage of being based on a proven design already in use in the European carbon therapy facilities.

3.4 The synchrotron

An advanced version of the synchrotron described in the initial proposal for the SEEIIST facility [1], featuring higher beam intensity and improved injection and extraction, has been developed. While its lattice is based on the well-known warm-magnet technology of PIMMS [6] [2], its design parameters and novel features are intended to give it a lead among other ion therapy facilities in the world, with major innovative developments in the dose delivery to the patient due to the large stored current and flexible extraction possibilities.

3.4.1 Synchrotron layout

The layout of the accelerator system is based on the 75-m-circumference PIMMS synchrotron [6] [2]. The ions are produced in one of the three sources and pre-accelerated in the linac up to the 5 MeV/u injection energy. After the energy for treatment is reached (see **Table 5**), the beam is extracted to the HEBT line and sent to the treatment or to the experimental rooms.

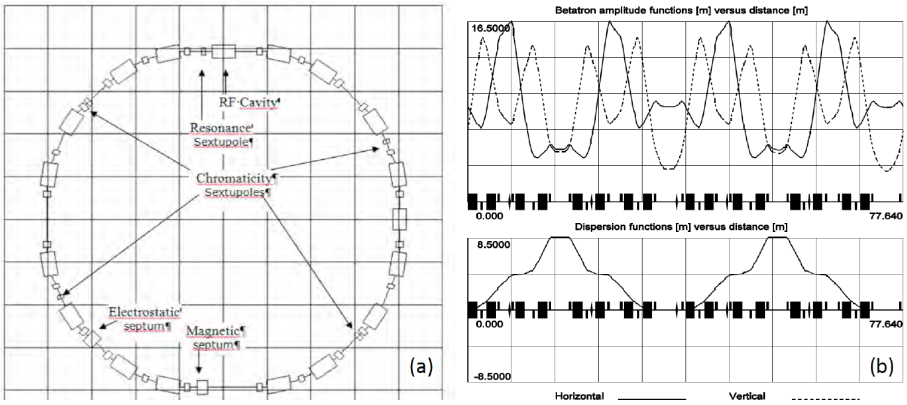

Fig. 57: (a) Layout of the baseline synchrotron with warm magnets. (b) Optical functions: betatron functions (top) and dispersion (bottom) [2].

The synchrotron comprises two symmetric, achromatic arcs joined by two dispersion-free sections, as shown in **Fig. 57**. It has 16 main dipoles. The 24 quadrupoles are grouped into three families that allow enough flexibility to match all the needed tunes while conserving the dispersion-free regions. The four lattice sextupoles allow independent adjustment of the horizontal and vertical chromaticity; these magnets are individually powered to allow some additional flexibility in setting up the extraction.

For the orbit correction, there are eight vertical beam position monitors and the same number of associated vertical correctors. Additionally, there are ten horizontal monitors with associated correctors.

One of the two dispersion-free sections contains the magnetic extraction septum. The other contains the resonance-driving sextupoles and the injection electrostatic septum. The orbit bumps are created with two horizontal kickers each, positioned at a proper phase advance.

The RF system consists of a FINEMET®-loaded wideband cavity powered by solid-state amplifiers connected to a digital low-level RF system, as installed for MedAustron [117]. These are state-of-the-art cavities for low-energy accelerators [118], and they easily allow operation in multi-harmonic mode [119]. The technology has been successfully tested and deployed for the upgrade of the CERN PS booster [120], with the double-harmonic mode used at low energy to increase the bunch length and reduce space charge. Unlike the PIMMS design, the RF cavity is located in a non-zero-dispersion section; this is a choice common to other accelerators, such as the CERN PS booster, and in general, in rings where dispersion-free sections are not available.

A multi-turn (MT) injection allows the accumulation of the beam from the linac to reach the required intensity. Extraction is performed by RF-knock out (RF-KO) at multiple energies (on multiple flattops) during the same accelerator cycle, as shown in **Fig. 52**. For the novel FLASH dose delivery modality, a "fast" slow-extraction technique is being developed.

3.4.2 Multi-turn injection in the synchrotron

The main challenge for the proposed new facility is the increase of the beam intensity with respect to existing European facilities—for C-ions up to 2×10^{10} ions/cycle. This requires increasing the ion source intensity, a better linac transmission (as described in Section 3.2), and the optimisation of the MT injection process.

Figure 58 shows the results of simulations of the MT injection process [121] with 2×10^{10} carbon ions accumulated in the accelerator. The kicker strength function, which provides an orbit bump varying with time, has been optimised to maximise the intensity and minimise the emittance of the circulating beam after a 30-turn injection. Increasing the number of injected turns further would excessively dilute the emittance. **Table 8** summarises the optimal set of injection parameters and the resulting beam characteristics.

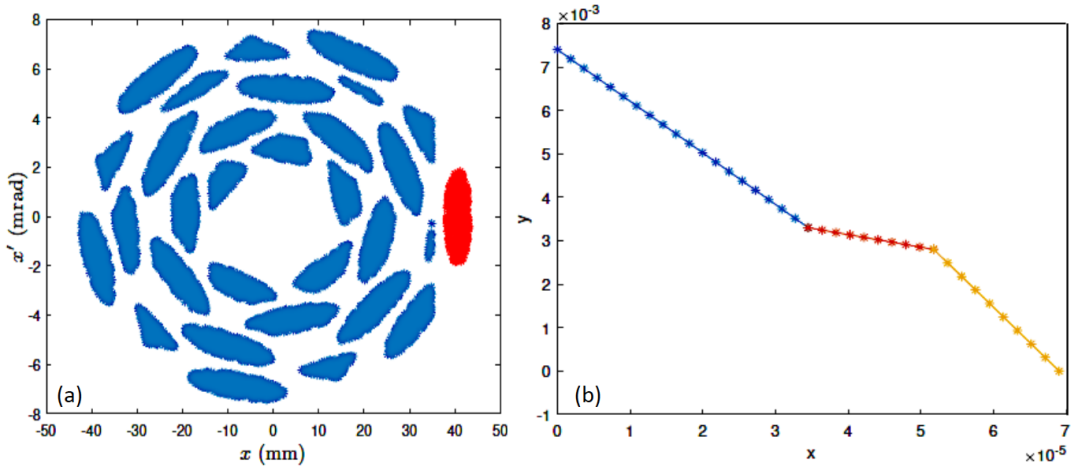

Fig. 58: (a) Phase space of the circulating beam after 30 turns, in blue. The injected beam from the linac is in red. (b) Kicker strength (rad) as a function of time (s), to produce a maximum orbit bump of 44.7 mm at the injection septum location.

Table 8: Optimised injection parameters and circulating beam characteristics.

Number of injected turns	30

Injected beam emittance	0.7 μm
Horizontal tune	1.82
Ratio of the β-function of the injected beam to the circulating beam	0.5
Effective number of stored turns (injection efficiency %)	21 (70%)
Resulting circulating rms emittance	5.6 μm

The effective number of injected turns is 21, and the current needed from the electron cyclotron resonance (ECR) source at the injection point is 350 μA, within a 0.7-μm normalised emittance. These values include the transmission efficiency of the injector linac and are considered feasible with new-generation sources, as discussed in Section 3.2.

The beam characteristics for one of the studied options are given below, while further optimisations have been reported in international accelerator conferences such as IPAC and other specialised conferences [122]. The final circulating beam emittance is 5.6 μm (rms), much larger than the 1-μm normalised emittance (rms) expected for a 10^9-ion beam in the original PIMMS design. Similar optimised simulations showed that to inject 2×10^{10} C-ions and keep the emittance below 1 μm, the number of effective turns must be 7.8, which would require—considering a realistic linac transmission—a current from the source of about 1 mA, which is beyond the reach of present ion sources. The stored beam will therefore be flat, with a normalised horizontal emittance of 5.6 μm and a vertical emittance of 1 μm. The value for the vertical emittance is required for the gantry operation and is similar to the value for the PIMMS design. Careful studies and machine-development experiments need to be conducted on existing synchrotrons to prove that such a flat beam can be stored and accelerated without emittance exchange.

3.4.3 Resonant extraction from the synchrotron

In the slow-extraction process, the beam is extracted over thousands to millions of turns, with a typical spill duration between 0.1 and 10 s, as discussed in Section 3.4.1.

The beam is brought close to a third-order resonance [6], which is excited with one or more dedicated sextupoles, and the extraction is driven by bringing the particles into an unstable state in a controlled way. **Figure 59** shows the so-called "Steinbach diagram" (named after one of the pioneers of slow extraction), which illustrates the mechanisms by representing the beam particles in the amplitude versus tune space. The unstable region in the diagram is represented by the upside-down triangle centred at the resonant tune. The first extraction method, which is used in the medical synchrotrons derived from the PIMMS design [6] [2], is the so called "betatron core" [123]: a set of coils that change the beam energy and tune via inductance, bringing the particles into the unstable region (the beam is moving rightward in the diagram). The second method, RF-KO, employs a transverse exciter that increases the oscillation amplitude of the particles until they become unstable (the particles are moving upwards). The baseline for the new facility will be the RF-KO extraction, which has the advantages of being able to produce spills of shorter duration (down to about 100 ms) and allowing for better control of the extracted beam current. This latter feature is critical for treatment plans that use gating due to respiration. In addition, the RF-KO extraction is conducted without debunching the circulating beams, which allows for multiple energy extraction, which is planned to be a standard mode of operation of the new facility (**Fig. 52**). It is, however, necessary to ensure that the transverse exciter has enough power to reach a short spill duration. A new type of exciter is being designed within the I.FAST [104] EU innovation pilot project for accelerator R&D, and this will become available for implementation in any new facility.

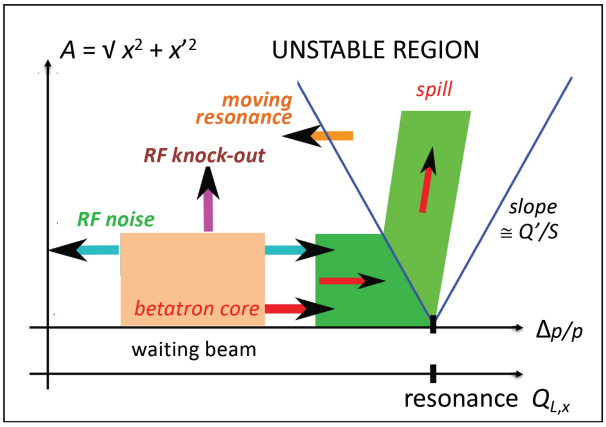

Fig. 59: Steinbach diagram illustrating the driving mechanisms of resonant slow extraction. (Adapted from [123].)

An important aspect of slow-extraction methods is the temporal structure of the spill. The problems with the temporal structure of the spill arise from the power converters, which regulate the current in the magnets with various frequencies. These frequencies are transmitted to the beam and are finally reflected in beam-intensity fluctuations at millisecond and shorter time scales. There are numerous techniques to ensure a sufficiently good spill structure. The most popular of these are fast feedback with air-core quadrupoles [124] or transverse RF kickers, injection of specific frequencies into the power converter regulation loop [125], or the use of feedback on the delivered dose by rescanning the tumour. Spill control and quality are active areas of R&D.

The production of a FLASH-type beam will require a spill that is 100–1000 times more intense than the typical slow-extracted beam, with a maximum duration of 500 ms, so that dose rates up to 50 Gy/s can be achieved. The design of the new facility should remain flexible and allow this new modality, for which other approaches are being studied.

Another way to obtain the required intensities would be through the use of second-order resonance, which is stronger than the third-order resonance and leads to faster extraction of particles [107]. This method is used in the oldest functional proton therapy facility, in Loma Linda University Medical Center (CA, USA). Simulations and tests must be conducted to assess the particle extraction rate. Moreover, the ring could optionally be equipped with a fast-extraction system to extract the entire beam in less than one revolution period, i.e. less than 0.3 μs, for research.

The development of optimal dose delivery and control methods in the FLASH mode is an interesting topic to be included in the scientific programmes related to the accelerator technology of any new RI.

3.4.4 Required R&D and risk comparison

Medical synchrotrons based on normal conducting magnets are well understood, and the risks associated with this technology are low. However, the advanced warm synchrotron proposed for a new facility requires developments to reach record intensities and flexible beam delivery by improving:

(i) the source, to increase the ion intensity in the same beam emittance;

(ii) the linac, to improve transmission;

(iii) the multiturn injection process;

(iv) the extraction system, to ensure flexibility (e.g. high dose rates, MEE).

The increase in the ion source current is considered to pose relatively low risk, and suitable designs are already close to market. Improving the linac transmission might be more critical; however, new linac designs and more modern beam optics simulation tools have strong potential to lead to higher transmission. The R&D activities examining multiturn injection mainly involve simulations and tests in operative facilities.

Altogether, the level of R&D required to build an advanced warm-magnet synchrotron configuration at increased beam intensity is low. The only component requiring both simulation studies and prototyping is the linac, with the construction of another copy of the standard injector shown in **Fig. 53** being a straightforward mitigation in case of problems related to this R&D.

3.4.5 Alternatives to the baseline design

A new RI for research and therapy with ion beams must be based on a reliable accelerator design that can be built in a reasonable amount of time, without the need for additional accelerator R&D, and with minimal risks for the accelerator operation, its priority being delivering beam to the clinical and experimental users. This is why the baseline synchrotron design presented in this document is based on an advanced version of the PIMMS synchrotron developed at CERN during 1996–2000 and already implemented in the CNAO and MedAustron carbon therapy centres [6]. Because its feasibility and reliability have already been proven, its main components can be rapidly constructed in industry.

Since the development of PIMMS, however, accelerator science and technology have made impressive progress. Hence, the NIMMS initiative, in close collaboration with a network of partner laboratories and universities, is investigating and developing technologies that could be used in an advanced ion therapy and research facility, with the goals of reducing the cost and dimensions of the facility, and of providing higher performance and operational flexibility.

Some components under development in NIMMS are already part of the baseline design presented in this report. In this section, three synchrotron layouts under study within NIMMS or its collaborations are presented. They represent valuable alternatives to the baseline PIMMS layout but require some additional analysis to come to a complete technical design that could be the basis for a new construction. These are: (a) a synchrotron with fewer magnets; (b) a superconducting synchrotron with fewer magnets and smaller dimensions; and (c) a smaller synchrotron limited to lighter helium ions.

3.4.5.1 Alternative synchrotron lattices

European ion therapy accelerators share a similar lattice structure based on the FODO cell sequence (where F stands for focusing, D for defocusing, and O for drift), with variations in the number of periods and magnets along the ring. The number of magnets ranges between six for HIT and 16 for the PIMMS designs: while a small number of magnets simplifies operation and reduces cost, a larger number of magnets provides flexibility in the tuning of the machine. Two lines of development have therefore been identified to define a new optimised alternative lattice for the synchrotron of a new facility, particularly with the requirements and constraints of the SEEIIST facility in mind.

The first direction being explored is a revision of the standard FODO lattice with a possible configuration having fewer magnets than PIMMS and the addition of dispersion-free sections, which is a desired requirement to simplify injection, acceleration, and extraction dynamics. To achieve two long straight sections with zero dispersion, the solution chosen for PIMMS was to modify the FODO lattice and introduce a third quadrupole family, making it a FODOF lattice.

Another alternative, proposed by the University of Melbourne [126], is to use a different lattice based on a double-bend achromat (DBA) cell. **Figure 60** shows a schematic of the layout of an optimised DBA design with 12 dipoles and a circumference of only 55 m. The choice is mainly driven by the preference for dispersion-free drift sections. In comparison with a compact PIMMS type FODOF lattice, the DBA requires fewer quadrupole magnets.

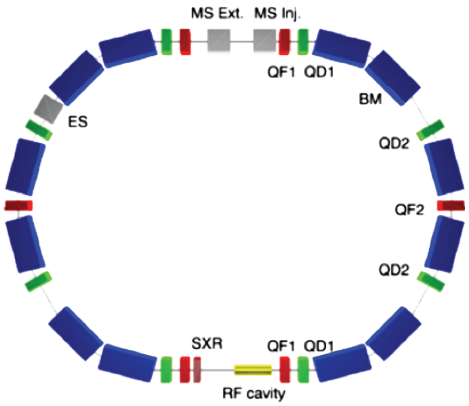

Fig. 60: Layout of University of Melbourne DBA synchrotron design for 430 MeV/u carbon ions.

3.4.5.2 New superconducting design

Superconductivity is the main avenue towards reducing synchrotron dimensions, thanks to the much higher magnetic fields that can be achieved compared to conventional warm magnets; additionally, a layout based on superconducting magnets is expected to have lower construction and operation costs related to the reduction in accelerator size and in electrical power consumption. The reliability of this technology has been demonstrated by the successful operation of the LHC at CERN, which is equipped with as many as 1400 very long superconducting (SC) magnets. The simple operation and reduced maintenance of modern SC systems makes them a viable choice for the accelerator of a new facility.

The design of a compact SC synchrotron has been developed by the TERA Foundation [127], based on 90° magnets of the canted cosine theta (CCT) type at 3.5-T field, along with the design of a gantry based on the same type of magnet at 4 T, as discussed in Section 3.6. For this specific application, the CCT magnets, including nested alternating-gradient quadrupoles (AG-CCT), are based on a development pursued at Lawrence Berkeley National Laboratory for proton therapy gantries [128]. Examples of CCT magnets are shown in **Fig. 61**.

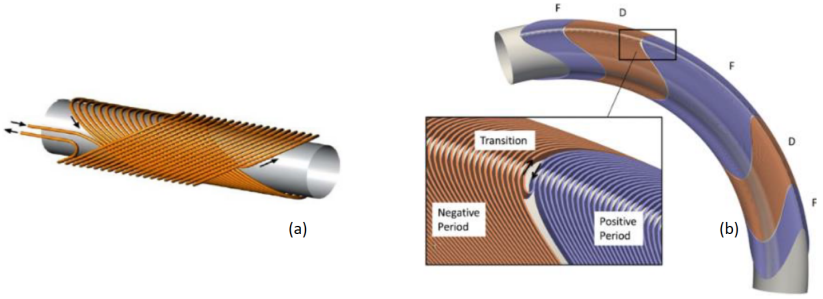

Fig. 61: Examples of CCT magnets. (a) Pure dipole: the two vertical magnetic fields produced by the two coils cancel along the tube axis and add in the transverse direction. (b) AG-CCT: windings needed to obtain sections that are alternatively focusing (F) and defocusing (D).

A wide collaboration has been formed, grouping the main European laboratories and industries in the field of SC magnets, with the goal of developing a specific magnet design to be used in ion therapy synchrotrons. The CCT will be closely analysed and compared with other suitable designs, to finally define the geometry of a prototype magnet to be built and tested. Starting from a conventional NbTi conductor, the programme will consider the alternative options of using Nb_3Sn or advanced high-temperature superconductivity (HTS). Both the design and the prototyping of the magnet are supported within the EU programmes I.FAST [104] and HITRI*plus* [105], which will result in the construction of several prototype magnets by 2025. The preliminary target parameters for the reference synchrotron magnet design and for the prototype to be constructed at the end of the design phase are given in **Table 9** [129] [130].

Table 9: Design parameters for the synchrotron magnet and for the prototype to be developed within the HITRI*plus* and I.FAST Horizon EU-funded projects.

Parameter	Synchrotron magnet	Prototype magnet
$B\rho$ Tm	6.6	6.6
B_0 dipole (T)	3.0	4–5
Coil apert. (mm)	70–90	60 (90)
Curvature radius (m)	2.2	2.2, ∞
Ramp rate (T/s)	1	0.15–1
Field quality (10^{-4})	1–2	10–20
Deflecting angle	90–	0–45°
Alternating gradient	Yes (triplet)	N/A
Quad gradient (T/m)	40	40
B_{quad} peak (T)	1.54–1.98	1.2
B_{peak} coil (T)	5.0–6.0	5.6–7.0
Operating current (kA)	< 6	< 5
Type of superconductor	NbTi (Nb_3Sn)	NbTi (curved), HTS (straight)
Operating temperature (K)	5 (8)	5 (20)

The basic parameters of a reference SC synchrotron design are presented in **Table 10**. The lattice parameters may still be improved with optimisation that can only take place once the magnet R&D programme can provide indications on the range of magnet parameters that can be reached.

Table 10: Main parameters of the superconducting synchrotron.

Circumference	27 m
Injection energy	7 MeV/u
Extraction energy	100 → 430 MeV/u
Straight section 1	3.0 m
Straight section 2	3.6 m
AG-CCT Max. bending field	3.5 T
AG-CCT Bending radius	1.89 m
AG-CCT Magnetic bending angle	90°

3.4.5.3 Helium ion design

Recent years have seen an increased interest in the use of helium ions for radiation therapy for cancer [68]. To exploit the potential of helium therapy, the design of a compact synchrotron optimised for acceleration of proton and helium beams has been investigated in the framework of NIMMS at CERN [122].

The accelerator required for helium is considerably smaller than a standard carbon ion synchrotron. The synchrotron is based on a new magnet design, benefits from a novel injector linac, and can provide both slow and fast extraction [131] for conventional and FLASH therapy. The production of mini-beams and operation with multiple ions for imaging and treatment are also considered.

For the lattice, a triangular shape was chosen for the sake of compactness and to ease magnet manufacturing, following a similar approach to that for the design of a compact medical synchrotron

for carbon ions [132] with superconducting magnets. A sketch of the synchrotron design and its preliminary optics, which are being optimised to properly accommodate the injection and extraction hardware, is shown in **Fig. 62**.

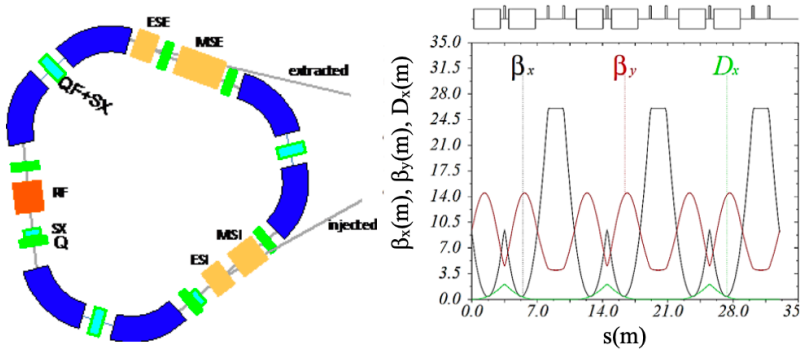

Fig. 62: Sketch of the lattice layout and a preliminary optics, generated with MAD-X [133].

The lattice is made up of three bending sections, each consisting of two 60° magnets with a strong quadrupole in between, to have zero dispersion in the three straight sections. The straight section hosts the injection and extraction hardware, as well as the RF cavities.

Because of the maximum beam rigidity of 4.5 Tm and the choice of the maximum field of 1.65 T, the resulting bending radius is 2.7 m. The straight sections are about 5 m long to accommodate the required hardware, leading to a total circumference length of about 33 m.

The 60° magnets have a small defocusing gradient to reduce the vertical beta functions in the bends, and the quadrupoles in between also carry sextupolar coils to control chromaticity. Two additional quadrupoles are needed in each straight section for the optics and working point adjustment, as well as sextupole(s) at the correct phase advance to excite the third-order resonance for slow extraction, and orbit correctors, which will also generate the extraction bump. These functions will be combined as much as possible in a single corrector magnet carrying multiple components. In general, the synchrotron magnets were designed for compactness and simplicity, limiting power consumption, and keeping the option open for a later upgrade to higher energies and heavier ions [122].

Figure 63 shows a preliminary layout of the synchrotron ring, with the total surface are covered by the complex being of the order of only 1600 m^2. This compact synchrotron could be the central element of a facility devoted to a parallel programme of cancer research and treatment with proton and helium beams, to both treat patients and contribute to the assessment of helium beams as a new tool to fight cancer [122].

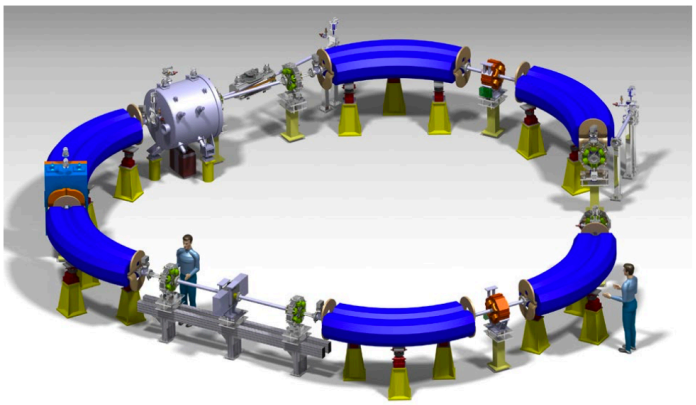

Fig. 63: View of the 33-m-circumference synchrotron.

3.5 Beam transfer to the treatment and experimental rooms

3.5.1 Specifications

In the basic layout of **Fig. 50**, the HEBT line transports the beam from the synchrotron to three therapy rooms and two experimental rooms, with expected losses below 5%.

The optics system allows adjustable sizes of 4−10 mm full width at half maximum (FWHM) at the isocentre for the C-ions, as shown in **Table 11**. The experimental beamline has a double isocentre: one for a conventional field size [(20 × 20) cm^2], and the other, after a longer drift, with an enlarged field size [(40 × 40) cm^2].

Table 11: Specifications of the HEBT line.

Adjustable beam width (FWHM) at isocentre for protons and helium ions at max energy (mm)	7–15
Adjustable beam width (FWHM) at isocentre for C-ions at max energy (mm)	4–10
Transverse field for scanning in the fixed bean treatment rooms (cm^2)	25 × 25
Transverse fields for scanning in the experimental hall (two positions) (cm^2)	20 × 20 40 × 40
Maximum transverse scanning speed (m/s)	20
Distance from scanner magnets to isocentre in the horizontal and vertical beamlines (m)	7.4
Momentum spread (95%), $\Delta p/p$ (%)	< 0.1
Dispersion at isocentre, D (m)	< 0.1
Dispersion gradient at isocentre, dD/ds	< 0.1

The common part of the HEBT line contains a beam-chopping system, which prevents any beam particles entering the beamline within 200 μs after an interlock signal. This is used in combination with switching off the RF-KO exciter to remove unwanted beam in the gaps during spill pauses.

3.5.2 Design of the transfer lines

The HEBT lines connect the synchrotron extraction region to the three irradiation rooms and the two experimental stations.

The two experimental beamlines end in the same large and configurable room with two separate entrances. The spacious experimental hall can easily be divided into two or more experimental caves according to the needs of the experiments. The large size of the caves will facilitate time-of-flight measurements, which are often very important for experiments. For the research programme, the two main lines of the experimental hall will be equipped with scanning systems, at least one of which will feature exactly the same scanning magnets and nozzle as the horizontal medical beamline for patient treatment (TR2).

Therapy rooms should provide enough space around the patient's bed to allow for comfortable access to the patient and for installation of additional diagnostic equipment such as MRI and CT scanners. In existing facilities, this space extends between 3.5 m (HIT) and 5 m (MedAustron) from the isocentre. In the proposed design for the new facility, almost 5 m of space is foreseen.

It is anticipated that 3-m-thick concrete walls will separate the rooms for radiation shielding, due to the potential for irradiating at intensities up to ten times higher than existing facilities. An indirect consequence of the thick shielding and the large area required around the patient is the availability of generous space for optimal design of the beamline optics.

The principal considerations regarding the design of the beam optics are as follows:

(i) The dispersion and dispersion derivative of the beam extracted from the synchrotron are matched to zero ($D_H = 0$, $D'_H = 0$) after the extraction section to allow for dispersion-free measurements and to limit the beam envelope in the common section of the transfer lines. The segment in which the dispersion is matched to zero is marked as DIS in **Fig. 50**.

(ii) A fast chopper, made using four steering magnets and an internal dump, allowing for fast spill abort, is installed in the common part of the HEBT lines.

(iii) The beam is bent from the main beamline towards the treatment rooms and experimental stations at a 45° angle using two 22.5° dipoles with a quadrupole doublet in between. The bending sections (marked BEN in **Fig. 50**) are achromatic. In addition, the dipoles have the same bending angle as those used in the synchrotron.

(iv) The horizontal and vertical sections (HSC and VSC in **Fig. 50**) adjust the final beam size and contain fast-scanning magnets for tumour painting. The 3-m-long drift space corresponds to where the beamline will traverse the shielding wall.

The main clinical parameters controlled by the beamline optics are the beam size in both planes, which translates into constraints on the Twiss parameters: β_H and β_V. The dispersion $D_{H,V}$ and dispersion derivative $D'_{H,V}$ need to be zero, which corresponds to no dependence on beam energy; additionally, $\alpha_H = \alpha_V = 0$, which reflects the condition of zero divergence at the isocentre.

The resonant slow-extraction process generates, in the horizontal phase space, a particular beam shape known as a “bar of charge”. Due to this effect, the beam size on the patient can be regulated in various ways.

The approach implemented at HIT aims to minimise the surface area, because the facility has been designed with strong restrictions on its footprint. As a result, the shortest beamline contains only six quadrupoles. In theory, these provide the six degrees of freedom necessary to set the six optical parameters on the patient. However, in practice, some settings are very difficult, and the beam envelope is large (with the beta function as large as 450 m), requiring very-large-aperture dipoles to avoid extensive beam losses.

A different approach has been developed by the PIMMS collaboration and applied in MedAustron. In this approach, the vertical beam size is regulated by the vertical beta function β_V, while the horizontal size is regulated by the rotation of the bar of charge in the phase space, i.e. by the phase advance between the extraction septum and the patient. This requires additional degrees of freedom. The PIMMS solution is mathematically elegant; however, it requires numerous additional quadrupoles and significantly longer beamlines.

Because the footprint of a new facility is not a priori strongly constrained, the approach to HEBT optics is a middle path, similar to that used in CNAO. The dispersion is matched to zero after extraction from the synchrotron and after each bending section; however, the beam size on the patient is adjusted with the use of the beta functions $\beta_{H,V}$ and not of the phase advance. The length and complexity of the beamlines is smaller than in MedAustron, while the number of quadrupoles is larger than in HIT, allowing for a small beam envelope and significant flexibility. Optimisation to further reduce the number of independently powered quadrupoles is still possible.

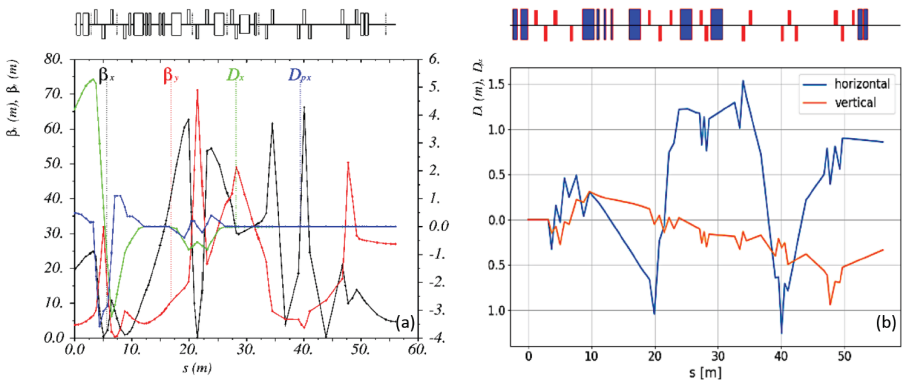

Fig. 64: (a) Possible optics for the horizontal transfer line to the first treatment room (TR1H). (b) Trajectory deviation due to random errors of the quadrupole alignment.

The additional peculiarity of the proposed HEBT line layout is the large separation between the experimental and treatment rooms and the location of a horizontal–vertical (H/V) treatment room (TR1) as the first room, which gives more flexibility to this beamline setting and leads to better shielding between the treatment rooms.

One of the possible solutions to the beam optics of the first horizontal line is shown in **Fig. 64**. The vertical beta function in the dipoles is below 50 m, allowing for a small vertical aperture. Analysis of the trajectory deviation due to the quadrupole alignment errors allows estimation of the number and position of the steering magnets and beam position measuring instruments.

The current layout of the HEBT beamlines contains:

(i) 15 bending magnets (six switching);

(ii) 50 quadrupoles, each 0.45 m long;

(iii) ten fast-scanning magnets;

(iv) ten steering magnets;

(v) 16 multi-wire proportional chambers for beam size and position measurement—some of these systems can be replaced by cheaper scintillating screens;

(vi) the superconducting gantry.

All these elements are costed in Section 3.11.

Beam position monitors (BPMs) and beam loss monitors are also expected to be installed for the fast-extracted high-intensity beam, as well as beam current monitors (BCMs). BPMs and BCMs do not work for the slow-extracted beams, but they are extremely useful to precisely monitor, and therefore control, the beam characteristics. Ionisation profile monitors might also be employed for continuous monitoring of the beam quality, although they are not essential. For a review of beam instrumentation solutions used in existing facilities see Refs. [134] [135].

3.6 The rotating C-ion gantry

3.6.1 Hadron therapy gantries

Gantries are used to deliver the dose to the patient from several angles and thus spare OARs. They consist of a beamline supported by a mechanical structure that rotates. Gantries are heavy and bulky elements in a hadron therapy facility due to the size and weight of the magnets, which depend on the beam rigidity, and the large supporting structure, which has to guarantee the mechanical rigidity and precision of the system. Only three C-ion gantries exist today, compared to more than 100 proton gantries (the beam rigidity for carbon ions is a factor of three higher than for protons).

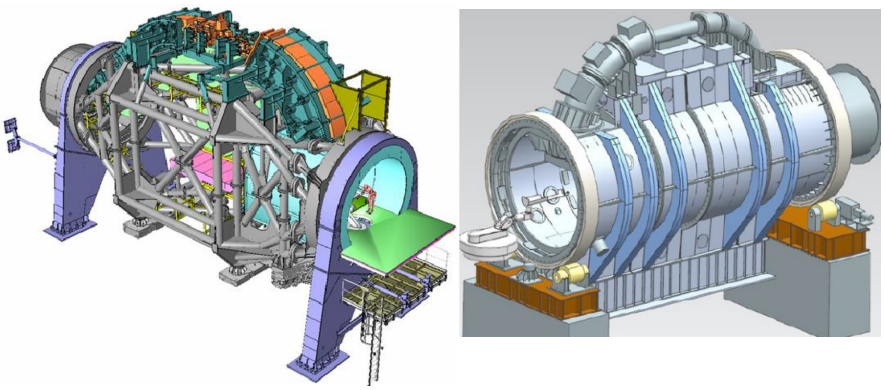

Fig. 65: Left: the 430-MeV/u HIT C-ion gantry has a 6.5-m external radius, is 25 m long, and weighs 600 tons [136]. Right: the 430-MeV/u NIRS C-ion gantry, which has SC magnets of 2.9 T, has a 6-m external radius, is 15 m long, and weighs about 300 tons [137].

The left-hand panel of **Fig. 65** shows the first C-ion gantry ever built, designed by GSI for HIT. It weighs 600 tons and consumes about 400 kW at maximum field [138]. The right-hand panel of **Fig. 65** shows the Japanese C-ion gantry, which was designed and built by a collaboration among NIRS, KEK, and Toshiba. It is smaller in size and weighs "only" 300 tons, thanks to the use of SC magnets. The third one, in Gunma University, is similar to the NIRS one but slightly smaller.

In addition to the magnet technology, i.e. using SC magnets to reduce the size and weight of the gantry, another important choice is the position of the scanning magnets, which allow transverse painting of the tumour. In both the HIT and NIRS gantries, these are *upstream* of the last bending magnet. The advantage is a very large source-to-axis distance (SAD) and ideally parallel beam scanning; however, this requires large-aperture magnets, which are bulky and challenging.

In the most recent design by NIRS, as shown in **Fig. 66** superimposed on the original design, the scanning magnets are *downstream* of the last bending magnet, which has a small aperture. As a consequence, the SADs are relatively small—about 2.5 m—but the gantry, which is based on 90° bending magnets, is smaller both in terms of height and length [139].

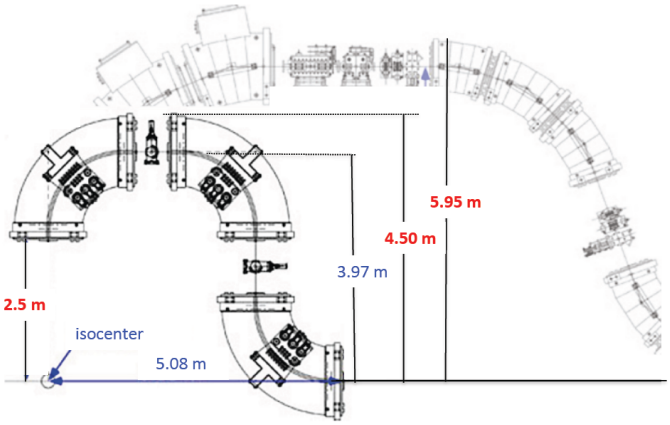

Fig. 66: Comparison of the compact design by NIRS, having a 4.5-m external radius, with their first design (**Fig. 65** right). The two gantries have 5-T and 2.9-T SC bending magnets, respectively [139].

The external diameter of an ion gantry is mainly determined by the magnetic field in the bending magnets and by the choice between either upstream or downstream scanning magnets. To keep the cost, weight, and complexity of the magnet low, the large majority of designs currently use downstream scanning magnets, transferring the challenges in the design to the latter elements.

3.6.2 Next-generation European gantry design

3.6.2.1 SIGRUM design

Seeking to develop an innovative, compact, and light C-ion gantry for new and/or running facilities, in 2018, the TERA Foundation designed a gantry [127] based on the SC magnets of the AG-CCT type similar to that used for the compact synchrotron (see Section 3.4) and characterised by unconventional mechanics. **Figure 67** presents a schematic layout and 3D implementation of this design. This design, known as the superconducting ion gantry with Riboni's unconventional mechanics (SIGRUM), has led to several variants [140].

The principles driving the SIGRUM design are simplification and compactness. An important simplification involves attaching the gantry to the wall of the treatment room and allowing a rotation of 220°. An electric motor equipped with a high-torque planetary gearset precisely moves the gantry to any angular position without the need for a counterweight.

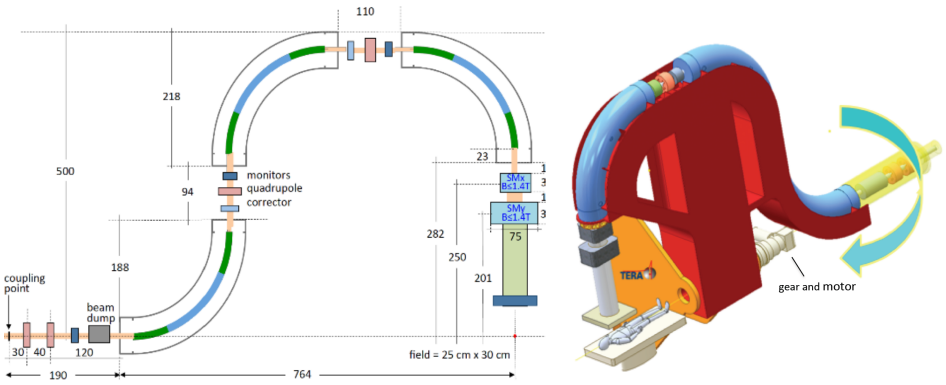

Fig. 67: SIGRUM gantry layout (left) and 3D implementation (right). As indicated by the green and blue colours, three quadrupoles are superimposed to the three 90° bending magnets ("nested quadrupoles"). The magnets have a bending radius of 1.65 m and reach a magnetic field of 4 T. The external radius is 5 m.

The choice to use such a motor in itself reduces the weight of (and the space occupied by) the gantry by at least a factor of two. However, this solution is feasible as long as the torque is "small enough"; thus, the design of the first version [127], presented in **Fig. 67**, focused on the reduction of the weight and of the external radius of the structure:

(i) the scanning magnets are downstream of the last dipole, which allows its aperture to be reduced;

(ii) the SADs in the horizontal and vertical planes are 2.1 and 2.5 m, respectively;

(iii) the magnets have a maximum field of 4 T, corresponding to a bending radius of 1.65 m;

(iv) the choice of the AG-CCT magnets allows for a substantial reduction of the beam size thanks to the presence of nested alternating focusing and defocusing components in the 90° dipoles. This, in turn, reduces the magnet's aperture, as well as their total cross section and weight.

Thanks to these choices, the external radius is 5.0 m, and the magnet aperture small enough (60-mm diameter) to achieve a compact design. The optics are achromatic. The matching is independent of the gantry rotation angle, point-to-point, with a magnification factor of 1:1, and guarantees the required beam sizes at the isocentre, along with a momentum acceptance of 1%.

The mechanical support structure for the gantry has been designed to maintain the deformations below 1 mm when the torque is maximum (the gantry beamline is horizontal). The rotating part of the gantry (magnets and mechanical structure) weighs 35 tons, and, together with the support fixed to the wall, the total weight comes to only 50 tons.

Because of the challenges involved in making 4-T, strongly curved, 90° superconducting magnets with nested gradients, in 2020, a collaboration between TERA and CERN proposed a second more

conservative version, the layout of which is shown in **Fig. 68**. This is based on 45° SC magnets with a 3-T maximum magnetic field, using the standard cosine-theta magnet design [140]. This gantry is, of course, much larger than the 4-T original version [127] shown in **Fig. 67**, but it significantly reduces the risks associated with the magnets and makes it feasible to have the gantry built within an 8–10-year timeframe.

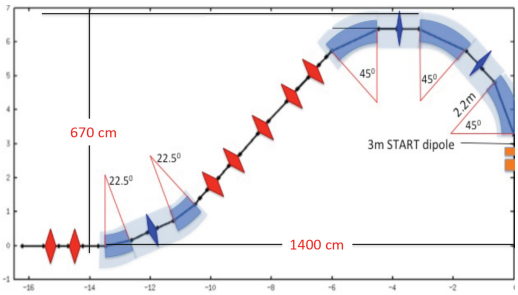

Fig. 68: SIGRUM gantry, conservative version, with 3-T SC magnets. This requires two 22.5° bending magnets (contained in the first cryostat) and three 45° bending magnets (contained in the second cryostat).

3.6.2.2 Scanning magnets

Along with the main SC bending magnets, the most important and challenging system is the scanning magnets. Since the position of the scanning magnets is downstream and the SAD is as small as possible to reduce the total dimensions of the gantry, those magnets need fast and powerful power supplies to allow a beam-painting speed of up to 20 m/s over a (30 × 30)-cm^2 treatment field. **Figure 69** shows the *x*/*y* scanning system for the 3-T SIGRUM design [140], which has SADs of 240 and 280 cm.

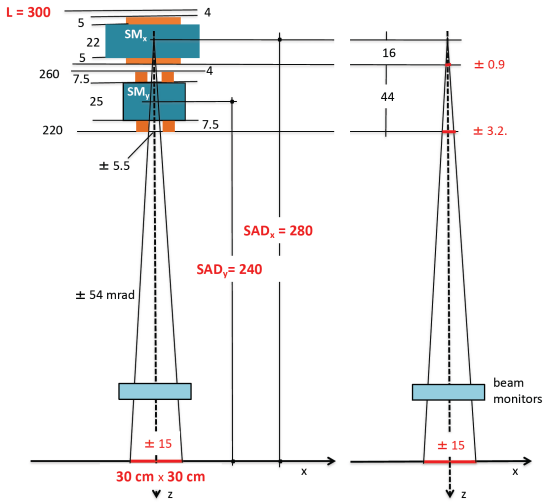

Fig. 69: Layout of the scanning system of the 3-T SIGRUM gantry [140].

3.6.2.3 Gantry studies within EU collaborations

The SIGRUM gantry conservative layout [140] is now being further developed within HITRI*plus* [105] and as part of EuroSIG [141], a collaboration between CERN, CNAO, INFN, and MedAustron aiming to have a C-ion gantry installed at the running therapy centres at CNAO and MedAustron in the next decade. This European gantry can, of course, also be considered for a new ion therapy facility with similar timescale planning. Two very distinct gantry options were considered by an international review committee, following the initiative of CERN, CNAO, and MedAustron, aiming to identify the best and most practical solution to be implemented in the next decade. The two options were the SIGRUM rotating gantry [140] and GaToroid [142] [143], an innovative concept for a fixed toroidal gantry, operating mechanically and electrically in steady state, as schematically represented in **Fig. 70**.

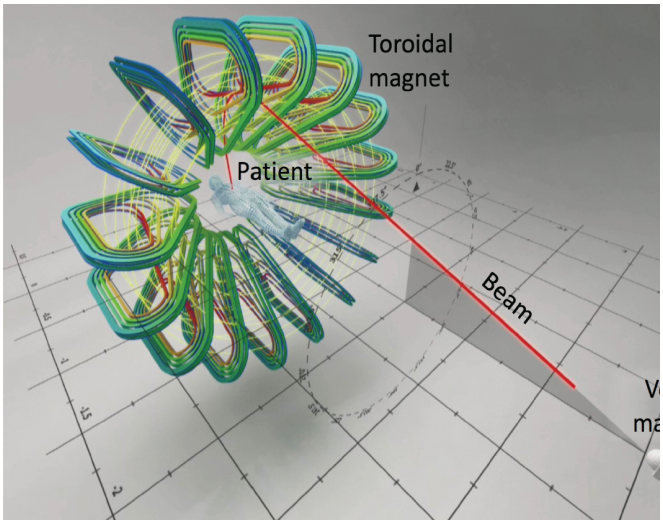

Fig. 70: Schematic representation of the GaToroid components. The patient is located in the field-free bore of the toroidal magnet. (Courtesy of D. Dominguez, CERN Design and Visual Identity Service, and L. Bottura, CERN, inventor.)

Given the timeframe of 8–10 years for the installation of a carbon ion gantry, the committee suggested focusing on the design of the most conventional among the proposed designs, namely a rotational gantry such as SIGRUM, and recommended a revision of the general and clinical requirements, as discussed with the medical physicists and doctors of CNAO and MedAustron.

The best solution, which optimises the flexibility of the optics, the aperture of the SC magnets, compactness, and its impact on weight and cost [144], was selected after analysing more than 30 configurations [141], starting from the conservative SIGRUM optics but reintroducing the possibility of having 4-T bending magnets. **Figure 71** shows the selected layout, which has 45° dipole magnets and is characterised by:

(i) a single family of superconducting dipoles, i.e. all dipoles are identical and provide only a pure dipole field, with no quadrupole gradient;

(ii) four warm quadrupoles and five superconducting quadrupoles, responsible for a flexible optics matching (parallel-to-point), with modulation of the magnification factor;

(iii) achromatic and angle-independent optics;

(iv) compatibility with a 70-mm magnet aperture and a momentum acceptance of $\Delta p/p = 0.1\%$.

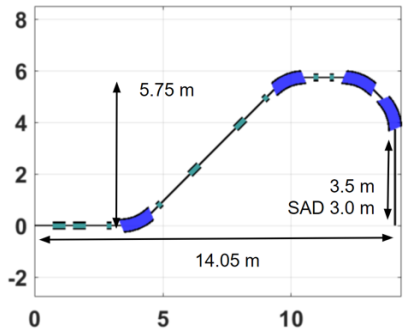

Fig. 71: Layout of the European gantry. Main gantry dimensions are reported with arrows. The radius of the gantry is reported at the beam and not at the external magnet dimension. (Courtesy of M. Pullia, CNAO [141] [144]).

Several solutions were also explored for the mechanical structure [141] [145], for both 220° and 360° rotation angles, and these were compared according to criteria of design robustness, size, weight and complexity, deformation and precision performance, costs, as well as environmental impact. Two options were retained. For the partial rotation, a balanced structure attached to the building wall was

proposed, differing from the original SIGRUM, which has an unbalanced structure. For the complete 360° rotation, a more traditional barrel configuration was considered the most appropriate and finally selected, as it was the preferred choice by the medical doctors and the increase in costs and dimensions with respect to the 220° solution was considered acceptable. **Figure 72** shows its conceptual mechanical layout.

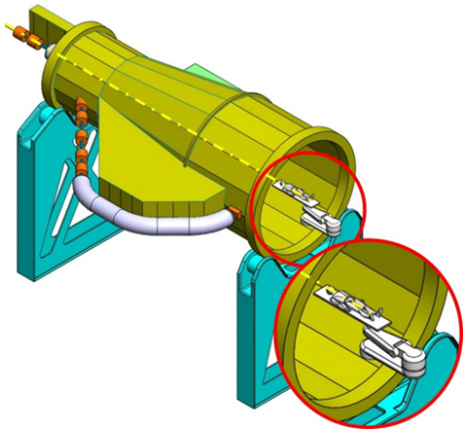

Fig. 72: Mechanical structure for the European gantry. (Courtesy of L. Piacentini, CERN and RTU [141] [145].

3.7 Radioisotope production

Accelerator-produced radioisotopes are widely used in modern medicine for imaging, for cancer therapy, and for combinations of therapy and diagnostics (theragnostics). Clinical trials are well advanced for several radioisotope-based treatments, and this is expected to lead to a strong demand for radioisotopes that are usually produced by dedicated accelerator systems.

As an alternative to using a dedicated accelerator, such as a medium-energy (30-MeV) cyclotron, the linac injecting into the synchrotron of an advanced ion therapy facility can be easily designed to allow dual-mode operation. This approach allows the production of a wide range of radioisotopes in parallel with operation as synchrotron injector, achieving this at a much lower cost than using a dedicated accelerator. The structure of the dual-mode linac has already been presented in **Fig. 54**, and it is repeated here for convenience as **Fig. 73**.

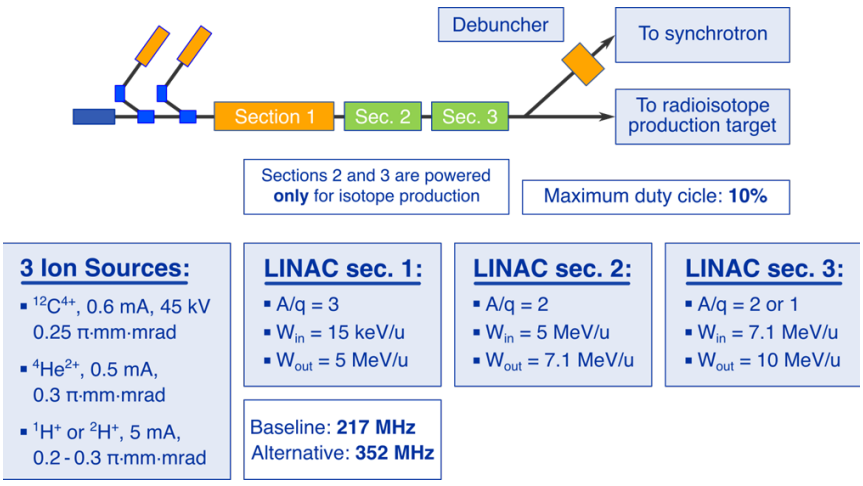

Fig. 73: Scheme of the dual-mode injector linac.

In this configuration, a radioisotope production target is placed in a shielded room directly in front of the linac. A switching magnet at the linac exit can select some beam pulses to be sent to the transfer line towards the synchrotron, while other pulses will go to the isotope production target. Since the pulse repetition frequency required for synchrotron injection is < 1 Hz and the linac can easily be operated up to 50 Hz, most of the pulses can be used for isotope production, reaching the average currents required for efficient production. Typically, 2-ms beam pulses at 50 Hz repetition could be

used for isotope production, leading to a duty cycle of 10%, which is considered to be the maximum achievable in the linac using standard RF cavity designs. Beyond this value, special construction techniques would be needed, leading to considerably higher construction costs. At the same time, a duty cycle of 10% is considered to be large enough to keep the temperature in the target during operation within acceptable limits.

For radioisotope production, proton or fully stripped helium (alpha) beams would be used. In the isotope production mode, the first linac section designed for carbon at $A/q = 3$ is operated at the lower voltage required for protons or helium. The second and third sections designed for $A/q = 2$ are switched on as needed, according to the energy and type of particles required for the isotope to be produced. The energy of the second section has been defined with the goal of producing ^{211}At for targeted alpha therapy at its optimum energy of 28 MeV [146].

With respect to a linac devoted only to synchrotron injection, the configuration presented in **Fig. 73** presents some additional costs related to the cooling of the accelerating structures and to the larger dimensions and energy capacity of the modulators that drive the RF system. In particular, the RF cavities require larger cooling channels, which has an impact on the production cost and might lead to some reduction in power efficiency (shunt impedance). These costs are, however, estimated to be about 10%–20% of the overall cost of the linac, making the dual-mode system much less expensive than a dedicated accelerator. A similar dual-mode operation has been envisioned for CERN's new proton injector, Linac4, which is designed to serve as both an injector to the PS booster ring and as the initial stage of a high-power proton linac, the Superconducting Proton Linac [147]. So far, only the first operation mode has been used.

With a duty cycle of 10% and a maximum $^{4+}$He current of 200 μA, calculations show that up to 250 doses of ^{211}At could be produced in 7 h of target bombardment, enough to cover the daily needs of a small–medium-sized hospital [146].

Table 12 Accelerator-produced doses for patient treatment ($\text{Doses}_{\text{treat}}$), considering the preparation time (t_{prep}) after the end of bombardment (EOB).

Element	Half-life (min)	t_{prep} (min)	$\text{Doses}_{\text{EOB}}$	$\text{Doses}_{\text{treat}}$
^{18}F	109.7	30	200	181
^{11}C	20.4	40	32÷70	8÷17
^{211}At, ovarian cancer	432	420	52÷260	27÷132
^{211}At, brain cancer	432	420	15÷74	8÷38

A compact linear accelerator is a very attractive option for producing an interesting selection of medical radioisotopes at a hospital site. With 7 MeV proton beams at 30 mA or 7 MeV/u alpha beams at 20 mA, the production of radiopharmaceuticals containing ^{18}F, ^{11}C, and ^{211}At (the first two for PET imaging, the latter for therapy) is sufficient to cover the daily needs of a small–medium-sized hospital. Doses made available at the beginning of a therapy day by the two linac-based systems are shown in **Table 12**. Compared to proton PET cyclotrons of comparable beam specifications, compact proton linacs require thinner shielding and have lower costs, easier maintenance, and lower weight. An α-linac designed to produce ^{211}At—necessarily limited to 7 MeV/u energy to avoid co-generation of ^{210}At—would be well-suited to targeted alpha therapy and might also produce PET-imaging isotopes if equipped with an additional proton source.

3.8 Software

3.8.1 Accelerator control system

The accelerator control system (ACS) is responsible for the control and monitoring of hundreds of devices in the injector, synchrotron, and beam transfer lines with sub-microsecond synchronisation. The

purpose is to produce ion beams with the desired characteristics at the entrance to each one of the five rooms (two for experiments and three for patients' treatments), and at the end of the lines in which the two experimental beams will branch out. These devices include, but are not limited to:

(i) ion sources;

(ii) RF systems;

(iii) magnet power supplies;

(iv) synchrotron injection and extraction hardware;

(v) beam diagnostics;

(vi) vacuum devices;

(vii) beam stopping devices.

As these devices have very different data communication and workflow requirements, the ACS will be architecturally organised into multiple tiers:

(i) Presentation tier (T1): presents information produced by the system to the users, processes user inputs, and interfaces to external systems.

(ii) Service tier (T2): includes the common control system services used on the equipment tier, such as allocation of the required devices for beam production, communication between devices, configuration management, data logging, archiving, and alarms.

(iii) Equipment tier (T3): contains the electronic controllers (based on modular computing and I/O platforms, such as PLC, PXIe, uTCA, VME, etc.) that control and supervise the individual accelerator devices. This tier is characterised by short reaction times, soft real-time operation, and safety requirements. It includes a timing system that allows very precise coordination of the accelerator and beam transfer equipment.

3.8.2 Treatment control system

To successfully execute patient treatments, radiotherapists must be able to control the equipment in the treatment room, such as:

(i) the patient positioning system (PPS);

(ii) the gantry and the movable beam nozzle;

(iii) the patient position verification system;

(iv) the room safety system.

This equipment and the particle therapy machine—the accelerator and the dose delivery system (DDS)—need to be controlled and configured with data, as prescribed by the oncology information system (OIS) and the TPS. This functionality is typically implemented in a treatment control system (TCS), which also features the user interfaces that the clinical personnel use to execute the workflow of a treatment fraction. These operations include:

(i) retrieving plan data generated by the TPS and managed by the OIS;

(ii) preparing patient-specific equipment and patient immobilisation;

(iii) patient alignment—acquisition of 2D or 3D daily images, registration of daily images to the planning data, and generation of daily alignment vectors;

(iv) positioning equipment (PPS, gantry, nozzle) into the treatment configuration;

(v) beam delivery—using the DDS and ACS;

(vi) generating and storing delivery reports;

(vii) handling potential error and warning situations.

All this functionality needs to be executed through a user-friendly user interface, guiding the radiotherapist through the workflow and presenting the right information at the appropriate step in the process. To increase the workflow efficiency, many of the operations must be able to be executed remotely from a treatment control room.

Much of the same functionality is required by the research personnel using the equipment in the research or clinical rooms of the facility, especially in the case of animal irradiations. In addition, the TCS must support research personnel with functionality to be able to automate certain operations of the workflow and provide access to detailed information from the subsystems, for example the DDS. The design of the software should be modular to support integration of advanced devices (e.g. patient imaging, sample handling and positioning) in the treatment and research rooms.

The time spent on quality assurance (QA) of the machine and the treatment plan should be minimised to maximise the available time for clinical and research use of the machine. Therefore, the TCS should support automation of QA in the form of semi-automated and automated QA workflows (device positioning, delivery, integration with external QA equipment) and availability of delivery log data for log-based QA.

3.8.3 Dose delivery system

The DDS is the main driver of the beam delivery in a particle therapy accelerator. The DDS receives the delivery instructions, custom-generated by a TPS, from the TCS. To execute the delivery, the DDS requests a beam of appropriate parameters (energy, width, intensity) from the ACS and uses a pair of scanning dipole magnets to scan the beam over a layer of the tumour by controlling its lateral position. The DDS monitors all clinically relevant parameters of the beam, such as the delivered dose, beam position, width, and energy. To enable reconstruction of the beam delivery and tracking of treatment progress, it generates reports of the values measured during irradiation.

The dual clinical and research use of the proposed future facility imposes the following requirements on the DDS:

(i) Performant scanning dose delivery with in-built real-time monitoring and interlock functionality. Modern digital technologies, such as field-programmable gate FPGA arrays, should be used, and system redundancy should be considered to guarantee fast, precise, and safe dose delivery to patients.

(ii) The architecture of the system should be modular to support new research and clinical equipment—novel beam monitoring systems, tumour tracking systems, low-dose proton radiography equipment, ion beam tracking with PET or prompt gamma tracking, etc.

(iii) The software should be customisable to support research of novel beam delivery techniques:
- oblique raster scanning [148];
- FLASH;
- mini-/microbeams;
- hypofractionation.

The hardware and software should support the delivery of multiple particle species. The DDS should be able to be integrated with research equipment, such as dosimetry devices, to synchronise the operation of the machine and equipment in the research room. Interfaces should allow efficient and potentially automated operation of the DDS without the use of clinical software, such as the TCS, OIS, and TPS, to simplify irradiations for research purposes.

3.8.4 Treatment planning system

The TPS is used to generate a treatment plan for a specific patient based on patient images and the prescription given by the radiation oncologist. It is a complex piece of software, integrating detailed physics (dose calculation), mathematics (plan optimisation), and graphical (contouring) algorithms.

The TPS has to import image datasets from multiple modalities (CT, PET, MRI) and support the alignment of these images to one another (image registration). In this first stage, the tumour and important anatomical structures have to be identified. This process is called contouring, and it is either performed manually or automated using anatomical atlases or deep-learning algorithms.

In the second stage, the image dataset and the contours are taken along with prescription input to produce a treatment plan, a set of instructions on how to deliver radiation. To produce a treatment plan and allow for its optimisation and evaluation, the TPS computes the expected dose distribution in the patient's anatomy, considering different tissue types and the characteristics of the beam delivery device. These treatment plans can also be modified to compensate for changes in patient anatomy over the course of treatments, usually referred to as adaptive therapy.

To support the study of the radiobiological effects of different particle species, the TPS should be able to model the effects of varying RBE. In addition, the design of the TPS should be open enough to allow extension of its functionality to novel delivery methods, such as FLASH, mini-/microbeams and oblique raster scanning. Due to the heavy computational requirements of the certified TPS, automation of the workflow through scripting and off-loading of calculations to a GPU-based hardware should be supported.

3.8.5 Oncology information system

The OIS is the clinical software that manages the entire patient journey through the facility. Using the OIS, the clinical personnel are able to connect and track the patient data generated during a particle therapy course, such as patient images, treatment plans, and delivery reports, in an electronic patient chart and integrate them into the overall hospital information system.

The OIS connects the software systems of the particle therapy facility to allow the clinical personnel to:

(i) create and maintain electronic patient charts;

(ii) import, keep, and display documents related to patient treatment;

(iii) create, access, modify, store, and archive patient treatment course plans;

(iv) transfer a "treatment order" to a treatment machine;

(v) import the actual radiotherapy session report from a treatment machine to enable treatment plan tracking and control;

(vi) record a complete history of actual delivered radiation doses;

(vii) prepare a detailed report of performed treatments;

(viii) generate a list of services provided to streamline the billing process.

3.9 Buildings architecture and site

The layout of the accelerating structures and beam delivery systems proposed for a new facility, as implemented for the future SEEIIST RI, is presented in

Fig. 74. The main principles of the architectural design, which are also adopted for the SEEIIST facility, are as follows:

(i) Three treatment beamlines and two experimental beamlines are planned, oriented in opposite directions, to physically separate the treatment and the research areas of the facility.

(ii) The three treatment rooms are equipped with a (a) horizontal beamline, (b) horizontal and vertical beamline, and (c) rotating gantry.

(iii) The two experimental beamlines enter a reconfigurable hall where shielding blocks can be moved to arrange the space and the shielding according to the requirements of the experiments. Space is allocated for splitting the beamlines inside the experimental hall. Access for animals is provided from a separate side of the experimental hall.

(iv) From a radiation protection point of view, the facility is structured into six radiation-shielded zones, each being accessible while the others are in operation. The main shielded zone includes the accelerator and the beam transport lines; the linac injector and the ion sources are in a separate zone that is usually accessible during accelerator operation. Each treatment room constitutes a separate zone. The experimental room is the last zone, which can be subdivided into individual smaller shielded areas (bunkers) according to the needs of the different experiments.

(v) The linear accelerator is connected to an additional shielded area that might be used in a second stage of the facility development for the production of radioisotopes using the low-energy beam.

(vi) Adequate space is allocated for loading and unloading of equipment, particularly next to the experimental hall.

(vii) The operational part of the facility is constructed as a fully shielded area that can be considered as a "building block" of any final architectural design chosen for the facility, which will adapt to the local environment for the final site.

(viii) Future extensions are possible, e.g. to add a fourth treatment room equipped with a second gantry and to extend the experimental hall with another beamline. Similarly, new ion sources can be added in the source area.

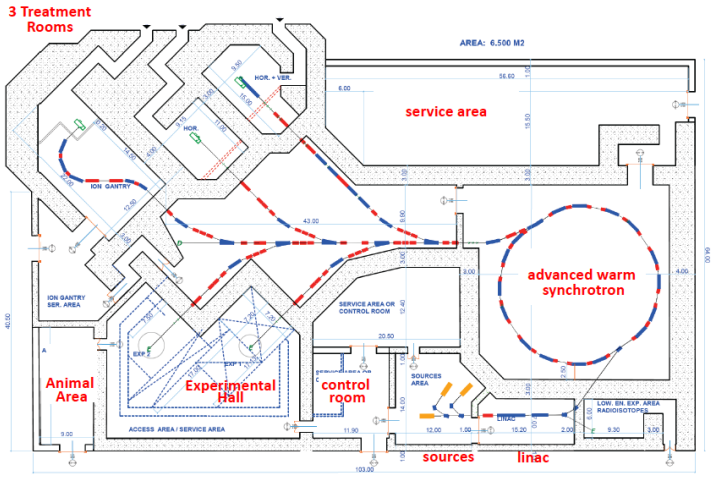

Fig. 74: Layout of the accelerating and beam delivery structures of the proposed RI optimised for SEEIIST.

The area of the overall facility, including beam transport, treatment, and experimental rooms, is about 6500 m^2, with the accelerator occupying 1200 m^2 (900 m^2 for the synchrotron and 300 m^2 for the linac and the ion sources).

Fig. 75: General 3D view of the overall facility including auxiliary buildings, designed for SEEIIST, with the accelerator system bunker shown with the roof open. (Courtesy of Kaprinis Architects.)

Figure 75 shows a 3D view of the overall facility, as designed for SEEIIST, showing the position of the clinical section connected to the treatment rooms, the accelerator bunker in the middle (with the roof open to see the accelerator components), and the experimental building to the right.

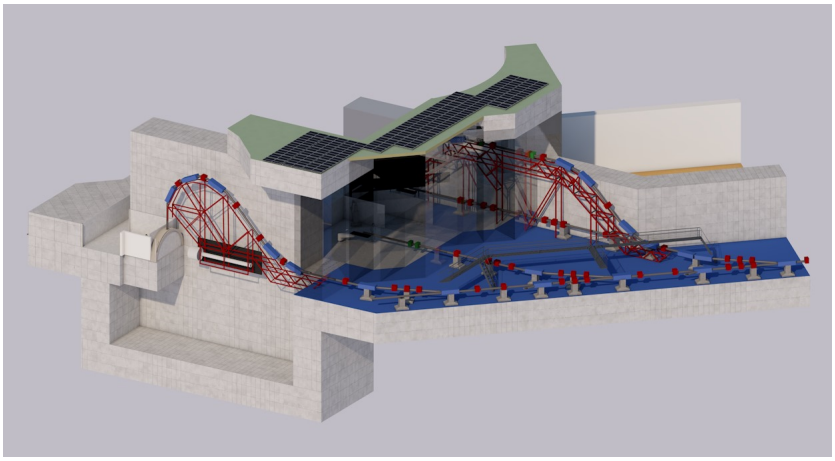

Fig. 76: 3D view of the treatment room area and of the final part of the beam transport line. (Courtesy of Kaprinis Architects.)

Figure 76 presents a 3D view of the critical area including the end of the beam transport line and the treatment rooms. In particular, this shows the footbridge that allows movement inside the beam transport area for servicing equipment, the large vertical beam transport line going to the first treatment room, and the 220° rotating superconducting gantry with its underneath vault, which allows for rotation and provides access for servicing the gantry elements.

3.9.1 Site requirements

The layout of the bunker shown in

Fig. 74, which covers an area of about 6500 m^2, does not include the laboratories and the animal house. Additional surface buildings, as shown in **Fig. 75**, covering an overall area of 14,000 m^2, will host laboratories and offices for three types of staff: those involved in the running of the facility, those who will provide tumour treatments, and the numerous visiting scientists coming from collaborating institutes.

A preliminary architectural design, conceived for the complete SEEIIST facility, including scientists' offices and laboratories as well as administrative buildings, is presented in **Fig. 77** and **Fig. 78**.

Fig. 77: Overall concept of the SEEIIST facility seen from the side of the scientists offices and laboratories. (Courtesy of Kaprinis Architects.)

Fig. 78: Overall concept of the SEEIIST facility seen from the side of the administrative buildings and the patient treatment areas. (Courtesy of Kaprinis Architects.)

In this conceptual design, the overall area required by the different buildings is 14,000 m^2, corresponding to a rectangle of about 115 m × 125 m. At this stage, it can be said that to cover all needs and possible future upgrades, the overall site must have an area not less than 200 m × 250 m.

The electric cabin serving the facility should have a capacity of no less than 15 MVA, and the water flux, at 6–10°C for cooling the equipment, should be produced in a cooling tower delivering at least 1000 m^3/h.

Assuming that only outpatients would be irradiated, the facility should be located not far from a hospital that could provide the necessary care for the patients, integrating the offerings of the facility. The presence of a radiotherapy department in the hospital, featuring modern linacs for X-ray therapy and the corresponding medical imaging tools (CT, PET, CT/PET, and MRI), would represent an important asset. This would also reduce the investments needed to install and maintain some of these costly diagnostic tools in the new RI. In any case, the instruments installed in the facility should complement those available in the nearby hospitals.

As discussed above, for the animal studies programme, an in-house animal facility should be established for permanent housing of small rodents. The animal facility should be placed not far from

the accelerator building. The animal preparation area should have a direct connection to the experimental beam room to avoid patient areas being exposed to allergens. The animal facility should also include an isolated section that can serve as temporary housing for visiting large animals brought in by visiting scientists. After treatment, these animals will be taken to the home institution for follow-up. All facilities for housing and treatment of animals should comply with EU regulations.

Larger animals could be brought to the site as needed, based on a scientific collaboration agreement with a veterinary department. As foreseen for SEEIIST, this department could be located in one of the collaborating countries that does not host the main facility.

As for all the facilities of this type, the roads should be such that heavy pieces of equipment can be transported. Furthermore, there should be an airport not too far away, since many scientists are expected to visit the laboratories to perform experiments, and patients, with their relatives, will have to spend on average 3–4 weeks in the facility. With a proton or carbon ion average irradiation course lasting 20 working days, 7500 sessions will be needed for treating the target of 375 patients/year. This means that every day, the facility will be visited by about 35 patients, and they will often be accompanied by one relative. Therefore, a guesthouse and/or nearby hotels are needed to host these patients with their relatives.

3.9.2 SC magnet advanced option layout

A superconducting synchrotron would allow the compact layout shown in **Fig. 79** to be realised. The reduction in the area required for the accelerator would be a factor of two: 600 m^2 for the superconducting option, including sources and injector, against 1200 m^2 for the warm-magnet option. However, the impact of the reduction in accelerator size will be less visible, about 10% when considering the overall area of the bunker, including beam distribution, treatment, and experimental rooms.

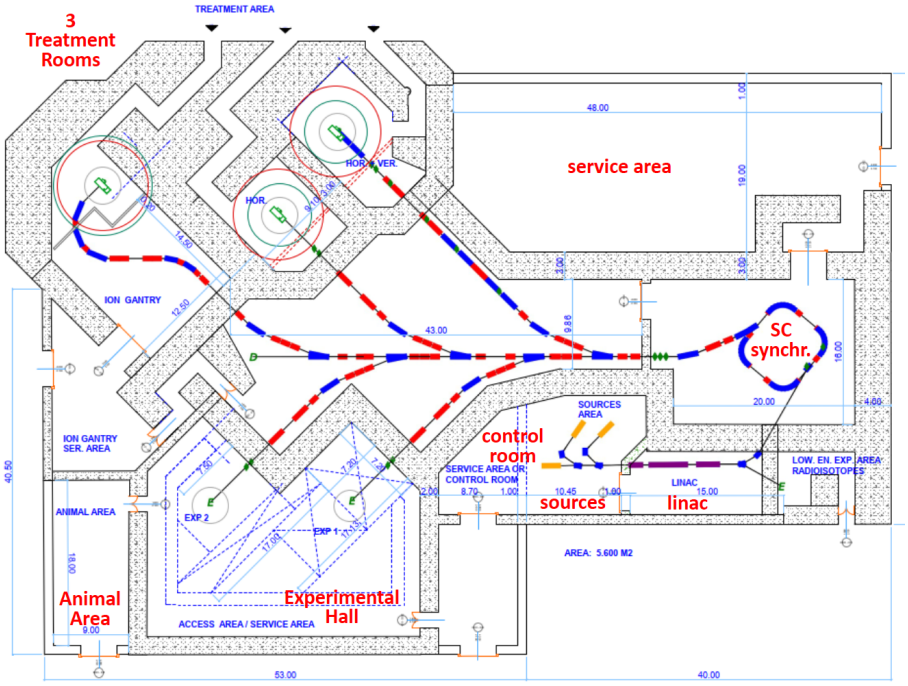

Fig. 79: Same layout as in **Fig. 74** but with a superconducting synchrotron.

A preliminary cost analysis indicates that the cost of a superconducting synchrotron is about 20% lower than that of the baseline warm-magnet version. This is due to the smaller ring dimensions and the smaller numbers of magnets and other components. To these savings, additional savings related to the smaller dimensions of the building must be added.

3.10 Energy management

3.10.1 Low environmental impact

A crucial asset and a clear priority while designing a new facility is to keep its environmental impact and energy consumption as low as reasonably possible while making ample use of renewable energy sources.

A growing awareness about the importance of these topics is making its way into the field of modern particle accelerators, in particular when addressing the specifications of very large facilities, which are very demanding in terms of capital investment and energy consumption [149]. This has triggered, particularly in the latest decade, a coordinated effort by several European institutions aimed at:

(i) maximising the ratio between the scientific throughput of any research facility and the electrical power required to operate it;

(ii) storing excess energy to compensate for power supply interruptions;

(iii) recovering waste heat;

(iv) adapting operation schemes to periods of lower industrial and residential power consumption in the surrounding area, on both daily and seasonal time scales.

Flagship programmes of the European Union in the field of particle accelerators, such as EuCARD-2 [150] [151] and ARIES [152], included energy efficiency among their work packages and rated them as very high-priority commitments. Further considerations are reported in NIMMS-Note-021 [153].

Respect for the environment is ensured not only by the use of renewable resources—and eventually by the use of the facility's waste heat at the end of the exploitation chain—but also by:

(i) responsible selection of construction materials for buildings, technical infrastructure, and machine components, and by

(ii) the complete design of the energy-efficient facility such that the highest overall throughput is achieved with the lowest possible use of electrical energy in terms of therapeutic doses delivered to patients, production of radioisotopes for the hospital, and well-scheduled and prioritised research beam times.

Adequate planning and engineering resources should then be allocated to address all these aspects in an integrated way, optimising the entire power chain from the "green" power sources to the efficient, high-tech tools used for the accelerator, irradiation rooms, and experiments. Designing a modern and compact facility with a smaller footprint than existing facilities of the same type will further reduce the environmental impact.

The various measures to keep the environmental impact small and to increase the energy efficiency of the facility are described in the rest of this section.

3.10.1.1 A holistic approach to energy efficiency

Beyond the availability of green energy sources, an environmentally sustainable infrastructure, such as the one that SEEIIST intends to construct, could put in place all possible measures to limit its overall environmental impact without compromising its ambitious scientific and technological goals.

The technical performance required to make the facility a first-class therapy and RI, as described in the present document, is, of course, the highest priority. On this basis, the design of the facility and its components should include, from its inception, all technically feasible and economically affordable measures to ensure the highest possible energy efficiency. This, in effect, acts as an "energy resource" in its own right by providing higher performance with lower power consumption. Moreover, the choice

of all materials for both technological and building components will be dictated by the lowest possible environmental impact.

The overall design of the facility, the choice of individual components, and the use of efficient operation modes can guarantee high performance at low power consumption. Indeed, one can in principle look at the efficiency (ε) of a facility in terms of the ratio between the total yield (Y) or throughput and the overall environmental impact (I). The latter includes the energy required (and what fraction of it comes from renewable sources), the choice of environmentally friendly materials and construction methods, the size of the layout, the effort taken to minimise faults that would keep the machine on (and consuming) but idle, and the amount of waste heat that cannot be recovered:

$$\varepsilon = \frac{Y}{I}. \tag{2.1}$$

Neither Y nor I are straightforward to define using simple formulas and, even if this were possible, the results would be expressed in different measurement units and thus be difficult to compare. Moreover, in the present case, the definition of the numerator in the efficiency ratio is complicated (indeed, enriched) by the status of a proposed facility, such as the SEEIIST RI, with the decision of devoting 50% of weekday time to therapy and the other 50% to research purposes. Indeed, while for pure science accelerators, the beam luminosity (or the total number of accelerated particles) and its energy contribute to the nominator of the efficiency ratio, the situation looks different for an RI devoted to both research and therapy.

As to the fraction of the machine's use directly dedicated to patient treatment, the throughput of the facility will probably be a reasoned composition of ion therapy hours and the quantity of medical radioisotopes, assuming that they will be produced as a by-product from the high-duty-cycle injector linac. As to the fractional use of the facility for medical research, it is intrinsically even less straightforward to define a throughput: experiments with short data acquisition times and long preparation times may indeed be favoured by their higher scientific significance. At present, Eq. (2.1) can be used only as a general qualitative guide; its definition could be better refined during the project's preparation phase.

All the measures aimed at maximising the efficiency ratios—proposed for the design, construction, and implementation phases—should be the subject of an ad-hoc budgetary plan. This should provide convincing arguments that, beyond the environmentally friendly appeal of the proposed solutions, the sum of the initial investment cost for an energy-efficient facility and the operation cost, amortised along a lifetime of 30 years, is properly considered.

3.10.1.2 High energy efficiency

Detailed specifications of the ion therapy cycles for the proposed new facility are going to be dictated by the medical doctors, considering, in addition, its conceived specific features, as outlined in Section 1.1, that simultaneously offer a strong scientific research programme with unique potential.

First of all, the higher beam intensity will translate into shorter treatment times, increasing the well-being of patients. The possibility of different dose delivery schemes, from hypofractionated to FLASH therapy doses, is expected to offer unique and yet largely unexplored therapeutic potential, but also higher throughput, which will contribute to higher energy efficiency.

In addition, the opportunity offered by multiple-flattop operation (as described in Section 3.4) will certainly be source of a better machine efficiency (higher throughput): it will significantly shorten the overall dead time due to injection and acceleration during the overall irradiation period.

3.10.1.3 Production of radioisotopes at low additional energy cost

The possibility to use the injector linac in a "parasitic" way for the production of medical isotopes in parallel with research or therapy could contribute to the overall yield of the facility if it is decided to implement this at a later phase of the facility design. To this end, as outlined in Section 3.6, the linac will feature a higher duty cycle than required for the medical synchrotron (10% versus 0.1%) and

possibly a higher energy (10 MeV/u versus 7 MeV/u) with respect to present machines, so as to provide the medical doctors with radioisotopes (^{18}F, ^{11}C, ^{211}At, and others). This feature, which is not available at presently operational heavy ion therapy centres, will complement the therapeutic portfolio of the proposed facility; it will require limited ad-hoc investment in the construction phase, and it has the potential to increase the overall throughput of the facility with small additional energy consumption.

3.10.1.4 Optimisation of the entire operation cycle

Over and above all factors of higher throughput mentioned above, ample margins for energy-efficiency optimisation come from a careful planning of the entire machine cycle. The proposed RI shall eventually identify, schedule, and even automatically set up operation schemes. Activities requiring no or minor changes to the setups (e.g. the same beam type with similar current and energy) can be clustered.

An efficient operation cycle can be largely eased by the availability of advanced routines for the high-level control of accelerators and beamlines, which must be accompanied by beam instrumentation and tools for component diagnostics that are able to anticipate the detection of faults. This feature is deemed to be crucial for improving the overall machine duty cycle, not only by reducing the time needed for beam preparation but also by anticipating technical issues. These, when not diagnosed in real time, may cause periods of machine unavailability, which could range between minutes and several hours. An effort to keep the machine operation setup updated with modern machine-learning algorithms is a crucial asset in this respect.

The control system shall have to judge, in case of faults, which parts of the machine shall have to be kept on and running (to enable an efficient and rapid restart) and which parts shall have to be turned down (for energy-saving purposes).

3.10.1.5 Minimisation of the environmental impact

In addition to planning and ensuring the largest possible throughput of the RI, as outlined in the previous section, the aim is to put in place a multi-faceted high-priority technological effort to limit the environmental impact of the machine, infrastructure, and buildings. This effort covers diverse aspects, which are addressed in the following paragraphs and which require a portfolio of various physics and engineering expertise. Emphasis is going to be put on keeping the layout compact, adopting up-to-date solutions for low-consumption high-tech components and their related infrastructure (including computing components), increasing the availability of the RI, recovering waste heat, and using environmentally compatible materials.

A smaller-footprint machine—As outlined in Section 3.2, the proposed facility will feature, even in its basic layout, extreme beam intensities, a large variety of ion species, and flexible injection and extraction schemes, while keeping a footprint that is not larger than that of the previous-generation (CNAO, MedAustron) facilities. Moreover, the opportunity to develop a synchrotron with superconducting dipoles, to be assessed during the R&D phase, with a higher maximum magnetic field (conservatively, by a factor of two to three), would allow the building of a synchrotron of smaller circumference. This would imply reducing the size of the buildings and their conventional infrastructure and reducing the number of beamline components, entailing a smaller overall environmental impact. A smaller facility is also appropriate for premises connected to a hospital.

Low-energy-consumption components—In addition to keeping the layout reasonably compact, the most up-to-date solutions in terms of efficiency can also be adopted, in particular, for the most energy-demanding components, such as magnet power converters, RF generators, and auxiliary systems (such as more efficient cryogenics compressors, conventional cooling, and air treatment systems). The superconducting gantry will be a noteworthy example of a high-tech, state-of-the-art component featuring these traits of power efficiency. One could possibly consider using optimised electromagnets (with lower resistive losses, albeit at higher investment costs) on the injector linac, the synchrotron, and the transfer lines, as well as pulsed normal conducting magnetic lenses. Clearly, the possible choice of advanced superconducting magnets for the synchrotron would imply an electrical consumption “at the

plug" that would be around a factor of 15 lower than with normal conducting magnets (considering the gain in magnetic field and the smaller number of components required for the smaller circumference): this value derives from a comparison between normal conducting and superconducting dipoles made for the FAIR SIS100 dipoles [154].

Green computing—The increasing energy requirements of computing centres are becoming a growing concern on a global scale. The new proposed RI will not be exempt from this concern, as several high-tech computing and data-management centres will be required: for operation of the facility, the treatment protocols, and the management of patient data and of clinical and research data to be shared among several facilities in an international network. Therefore, special care is to be devoted to green computing infrastructures, taking care to limit energy usage via, for instance, the proper choice of single products (laptops, PC servers, storage units, etc.), the purchase of CPUs that offer high computing power per watt consumed, planning hard disks to be in standby mode when not in use, etc. Thermal dissipation can also be improved by using suitable system design for the entire data centre with a high node density and the best possible arrangement of components in the available physical space and using efficient, passive ventilation cooling. Data centres are particularly suited to being directly fed by renewable energy sources such as solar or wind. Eco-compatible IT materials in particular should be adopted, avoiding substances that may be harmful to the environment (see e.g. the EU RoHS Directive: Pb, Hg, Cd, and some plastics must be excluded). This is of particular importance given the very fast replacement rate of IT components.

Minimisation of downtime—Beyond improving the efficiency of the facility's operation cycle and using modern methods to anticipate component failures or deviation of the machine's operational parameters, as outlined above, all reasonable measures should be taken in the design, purchase, and construction phases to increase the mean time between failures of all machine components and infrastructures. This implies the most important benefit, namely to avoid interrupting the experimental program and medical treatment while reducing the length of downtimes during which the energy consumption may be almost constant, but with zero throughput. For those cases in which prompt fault recovery may not be possible, spare components should be made available online, properly connected via both hardware and software to the facility, so as to be able to switch to them quickly. As with many energy-efficiency measures, all-encompassing considerations on investment costs, operational efficiency, and the probability of faults have to be made on a case-by-case basis.

Accelerator facilities are often plagued by unwanted short-duration power failures that turn into long time spans being required for machine setup recovery: indeed, they typically require retuning of the machine, often with constant energy usage (efficiency denominator) while delivering no time for medical therapy or experiments (zero throughput—efficiency numerator). Beyond causing an annoying discontinuity in patient treatment, which is the most important "efficiency" factor, they also affect long-term energy efficiency. To mitigate this type of inefficiency, the use of short-term energy-recovery storage systems, such as capacitor banks or other technologies, could be considered.

Recovery of waste heat—As all energy consumed by the proposed RI will eventually end up as waste heat, engineering studies should be undertaken to recover machine waste heat for purposes such as providing warm water or heating the facility itself. Depending on the amount of waste heat, this could be limited to the facility or possibly extended to the surrounding industrial or living areas. This would further increase the social acceptance of such a facility by the neighbouring context due to immediate tangible benefits.

Environmentally compatible construction materials—The aim is to adopt the most recent EU standards for green construction (also called green building or sustainable construction) for the proposed new facility. Such concepts address the use of resource-efficient and environmentally responsible processes in construction to ensure lifetime sustainability of the buildings. The focus is also on the competitiveness of the sector, not least in the field of sustainable construction. This includes undertaking building operations, site design, maintenance, repair, and demolition with the least possible harm to the environment. The process requires close collaboration of the construction engineers and the architects in the entire construction project. The aim is to ensure that the building and construction

methods are cost-effective, durable, and reduce the overall effects on the environment and human health, with a central focus on efficient use of energy and resources, water preservation, improved occupational health, and reduction of pollution and wastage.

In particular, any new facility in Europe has to fulfil the requirements from the following set of EU rules:

(i) The original energy performance of buildings directive (EC, 2002), its update (EC, 2010), the energy-efficiency directive (EC, 2012), the amending directive on energy efficiency (EC, 2018c), and the directive on the energy performance of buildings (EC, 2018d).

(ii) The original renewable energy directive (EC, 2009) and the revised renewable energy directive (EEC, 2018b).

A possible dedicated sustainability hub supporting the new facility could become an important pillar of the RI and play a crucial role not only in the design and construction phases, but also throughout the entire lifetime of the facility.

Energy-efficient technologies are steadily improving in both complex and conventional apparatuses and infrastructures. Therefore, whenever maintenance measures or upgrade opportunities arise, amelioration of the environmental aspects of the facility—even after operations have started—could be addressed, and measures for improving energy efficiency can continuously be put in place. This will likely include measures that could both increase the yield and decrease costs (operational and environmental).

To this end, the layout of the facility, along with the logistics and technical infrastructure, will be designed in such a way as to ease replacement of components with better-performing or lower-consumption ones (e.g. supplies, magnets, cryogenics equipment, and air conditioning): the buildings themselves, as well as cranes, cable trays, galleries, etc., shall be designed to facilitate the manipulation, replacement, and reconfiguration of components in the halls, with minimal compromise of the overall footprint and minimal additional costs.

3.11 Investments and personnel for constructing and running the RI

3.11.1 Construction costs

Table 13 lists the investments required for constructing, mounting, checking, commissioning, and integrating all the instruments needed to:

(i) accelerate and distribute the ion beams;

(ii) to prepare the experimental hall for receiving the apparatus that will be mounted and dismounted according to need and used by the internal and visiting scientists to perform their experiments.

On the basis of the experience in realising the existing European ion therapy centres, it is estimated that 5.5 years will be needed from the beginning of the on-site construction to the end of the commissioning of the first beamline in the experimental hall before the experimental programme can start. At least another year will be needed to commission the first clinical beam of the two rooms devoted to patient treatment with fixed beams.

In compiling **Table 13**, it has been assumed that the construction of the new facility would be entrusted to a “main contractor” company that would provide all the work needed for procurement, construction, installation, and on-site commissioning of the various high-tech components, integrating them into buildings constructed by a “building company”. Indeed, the design of the facility should be the responsibility of the proposed new RI project, which would provide all the necessary information to allow the building company to construct the buildings and to allow the main contractor to realise, mount, and test the high-tech part of the RI.

The proposed RI should have its own "construction team"; one full-time equivalent of senior personnel per system has been considered as the average work required for the 5.5 years of the realisation project (row 1 of **Table 13**). The administrative experts of the construction team should prepare the contracts with the main contractor, the building company, and all the hardware and software companies that will work for the facility. The other technical members of the construction team will interface with the many external institutes, which would continue to support the initiative and provide not only the necessary expertise but also the technical specification and designs, which will be passed to the main contractor and to the building company. The construction team should also define the interface between the works entrusted to these two companies. About one year before start-up, this team should be joined by the staff needed to run the facility, who will have to be trained either externally, at other running centres, or in house by senior members of staff.

As shown in row 3 of **Table 13**, over the 5.5 years needed before the start of the first experiment, the construction team is estimated to cost, on average, EUR 3 million per year; however, the funds needed are expected to be lower at the beginning and higher at the end.

The entries of **Table 13** have been estimated assuming that the layout is that shown in **Fig. 73**, based on the CNAO design, with all the improvements discussed in Section 3.2. All the prices are based on detailed commercial offers obtained in 2016 by CNAO, from many different companies, for a similar facility; the prices have been updated (before the war in Ukraine) with a 10% increase to consider the time elapsed. The quoted prices include construction, procurement of the various parts (if the main contractor needs to buy some of them), project management within the main contractor, shipping, installation, and commissioning of the parts. The cabling is included in the cost of the components, while the IT infrastructure and its cabling are part of the cost of the building.

At variance with all the other components, the price of the gantry (row 25) is not based on an offer. The cost of the hardware and software realisation of the gantry has been estimated to be EUR 18 million, to which a 30% contingency has been added to obtain EUR 23.5 million. The design of this device is the focus of a large R&D European effort with the participation of top experts, as described in Section 3.6 and [141].

Table 13: Investments in thousands of Euros.

	kEUR
General expenses during construction and commissioning (5.5 years)	
1. Construction team managing the project	9500
2. Budget to cover administrative and general expenses	7350
3. Total for expenses during constr. and comm.	**16,850**
Accelerator system and beamlines	
4. Three sources	8250
5. Magnets, vacuum systems, mechanics, and supports	30,300
6. Beam diagnostics	9650
7. Power supplies	22,700
8. 7 MeV/u injector system	15,400
9. Safety and radiation systems	1200
10. General control system	12,100
11. Total for accelerator systems	**99,600**
Instrumentation for non-clinical research	
12. Common equipment for the experimental hall	1500
13. Equipment for radiobiology experiments	550
14. Equipment for animal studies	1600
15. Equipment for medical physics experiments	850
16. Equipment for materials science experiments	650
17. Total for non-clinical research	**5150**
Instrumentation for clinical research with hor./vert. beams	
18. Control system	6050
19. Nozzle	5600
20. Treatment planning system (TPS)	4050
21. Oncological information system (OIS)	4600
22. Patient positioning and verification systems	6950
23. Dosimetry devices	650
24. Total for clinical research	**27,900**
25. Total for the carbon ion gantry	**23,500**
26. TOTAL HIGH-TECH COMPONENTS	**173,000**
27. Building	**45,000**
28. TOTAL	**218,000**

A contingency is considered at the level of 15% for the high-tech components (row 26), reduced by the cost of the gantry, which already includes a EUR 5.5 million contingency (30% of the estimated

cost). Overall, the cost of the proposed facility for SEEIIST—without buildings—is EUR 167.5 million, and the contingency is EUR 28 million.

Before concluding this section, it has to be underlined that the investments of **Table 13** *do not* include:

(i) the instrumentation for medical diagnostics (CT, PET, CT/PET, MRI, etc.);

(ii) the X-ray therapy instruments that could be needed to treat some patients with conventional radiation, for instance, in the framework of a combined treatment with carbon ions.

These needs will strongly depend on the instrumentation available in a nearby hospital, if any. If no hospital is close enough, the overall investment for points (i) and (ii) would be about EUR 8 million.

3.11.2 Personnel needed for running the RI

The different professional figures needed for running the facility are listed in **Table 14**.

The personnel of row 19 are such that the accelerator can run 24 h a day, seven days a week. Every year, four short maintenance periods will be scheduled, one per quarter, during which the technical staff will be in charge of performing and coordinating system maintenance. The table shows that during the operation phase:

(i) 39 people are needed for running the facility;

(ii) 28 people are foreseen to support the external groups performing experiments in the two experimental areas—in radiobiology (in vitro and in vivo), medical physics, and materials science—and to perform their own experiments;

(iii) 38 people are foreseen for the clinical programme in the three treatment rooms.

Table 14: Personnel required during the running phase.

General direction and staff	
1. Director General	1
2. Scientific direction	3
3. Communication and outreach	2
4. Legal affairs	1
5. Human resources	2
6. Quality and regulatory affairs	1
7. Radioprotection	1
8. Safety and prevention	1
9. Total for general direction and staff	**12**
Administration and finance	
10. Budget control and accounting	4
11. Procurement and logistics	3
12. Patients' front desk	4
13. Total for administration and finance	**11**
Accelerator and high-tech: Operation, maintenance, and upgrades	
14. Technical Director	1
15. Experts (physicists and engineers)	20
16. Technical operators	9
17. Information technology support	4
18. Buildings and plant	5
19. Total for accelerator and high-tech	**39**
Experimental Department	
20. Director of the Experimental Department	1
21. Staff	27
22. Total for the Experimental Department	**28**
Medical Department	
23. Director of the Medical Department	1
24. Secretariat of the Medical Department	1
25. Medical officers	2
26. Physician	9
27. Medical physicists	6
28. Radiation and diagnostics technicians	12
29. Nurses	4
30. Bioengineers and experts in IT	3
31. Total for the Medical Department	**38**
32. TOTAL	**128**

Table 15: Personnel of the experimental department.

	Speciality	Units
General	Secretariat of the department	2
	Software engineers	1
	Technicians running the experimental areas	2
	Total	**4**
Radiobiology in vitro	Senior radiobiologists	1
	Junior radiobiologists	2
	Radiobiology technicians	3
	Total for the radiobiology programme	**6**
Animal studies	Senior veterinary	1
	Junior veterinary	2
	Technicians (including the animal facility)	3
	Total for the animal programme	**6**
Medical physics	Senior physicists	1
	Junior physicists	2
	Technicians	3
	Total for the medical physics programme	**6**
Materials science	Senior physicists	1
	Junior physicists	1
	Technicians	2
	Total for the materials science programme	**4**
	TOTAL	**27**

Table 15 describes the competences required of the staff belonging to the experimental division (row 21 of **Table 14**). At the present stage, it is impossible to know what the needs of the various programmes will be, and the content of this table is an educated guess. However, it highlights a very important aspect of the proposed RI: at variance with what happens in all existing facilities, the new proposed facility will support external experimental teams with a large group of local scientists and experts who, in most cases, will also participate in the experiments of the visiting groups.

3.11.3 Running costs during the exploitation years

It is well known that high running costs are a major problem for all RIs. This will not be the case for the proposed new RI because of the income expected from patient treatments, which can *significantly reduce these costs*. This is evident from **Table 16**, which has been filled using the many years of experience of CNAO. In particular, the CNAO salaries have been used to compute the yearly cost of the personnel of row 5.

As shown in row 7, the yearly running costs are EUR 18.1 million, from which the income expected from the treatments of the human patients has to be subtracted.

In filling row 8, the hypothesis has been made that, after 3–4 years of treatments, 250 patients/year would be irradiated in each one of the three rooms if the facility is able to run full time. With the 50% choice, this corresponds to a total of 375 patients/year in all three rooms, assuming that the large majority of these patients will be treated with carbon ions.

Table 16: Running costs per year.

Item	Yearly expenditure MEUR
1. Investments in the internal research programmes	1.6
2. Consumables for irradiating patients	0.5
3. Maintenance and upgrades	4.8
4. Power and utilities	2.0
5. Personnel (128 staff)	7.7
6. General expenses	1.5
7. Total	**18.1**
8. Income for 375 patients/year at 25,000 EUR/patient[(a)]	**−9.3**
Part of the yearly running cost to be covered by external sources	**8.8**

(a) This number of patients will be reached after about 3–4 years of treatments.

With an average fee of 25,000 EUR/patient—a typical European cost for a full carbon ion course, which is more expensive than a proton therapy treatment—the income of row 8 (9.3 million EUR/year) will correspond to about half of the total running cost.

Of course, the basic decision to irradiate patients *only* 50% of the weekday time reduces the potential income and thus increases the yearly running cost to be financed by external sources: about EUR 9 million with the assumptions made in filling **Table 16**. The balance is delicate and depends upon the number of patients who can be treated in the available time. This is a *clear advantage* of the chosen running scheme because, if the imbalance were too large, it would be always possible to increase the flow by 100 patients/year to raise an additional income of about 2.5 million EUR/year. This addition will not necessarily imply that the time dedicated to research activities in the two experimental areas will be reduced. In fact, since these experiments usually require long installation and calibration times but short runs, after years of experience, it will be possible to run some of them *in parallel* with the irradiation of patients.

In summary, according to the organisational scheme presented in **Table 15** and **Table 16**, only about 30% of workers belong to the medical department (row 31 of **Table 16**), but their clinical activities produce the income of row 8, which reduces the total expenditure required to run the RI by a *factor of two*. This factor can be adapted by adjusting either the number of patients treated yearly or the fees. This is easily achievable, especially considering the ongoing tendency to decrease the number of sessions needed per patient when treating with C-ion beams. This can be done without renouncing the basic idea that makes the proposed RI a globally unique synchrotron-based ion facility that, while dedicated for a very large amount of time to research in radiobiology, animal studies, medical physics and materials science, will require limited external financing during its long lifespan of typically 30–40 years.

References and notes

[1] U. Amaldi, J. Balosso, M. Dosanjh, J. Overgaard, S. Rossi, M. Scholz, and B. Singers Sørensen, A Facility for Tumour Therapy and Biomedical Research in South-Eastern Europe, CERN, Geneva, 2019.

[2] P. J. Bryant, L. Badano, M. Benedikt, M. Crescenti, P. Holy, A. T. Maier, M. Pullia, S. Reimoser, S. Rossi, G. Borri, P. Knaus, F. Gramatica, M. Pavlovic, and L. Weisser, Proton-Ion Medical Machine Study (PIMMS), 2, CERN, Geneva, 2000.

[3] J. Bourhis, W. J. Sozzi, P. G. Jorge, O. Gaide, C. Bailat, F. Duclos, D. Patin, M. Ozsahin, F. Bochud, J.-F. Germond, R. Moeckli, and M.-C. Vozenin, "Treatment of a first patient with FLASH-radiotherapy," *Radiotherapy and Oncology,* vol. 139, p. 18–22, 2019.

[4] V. Favaudon, L. Caplier, V. Monceau, F. Pouzoulet, M. Sayarath, C. Fouillade, M.-F. Poupon, I. Brito, P. Hupé, J. Bourhis, J. Hall, J.-J. Fontaine, and M.-C. Vozenin, "Ultrahigh dose-rate FLASH irradiation increases the differential response between normal and tumor tissue in mice," *Science Translational Medicine,* vol. 6, p. 245ra93–245ra93, 2014.

[5] M. Dosanjh, F.-G. Angeles, R. Corsini, and M. Vozenin, "Very high-energy electrons for cancer therapy," *CERN Courier,* vol. 60, 2020.

[6] L. Badano, M. Benedikt, P. J. Bryant, M. Crescenti, P. Holy, A. T. Maier, M. Pullia, S. Rossi, and P. Knaus, Proton-Ion Medical Machine Study (PIMMS), 1, CERN, Geneva, 1999.

[7] The plan shown in panel (a) was designed by A. Magliari (Varian) and was awarded the top scoring in the 2016 American Association of Medical Dosimetrists and Radiosurgery Society Plan Study.

[8] T. F. De Laney and H. M. Kooy, Proton and Charged Particle Radiotherapy, Lippincott Williams & Wilkins, 2008.

[9] H. Paganetti, Proton Therapy Physics, Second Edition, CRC Press, 2018.

[10] C. M. C. Ma and T. Lomax, Proton and Carbon Ion Therapy, CRC Press, 2012.

[11] U. Amaldi and G. Hall, Particle Accelerators: From Big Bang Physics to Hadron Therapy, Springer International Publishing, 2014.

[12] U. Amaldi and G. Kraft, "Radiotherapy with beams of carbon ions," *Reports on Progress in Physics,* vol. 68, p. 1861–1882, 2005.

[13] A. J. Lomax, "Charged particle therapy: The physics of interaction," *The Cancer Journal,* vol. 15, 2009.

[14] D. Schardt, T. Elsässer, and D. Schulz-Ertner, "Heavy-ion tumor therapy: Physical and radiobiological benefits," *Rev. Mod. Phys.,* vol. 82, no. 1, p. 383–425, 2010.

[15] D. Belkić, "Review of theories on ionization in fast ion-atom collisions with prospects for applications to hadron therapy," *Journal of Mathematical Chemistry,* vol. 47, p. 1366–1419, 2010.

[16] H. Bichsel, "Chapter One - Stochastics of Energy Loss and Biological Effects of Heavy Ions in Radiation Therapy," in *Theory of Heavy Ion Collision Physics in Hadron Therapy*, vol. 65, D. Belkić, Ed., Academic Press, 2013, p. 1–38.

[17] W. D. Newhauser and R. Zhang, "The physics of proton therapy," *Physics in Medicine and Biology,* vol. 60, p. R155–R209, 2015.

[18] M. Durante and H. Paganetti, “Nuclear physics in particle therapy: A review,” *Reports on Progress in Physics,* vol. 79, p. 096702, 2016.

[19] C. Bert and M. Durante, “Motion in radiotherapy: particle therapy,” *Physics in Medicine and Biology,* vol. 56, p. R113–R144, 2011.

[20] H. Tsujii, T. Kamada, T. Shirai, K. Noda, H. Tsuji, and K. Karasawa, Carbon-Ion Radiotherapy: Principles, Practices, and Treatment Planning, Springer Japan, 2013.

[21] T. Friedrich, U. Scholz, T. ElsäSser, M. Durante, and M. Scholz, “Systematic analysis of RBE and related quantities using a database of cell survival experiments with ion beam irradiation,” *Journal of Radiation Research,* vol. 54, p. 494–514, 2012.

[22] R. Grün, T. Friedrich, T. Elsässer, M. Krämer, K. Zink, C. P. Karger, M. Durante, R. Engenhart-Cabillic, and M. Scholz, “Impact of enhancements in the local effect model (LEM) on the predicted RBE-weighted target dose distribution in carbon ion therapy,” *Physics in Medicine and Biology,* vol. 57, p. 7261–7274, 2012.

[23] M. Durante, “New challenges in high-energy particle radiobiology,” *The British Journal of Radiology,* vol. 87, p. 20130626, 2014.

[24] The RBE values in Figure 19a correspond to a 10% survival rate of human salivary gland cells. Cho, I., Yoo, S., and Cho, S., “Modelling the biophysical effects in a carbon beam delivery line by using Monte Carlo simulations,” *Journal of the Korean Physical Society*.

[25] T. Kamada, H. Tsujii, E. A. Blakely, J. Debus, W. D. Neve, M. Durante, O. Jäkel, R. Mayer, R. Orecchia, R. Pötter, S. Vatnitsky, and W. T. Chu, “Carbon ion radiotherapy in Japan: An assessment of 20 years of clinical experience,” *The Lancet Oncology,* vol. 16, p. e93–e100, 2015.

[26] O. Mohamad, T. Tabuchi, Y. Nitta, A. Nomoto, A. Sato, G. Kasuya, H. Makishima, H. Choy, S. Yamada, T. Morishima, H. Tsuji, I. Miyashiro, and T. Kamada, “Risk of subsequent primary cancers after carbon ion radiotherapy, photon radiotherapy, or surgery for localised prostate cancer: A propensity score-weighted, retrospective, cohort study,” *The Lancet Oncology,* vol. 20, p. 674–685, 2019.

[27] M. Durante, R. Orecchia, and J. S. Loeffler, “Charged-particle therapy in cancer: Clinical uses and future perspectives,” *Nature Reviews Clinical Oncology,* vol. 14, p. 483–495, 2017.

[28] M. Mima, Y. Demizu, D. Jin, N. Hashimoto, M. Takagi, K. Terashima, O. Fujii, Y. Niwa, T. Akagi, T. Daimon, Y. Hishikawa, M. Abe, M. Murakami, R. Sasaki, and N. Fuwa, “Particle therapy using carbon ions or protons as a definitive therapy for patients with primary sacral chordoma,” *The British Journal of Radiology,* vol. 87, p. 20130512, 2014.

[29] M. Takagi, Y. Demizu, N. Hashimoto, M. Mima, K. Terashima, O. Fujii, D. Jin, Y. Niwa, K. Morimoto, T. Akagi, T. Daimon, R. Sasaki, Y. Hishikawa, M. Abe, M. Murakami, and N. Fuwa, “Treatment outcomes of particle radiotherapy using protons or carbon ions as a single-modality therapy for adenoid cystic carcinoma of the head and neck,” *Radiotherapy and Oncology,* vol. 113, p. 364–370, 2014.

[30] T. Rackwitz and J. Debus, “Clinical applications of proton and carbon ion therapy,” *Seminars in Oncology,* vol. 46, p. 226–232, 2019.

[31] A. Iannalfi, E. D’Ippolito, G. Riva, S. Molinelli, S. Gandini, G. Viselner, M. R. Fiore, B. Vischioni, V. Vitolo, M. Bonora, S. Ronchi, R. Petrucci, A. Barcellini, A. Mirandola, S. Russo, A. Vai, E. Mastella, G. Magro, D. Maestri, M. Ciocca, L. Preda, F. Valvo, and R. Orecchia, “Proton and carbon ion radiotherapy in skull base

chordomas: A prospective study based on a dual particle and a patient-customized treatment strategy," *Neuro-Oncology,* 2020.

[32] H. Tsujii, J.-e. Mizoe, T. Kamada, M. Baba, S. Kato, H. Kato, H. Tsuji, S. Yamada, S. Yasuda, T. Ohno, T. Yanagi, A. Hasegawa, T. Sugawara, H. Ezawa, S. Kandatsu, and Yo, "Overview of clinical experiences on carbon ion radiotherapy at NIRS," *Radiotherapy and Oncology,* vol. 73, p. S41–S49, 2004.

[33] T. Okada, T. Kamada, H. Tsuji, J.-e. Mizoe, M. Baba, S. Kato, S. Yamada, S. Sugahara, S. Yasuda, N. Yamamoto, R. Imai, A. Hasegawa, H. Imada, H. Kiyohara, K. Jingu, and M. Shinoto, "Carbon ion radiotherapy: Clinical experiences at National Institute of Radiological Science (NIRS)," *Journal of Radiation Research,* vol. 51, p. 355–364, 2010.

[34] T. Kanai, Y. Furusawa, K. Fukutsu, H. Itsukaichi, K. Eguchi-Kasai, and H. Ohara, "Irradiation of mixed beam and design of spread-out bragg peak for heavy-ion radiotherapy," *Radiation Research,* vol. 147, p. 78–85, 1997.

[35] M. Goitein, "Trials and tribulations in charged particle radiotherapy," *Radiotherapy and Oncology,* vol. 95, p. 23–31, 2010.

[36] M. V. Mishra, S. Aggarwal, S. M. Bentzen, N. Knight, M. P. Mehta, and W. F. Regine, "Establishing evidence-based indications for proton therapy: An overview of current clinical trials," *International Journal of Radiation Oncology*Biology*Physics,* vol. 97, p. 228–235, 2017.

[37] P. Fossati, N. Matsufuji, T. Kamada, and C. P. Karger, "Radiobiological issues in prospective carbon ion therapy trials," *Medical Physics,* vol. 45, p. e1096–e1110, 2018.

[38] M. Uhl, L. Edler, A. D. Jensen, G. Habl, J. Oelmann, F. Röder, O. Jäckel, J. Debus, and K. Herfarth, "Randomized phase II trial of hypofractionated proton versus carbon ion radiation therapy in patients with sacrococcygeal chordoma-the ISAC trial protocol," *Radiation Oncology,* vol. 9, p. 100, 2014.

[39] A. V. Nikoghosyan, I. Karapanagiotou-Schenkel, M. W. Münter, A. D. Jensen, S. E. Combs, and J. Debus, "Randomised trial of proton vs. carbon ion radiation therapy in patients with chordoma of the skull base, clinical phase III study HIT-1-Study," *BMC Cancer,* vol. 10, p. 607, 2010.

[40] S. Rieken, D. Habermehl, A. Nikoghosyan, A. Jensen, T. Haberer, O. Jäkel, M. W. Münter, T. Welzel, J. Debus, and S. E. Combs, "Assessment of early toxicity and response in patients treated with proton and carbon ion therapy at the Heidelberg Ion Therapy Center using the raster scanning technique," *International Journal of Radiation Oncology Biology Physics,* vol. 81, p. e793–e801, 2011.

[41] M. Shinoto, S. Yamada, S. Yasuda, H. Imada, Y. Shioyama, H. Honda, T. Kamada, H. Tsujii, H. Saisho, and W. G. for Pancreas Cancer, "Phase 1 trial of preoperative, short-course carbon-ion radiotherapy for patients with resectable pancreatic cancer," *Cancer,* vol. 119, p. 45–51, 2013.

[42] M. Durante, F. Tommasino, and S. Yamada, "Modeling combined chemotherapy and particle therapy for locally advanced pancreatic cancer," *Frontiers in Oncology,* vol. 5, p. 145, 2015.

[43] L. Schaub, S. B. Harrabi, and J. Debus, "Particle therapy in the future of precision therapy," *The British Journal of Radiology,* p. 20200183.

[44] T. D. Malouff, A. Mahajan, S. Krishnan, C. Beltran, D. S. Seneviratne, and D. M. Trifiletti, "Carbon ion therapy: A modern review of an emerging technology," *Frontiers in Oncology,* vol. 10, p. 82, 2020.

[45] S. E. Combs and J. Debus, "Treatment with heavy charged particles: Systematic review of clinical data and current clinical (comparative) trials," *Acta Oncologica,* vol. 52, p. 1272–1286, 2013.

[46] W. D. Newhauser and M. Durante, "Assessing the risk of second malignancies after modern radiotherapy," *Nature Reviews Cancer,* vol. 11, p. 438–448, 2011.

[47] C. L. Tessa, T. Berger, R. Kaderka, D. Schardt, C. Körner, U. Ramm, J. Licher, N. Matsufuji, C. V. Dahlgren, T. Lomax, G. Reitz, and M. Durante, "Out-of-field dose studies with an anthropomorphic phantom: Comparison of X-rays and particle therapy treatments," *Radiotherapy and Oncology,* vol. 105, p. 133–138, 2012.

[48] M. H. Baron, P. Pommier, V. Favrel, G. Truc, J. Balosso, and J. Rochat, "A 'One-day survey': As a reliable estimation of the potential recruitment for proton- and carbon-ion therapy in France," *Radiotherapy and Oncology,* vol. 73, p. S15–S17, 2004.

[49] Q. Cheng, E. Roelofs, B. L. T. Ramaekers, D. Eekers, J. van Soest, T. Lustberg, T. Hendriks, F. Hoebers, H. P. van der Laan, E. W. Korevaar, A. Dekker, J. A. Langendijk, and P. Lambin, "Development and evaluation of an online three-level proton vs photon decision support prototype for head and neck cancer – Comparison of dose, toxicity and cost-effectiveness," *Radiotherapy and Oncology,* vol. 118, p. 281–285, 2016.

[50] M. Garcia-Barros, F. Paris, C. Cordon-Cardo, D. Lyden, S. Rafii, A. Haimovitz-Friedman, Z. Fuks, and R. Kolesnick, "Tumor response to radiotherapy regulated by endothelial cell apoptosis," *Science,* vol. 300, p. 1155–1159, 2003.

[51] Y. Yamada, M. H. Bilsky, D. M. Lovelock, E. S. Venkatraman, S. Toner, J. Johnson, J. Zatcky, M. J. Zelefsky, and Z. Fuks, "High-dose, single-fraction image-guided intensity-modulated radiotherapy for metastatic spinal lesions," *International Journal of Radiation Oncology*Biology*Physics,* vol. 71, p. 484–490, 2008.

[52] Y. Takahashi, T. Teshima, N. Kawaguchi, Y. Hamada, S. Mori, A. Madachi, S. Ikeda, H. Mizuno, T. Ogata, K. Nojima, Y. Furusawa, and N. Matsuura, "Heavy ion irradiation inhibits in vitro angiogenesis even at sublethal dose," *Cancer Research,* vol. 63, p. 4253–4257, 2003.

[53] J. M. Brown, D. J. Brenner, and D. J. Carlson, "Dose escalation, not 'new biology, ' can account for the efficacy of stereotactic body radiation therapy with non-small cell lung cancer," *International Journal of Radiation Oncology Biology Physics,* vol. 85, p. 1159–1160, 2013.

[54] T. Miyamoto, M. Baba, N. Yamamoto, M. Koto, T. Sugawara, T. Yashiro, K. Kadono, H. Ezawa, H. Tsujii, J.-E. Mizoe, K. Yoshikawa, S. Kandatsu, and T. Fujisawa, "Curative treatment of Stage I non-small-cell lung cancer with carbon ion beams using a hypofractionated regimen," *International Journal of Radiation Oncology Biology Physics,* vol. 67, p. 750–758, 2007.

[55] W. Tinganelli, M. Durante, R. Hirayama, M. Krämer, A. Maier, W. Kraft-Weyrather, Y. Furusawa, T. Friedrich, and E. Scifoni, "Kill-painting of hypoxic tumours in charged particle therapy," *Scientific Reports,* vol. 5, p. 17016, 2015.

[56] T. Shimokawa, L. Ma, K. Ando, K. Sato, and T. Imai, "The future of combining carbon-ion radiotherapy with immunotherapy: Evidence and progress in mouse models," *International Journal of Particle Therapy,* vol. 3, p. 61–70, 2016.

[57] M. Durante, S. Yamada, K. Ando, Y. Furusawa, T. Kawata, H. Majima, T. Nakano, and H. Tsujii, "X-rays vs. carbon-ion tumor therapy: Cytogenetic damage in lymphocytes," *International Journal of Radiation Oncology*Biology*Physics,* vol. 47, p. 793–798, 2000.

[58] M. Durante and S. Formenti, "Harnessing radiation to improve immunotherapy: Better with particles?," *The British Journal of Radiology,* vol. 93, p. 20190224, 2020.

[59] C. Barlow, M. A. Eckhaus, A. A. Schäffer, and A. Wynshaw-Boris, "*Atm* haploinsufficiency results in increased sensitivity to sublethal doses of ionizing radiation in mice," *Nature Genetics,* vol. 21, p. 359–360, 1999.

[60] B. V. Worgul, L. Smilenov, D. J. Brenner, A. Junk, W. Zhou, and E. J. Hall, "*Atm* heterozygous mice are more sensitive to radiation-induced cataracts than are their wild-type counterparts," *Proceedings of the National Academy of Sciences,* vol. 99, p. 9836–9839, 2002.

[61] L.-H. Ding, S. Park, M. Peyton, L. Girard, Y. Xie, J. D. Minna, and M. D. Story, "Distinct transcriptome profiles identified in normal human bronchial epithelial cells after exposure to γ-rays and different elemental particles of high Z and energy," *BMC Genomics,* vol. 14, p. 372, 2013.

[62] S. A. Amundson, K. T. Do, L. C. Vinikoor, R. A. Lee, C. A. Koch-Paiz, J. Ahn, M. Reimers, Y. Chen, D. A. Scudiero, J. N. Weinstein, J. M. Trent, M. L. Bittner, P. S. Meltzer, and A. J. Fornace, "Integrating global gene expression and radiation survival parameters across the 60 cell lines of the National Cancer Institute Anticancer Drug Screen," *Cancer Research,* vol. 68, p. 415–424, 2008.

[63] S. Eschrich, H. Zhang, H. Zhao, D. Boulware, J.-H. Lee, G. Bloom, and J. F. Torres-Roca, "Systems biology modeling of the radiation sensitivity network: A biomarker discovery platform," *International Journal of Radiation Oncology*Biology*Physics,* vol. 75, p. 497–505, 2009.

[64] J. H. Schiller, D. Harrington, C. P. Belani, C. Langer, A. Sandler, J. Krook, J. Zhu, and D. H. Johnson, "Comparison of four chemotherapy regimens for advanced non–small-cell lung cancer," *New England Journal of Medicine,* vol. 346, p. 92–98, 2002.

[65] B. J. Moeller, J. S. Yordy, M. D. Williams, U. Giri, U. Raju, D. P. Molkentine, L. A. Byers, J. V. Heymach, M. D. Story, J. J. Lee, E. M. Sturgis, R. S. Weber, A. S. Garden, K. K. Ang, and D. L. Schwartz, "DNA repair biomarker profiling of head and neck cancer: Ku80 expression predicts locoregional failure and death following radiotherapy," *Clinical Cancer Research,* vol. 17, p. 2035–2043, 2011.

[66] F. Merz, F. Gaunitz, F. Dehghani, C. Renner, J. Meixensberger, A. Gutenberg, A. Giese, K. Schopow, C. Hellwig, M. Schäfer, M. Bauer, H. Stöcker, G. Taucher-Scholz, M. Durante, and Be, "Organotypic slice cultures of human glioblastoma reveal different susceptibilities to treatments," *Neuro-Oncology,* vol. 15, p. 670–681, 2013.

[67] F. Tommasino, E. Scifoni, and M. Durante, "New ions for therapy," *International Journal of Particle Therapy,* vol. 2, p. 428–438, 2016.

[68] T. Tessonnier, S. Ecker, J. Besuglow, J. Naumann, S. Mein, F. K. Longarino, M. Ellerbrock, B. Ackermann, M. Winter, S. Brons, A. Qubala, T. Haberer, J. Debus, and O. Jäkel, "Commissioning of helium ion therapy and the first patient treatment with active beam delivery," *International Journal of Radiation Oncology*Biology*Physics,* Vol. 116, p. 935–948, 2023.

[69] M. Durante, A. Golubev, W.-Y. Park, and C. Trautmann, “Applied nuclear physics at the new high-energy particle accelerator facilities,” *Physics Reports,* vol. 800, p. 1–37, 2019.

[70] M. Durante and K. Parodi, “Radioactive beams in particle therapy: Past, present, and future,” *Frontiers in Physics,* vol. 8, p. 326, 2020.

[71] M. Baumann, M. Krause, J. Overgaard, J. Debus, S. M. Bentzen, J. Daartz, C. Richter, D. Zips, and T. Bortfeld, “Radiation oncology in the era of precision medicine,” *Nature Reviews Cancer,* vol. 16, p. 234–249, 2016.

[72] P. F. Cosper, L. Abel, Y.-S. Lee, C. Paz, S. Kaushik, K. P. Nickel, R. Alexandridis, J. G. Scott, J. Y. Bruce, and R. J. Kimple, “Patient derived models to study head and neck cancer radiation response,” *Cancers,* vol. 12, p. 419, 2020.

[73] F. Ishikawa, M. Yasukawa, B. Lyons, S. Yoshida, T. Miyamoto, G. Yoshimoto, T. Watanabe, K. Akashi, L. D. Shultz, and M. Harada, “Development of functional human blood and immune systems in NOD/SCID/IL2 receptor γ chainnull mice,” *Blood,* vol. 106, p. 1565–1573, 2005.

[74] M. R. Horsman, D. W. Siemann, D. J. Chaplin, and J. Overgaard, “Nicotinamide as a radiosensitizer in tumours and normal tissues: The importance of drug dose and timing,” *Radiotherapy and Oncology,* vol. 45, p. 167–174, 1997.

[75] H. B. Stone, “Leg contracture in mice: An assay of normal tissue response,” *International Journal of Radiation Oncology*Biology*Physics,* vol. 10, p. 1053–1061, 1984.

[76] A. J. van der Kogel, “Chronic effects of neutrons and charged particles on spinal cord, lung, and rectum,” *Radiation Research,* vol. 104, p. S208–S216, 1985.

[77] H. von der Maase, J. Overgaard, and M. Vaeth, “Effect of cancer chemotherapeutic drugs on radiation-induced lung damage in mice,” *Radiotherapy and Oncology,* vol. 5, p. 245–257, 1986.

[78] F. Lundbeck, “An experimental in vivo model in mice to evaluate the change in reservoir function of the urinary bladder due to irradiation alone or combined with chemotherapy,” in Acute and Long-Term Side-Effects of Radiotherapy, Berlin, 1993.

[79] M. E. Forbes, M. Paitsel, J. D. Bourland, and D. R. Riddle, “Early-delayed, radiation-induced cognitive deficits in adult rats are heterogeneous and age-dependent,” *Radiation Research,* vol. 182, p. 60–71, 2014.

[80] B. S. Sørensen, M. R. Horsman, J. Alsner, J. Overgaard, M. Durante, M. Scholz, T. Friedrich, and N. Bassler, “Relative biological effectiveness of carbon ions for tumor control, acute skin damage and late radiation-induced fibrosis in a mouse model,” *Acta Oncologica,* vol. 54, p. 1623–1630, 2015.

[81] P. S. Cuculich, M. R. Schill, R. Kashani, S. Mutic, A. Lang, D. Cooper, M. Faddis, M. Gleva, A. Noheria, T. W. Smith, D. Hallahan, Y. Rudy, and C. G. Robinson, “Noninvasive cardiac radiation for ablation of ventricular tachycardia,” *New England Journal of Medicine,* vol. 377, p. 2325–2336, 2017.

[82] H. I. Lehmann, C. Graeff, P. Simoniello, A. Constantinescu, M. Takami, P. Lugenbiel, D. Richter, A. Eichhorn, M. Prall, R. Kaderka, F. Fiedler, S. Helmbrecht, C. Fournier, N. Erbeldinger, A.-K. Rahm, R. Rivinius, D. Thomas, H. A. Katus, S. B. Johnson, K. D. Parker, J. Debus, S. J. Asirvatham, C. Bert, M. Durante, and D. L. Packer, “Feasibility study on cardiac arrhythmia ablation using high-energy heavy ion beams,” *Scientific Reports,* vol. 6, p. 38895, 2016.

[83] V. Dusi, G. Russo, G. I. Forte, and G. M. D. Ferrari, "Non-invasive ablation of cardiac arrhythmia. Is proton radiation therapy a step forward?," *International Journal of Cardiology,* vol. 313, p. 64–66, 2020.

[84] S. Mein, I. Dokic, C. Klein, T. Tessonnier, T. T. Böhlen, G. Magro, J. Bauer, A. Ferrari, K. Parodi, T. Haberer, J. Debus, A. Abdollahi, and A. Mairani, "Biophysical modeling and experimental validation of relative biological effectiveness (RBE) for ^{4}He ion beam therapy," *Radiation Oncology,* vol. 14, p. 123, 2019.

[85] B. Kopp, S. Mein, I. Dokic, S. Harrabi, T. T. Böhlen, T. Haberer, J. Debus, A. Abdollahi, and A. Mairani, "Development and validation of single field multi-ion particle therapy treatments," *International Journal of Radiation Oncology*Biology*Physics,* vol. 106, p. 194–205, 2020.

[86] T. Tessonnier, T. T. Böhlen, F. Ceruti, A. Ferrari, P. Sala, S. Brons, T. Haberer, J. Debus, K. Parodi, and A. Mairani, "Dosimetric verification in water of a Monte Carlo treatment planning tool for proton, helium, carbon and oxygen ion beams at the Heidelberg Ion Beam Therapy Center," *Physics in Medicine & Biology,* vol. 62, p. 6579–6594, 2017.

[87] F. Horst, G. Aricò, K.-T. Brinkmann, S. Brons, A. Ferrari, T. Haberer, A. Mairani, K. Parodi, C.-A. Reidel, U. Weber, K. Zink, and C. Schuy, "Measurement of ^{4}He charge- and mass-changing cross sections on H, C, O, and Si targets in the energy range 70–220 MeV/u for radiation transport calculations in ion-beam therapy," *Physical Review C,* vol. 99, no. 1, p. 014603, 2019.

[88] A. Ferrari, P. R. Sala, A. Fasso, and J. Ranft, FLUKA: A Multi-Particle Transport Code (Program Version 2005), CERN, Geneva, 2005.

[89] M. Martišíková, T. Gehrke, S. Berke, G. Aricò, and O. Jäkel, "Helium ion beam imaging for image guided ion radiotherapy," *Radiation Oncology,* vol. 13, p. 109, 2018.

[90] W. Enghardt, P. Crespo, F. Fiedler, R. Hinz, K. Parodi, J. Pawelke, and F. Pönisch, "Charged hadron tumour therapy monitoring by means of PET," *Nuclear Instruments and Methods in Physics Research Section A: Accelerators, Spectrometers, Detectors and Associated Equipment,* vol. 525, p. 284–288, 2004.

[91] K. Parodi and W. Assmann, "Ionoacoustics: A new direct method for range verification," *Modern Physics Letters A,* vol. 30, p. 1540025, 2015.

[92] A. Mairani, T. T. Böhlen, A. Schiavi, T. Tessonnier, S. Molinelli, S. Brons, G. Battistoni, K. Parodi, and V. Patera, "A Monte Carlo-based treatment planning tool for proton therapy," *Physics in Medicine and Biology,* vol. 58, p. 2471–2490, 2013.

[93] T. T. Böhlen, J. Bauer, M. Dosanjh, A. Ferrari, T. Haberer, K. Parodi, V. Patera, and A. Mairani, "A Monte Carlo-based treatment-planning tool for ion beam therapy," *Journal of Radiation Research,* vol. 54, p. i77–i81, 2013.

[94] S. Mein, K. Choi, B. Kopp, T. Tessonnier, J. Bauer, A. Ferrari, T. Haberer, J. Debus, A. Abdollahi, and A. Mairani, "Fast robust dose calculation on GPU for high-precision ^{1}H, ^{4}He, ^{12}C and ^{16}O ion therapy: The FRoG platform," *Scientific Reports,* vol. 8, p. 14829, 2018.

[95] K. Choi, S. Mein, B. Kopp, G. Magro, S. Molinelli, M. Ciocca, and A. Mairani, "FRoG—A new calculation engine for clinical investigations with proton and carbon ion beams at CNAO," *Cancers,* vol. 10, p. 395, 2018.

[96] I. Dokic, A. Mairani, M. Niklas, F. Zimmermann, N. Chaudhri, D. Krunic, T. Tessonnier, A. Ferrari, K. Parodi, O. Jäkel, J. Debus, T. Haberer, and A. Abdollahi,

"Next generation multi-scale biophysical characterization of high precision cancer particle radiotherapy using clinical proton, helium-, carbon- and oxygen ion beams," *Oncotarget,* vol. 7, p. 56676–56689, 2016.

[97] A. Mairani, G. Magro, T. Tessonnier, T. T. Böhlen, S. Molinelli, A. Ferrari, K. Parodi, J. Debus, and T. Haberer, "Optimizing the modified microdosimetric kinetic model input parameters for proton and ^{4}He ion beam therapy application," *Physics in Medicine and Biology,* vol. 62, p. N244–N256, 2017.

[98] G. Magro, T. J. Dahle, S. Molinelli, M. Ciocca, P. Fossati, A. Ferrari, T. Inaniwa, N. Matsufuji, K. S. Ytre-Hauge, and A. Mairani, "The FLUKA Monte Carlo code coupled with the NIRS approach for clinical dose calculations in carbon ion therapy," *Physics in Medicine and Biology,* vol. 62, p. 3814–3827, 2017.

[99] Y. Simeonov, U. Weber, P. Penchev, T. P. Ringbæk, C. Schuy, S. Brons, R. Engenhart-Cabillic, J. Bliedtner, and K. Zink, "3D range-modulator for scanned particle therapy: Development, Monte Carlo simulations and experimental evaluation," *Physics in Medicine & Biology,* vol. 62, p. 7075–7096, 2017.

[100] P. Wang, M. Wang, F. Liu, S. Ding, X. Wang, G. Du, J. Liu, P. Apel, P. Kluth, C. Trautmann, and Y. Wang, "Ultrafast ion sieving using nanoporous polymeric membranes," *Nature Communications,* vol. 9, p. 569, 2018.

[101] S. Lehrack, W. Assmann, D. Bertrand, S. Henrotin, J. Herault, V. Heymans, F. V. Stappen, P. G. Thirolf, M. Vidal, J. V. de Walle, and K. Parodi, "Submillimeter ionoacoustic range determination for protons in water at a clinical synchrocyclotron," *Physics in Medicine & Biology,* vol. 62, p. L20–L30, 2017.

[102] M. Winkler, H. Geissel, H. Weick, B. Achenbach, K.-H. Behr, D. Boutin, A. Brünle, M. Gleim, W. Hüller, C. Karagiannis, A. Kelic, B. Kindler, E. Kozlova, H. Leibrock, B. Lommel, G. Moritz, C. Mühle, G. Münzenberg, C. Nociforo, and W. Plass, "The status of the Super-FRS in-flight facility at FAIR," *Nuclear Instruments and Methods in Physics Research Section B: Beam Interactions with Materials and Atoms,* vol. 266, p. 4183–4187, 2008.

[103] K. Kupka, M. Tomut, P. Simon, C. Hubert, A. Romanenko, B. Lommel, and C. Trautmann, "Intense heavy ion beam-induced temperature effects in carbon-based stripper foils," *Journal of Radioanalytical and Nuclear Chemistry,* vol. 305, p. 875–882, 2015.

[104] "I.FAST," [Online]. Available: https://ifast-project.eu/.

[105] "HITRIplus Project," [Online]. Available: https://www.hitriplus.eu/.

[106] Y. Iwata, T. Kadowaki, H. Uchiyama, T. Fujimoto, E. Takada, T. Shirai, T. Furukawa, K. Mizushima, E. Takeshita, K. Katagiri, S. Sato, and Y. Sano, "Multiple-energy operation with extended flattops at HIMAC," *Nuclear Instruments and Methods in Physics Research Section A: Accelerators, Spectrometers, Detectors and Associated Equipment,* vol. 624, p. 33–38, 2010.

[107] R. Taylor, E. Benedetto, M. Sapinski, and J. Pasternak, "Slow extraction modelling for NIMMS hadron therapy synchrotrons," *Journal of Physics: Conference Series,* vol. 2420, p. 012101, 2022. Also in Proc. IPAC'22.

[108] B. Schlitt, "Status of the 7 MeV/u, 217 MHz injector linac for the Heidelberg Cancer Therapy Facility," in *Proc. of the LINAC2004 Conf.*, Lübeck, Germany.

[109] B. Schlitt, "Commissioning and operation of the injector linacs for HIT and CNAO," in *Proc. of the LINAC2008 Conf.*, Victoria, Canada.

[110] B. Schlitt, “Commissioning and Operation of the Injector Linacs for HIT and CNAO, ” in *Proc. of Linear Accelerator Conference (LINAC'08), Victoria, British Columbia, Canada, 29 Sep–3 Oct 2008*, Geneva, 2008.

[111] Y. Iwata, S. Yamada, T. Murakami, T. Fujimoto, T. Fujisawa, H. Ogawa, N. Miyahara, K. Yamamoto, S. Hojo, Y. Sakamoto, M. Muramatsu, T. Takeuchi, T. Mitsumoto, H. Tsutsui, T. Watanabe, and T. Ueda, “Alternating-phase-focused IH-DTL for an injector of heavy-ion medical accelerators,” *Nuclear Instruments and Methods in Physics Research Section A: Accelerators, Spectrometers, Detectors and Associated Equipment,* vol. 569, p. 685–696, 2006.

[112] G. Castro, “The AISHa ion source at INFN-LNS,” *Journal of Physics*, 2022.

[113] A. C. Villlari, “PK-ISIS: A new superconducting ECR ion source at Pantechnik,” in *Proc. of ECRIS2010*, Grenoble, France.

[114] U. Ratzingerer, B. Koubek, H. Hoeltermann, H. Podlech, Bevatech GmbH, and M. Vretenar, “Linac design within HITRIplus for particle therapy,” in *31st Int. Linear Accel. Conf. LINAC2022*, Liverpool, UK.

[115] R. Tiede, G. Clemente, H. Podlech, U. Ratzinger, A. Sauer, and S. Minaev, LOSASR Code Development, CERN, Geneva, 2006.

[116] L. Nikitovic, T. Torims, and M. Vretenar, “Comparison of 352 MHz linac structures for injection into an ion therapy accelerator,” *Journal of Physics: Conference Series*.

[117] C. Schmitzer, “MedAustron Synchrotron RF Commissioning for Medical Proton Beams, ” in *Proc. of International Particle Accelerator Conference (IPAC'16), Busan, Korea, May 8–13, 2016*, Geneva, 2016.

[118] C. Ohmori, E. Ezura, K. Hara, K. Hasegawa, Y. Makida, R. Muto, M. Nomura, T. Ogitsu, T. Shimada, A. Schnase, K. Takata, A. Takagi, F. Tamura, K. Tanaka, M. Toda, M. Yamamoto, and M. Yoshii, “Development of a high gradient RF system using a nanocrystalline soft magnetic alloy,” *Physical Review Special Topics—Accelerators and Beams,* vol. 16, no. 11, p. 112002, 2013.

[119] C. Ohmori, M. Kanazawa, K. Noda, M. Kawashima, T. Misu, Y. Mori, A. Sugiura, A. Takagi, and T. Uesugi, “A multi-harmonic RF system using a MA cavity,” *Nuclear Instruments and Methods in Physics Research Section A: Accelerators, Spectrometers, Detectors and Associated Equipment,* vol. 547, p. 249–258, 2005.

[120] M. M. Paoluzzi, “The New 1-18 MHz Wideband RF System for the CERN PS Booster, ” in *Proc. 10th International Particle Accelerator Conference (IPAC'19), Melbourne, Australia, 19–24 May 2019*, Geneva, 2019.

[121] A. Advic, Multiturn injection of Carbon Ions in a Medical Synchrotron, Master’s Thesis, University of Sarajevo, 2020.

[122] M.Vretenar, M. E. Angoletta, G. Bisoffi, J. Borburgh, L. Bottura, K. Paļskis, R. Taylor, G. Tranquille, E. Benedetto, and M. Sapinski, “A compact synchrotron for advanced cancer therapy with helium and proton beams,” in *13th Int. Particle Acc. Conf. IPAC2022*, Bangkok, Thailand, 2022.

[123] G. Feldbauer, M. Benedikt, and U. Dorda, “Simulations of various driving mechanisms for the 3rd order resonant extraction from the MedAustron medical synchrotron,” p. 3, 2011.

[124] S. Rossi, An Air Core Quadrupole for the PIMMS Synchrotron, CERN, Geneva, 2000.

[125] R. Singh, P. Forck, and S. Sorge, “Reducing fluctuations in slow-extraction beam spill using transit-time-dependent tune modulation,” *Physical Review Applied,* vol. 13, no. 4, p. 044076, 2020.

[126] X. Zhang, *Lattice Design of a Carbon-Ion Synchrotron based on Double-Bend Achromat Lens,* 2020.

[127] E. Benedetto, N. Al Harbi, P. Riboni, L. Brouwer, S. Prestempon, and U. Amaldi, "A carbon ion superconducting gantry and a synchrotron based on canted cosine theta magnets," *submitted to Physics in Medicine and Biology,* 2020.

[128] L. Brouwer, S. Caspi, R. Hafalia, A. Hodgkinson, S. Prestemon, D. Robin, and W. Wan, "Design of an schromatic superconducting magnet for a proton therapy gantry," *IEEE Transactions on Applied Superconductivity,* vol. 27, p. 1–6, 2017.

[129] L. Rossi, "Magnet technology and design of superconducting magnets for heavy ion gantry for hadron therapy," in *14th Innternational Particle Accelerator Conference IPAC 23*, Venice, Italy, 11th May 2023.

[130] E. D. Matteis, "Straight and curved canted cosine theta superconducting dipoles for ion therapy: Comparison between various design options and technologies for ramping operation," in *Applied Superconductivity Conference 2022 (ASC22)*, Honolulu, USA, 26 October 2022.

[131] R. L. Taylor, J. Pasternak, E. Benedetto, and M. Sapinski, "Slow extraction modelling for NIMMS hadron therapy synchrotrons," in *IPAC'22*, Bangkok, Thailand, Jun. 2022, paper THPOMS019, Jun. 2022.

[132] E. Benedetto, "Carbon ion compact medical synchrotron: Key parameters," CERN-ACC-NOTE-2022-0017, NIMMS-Note 008, CERN, Geneva, 2022.

[133] F. Grote and H. Schmidt, "MAD-X – An Upgrade from MAD8," in *Proc. PAC'03*, Portland, OR, USA, May 2003.

[134] A. Peters and P. Forck, "Beam diagnostics for the heavy ion cancer therapy facility," *AIP Conference Proceedings,* vol. 546, pp. 519–526, 2000.

[135] R. Dölling, "Profile, current, and halo monitors of the PROSCAN beam lines," *AIP Conference Proceedings,* vol. 732, pp. 286–291, 2004.

[136] M. Galonska, S. Scheloske, S. Brons, R. Cee, K. Hoppner, J. Mosthaf, A. Peters, and T. Haberer, "The hit gantry: From commissioning to operation.," in *IPAC 2013: Proceedings of the 4th International Particle Accelerator Conference*, 2013.

[137] Quantum Life and Medical Science Directorate, "NIRS and Toshiba Complete World's First Rotating Gantry with Superconducting Technology for Heavy-ion Radiotherapy System," 8 January 2016. [Online]. Available: https://www.qst.go.jp/site/nirs-english/1376.html. [Accessed 9 February 2024].

[138] U. Weinrich and C. M. Kleffner, "Commissioning of the carbon beam gantry at the Heidelberg Ion Therapy (HIT) accelerator," in *Proc. European Particle Accelerator Conference (EPAC2008), Genova, Italy*, 2008.

[139] J. B. Farr, J. B. Flanz, A. Gerbershagen, and M. F. Moyers, "New horizons in particle therapy systems," *Medical Physics,* vol. 45, p. e953–e983, 2018.

[140] U. Amaldi, E. Benedetto, P. Riboni, D. Tommasini, and M. Karppiner, "Conceptual design of a light superconducting carbon ion gantry," 2020.

[141] U. Amaldi, N. Alharbi, E. Benedetto, P. Riboni, M. Vaziri, D. Aguglia, V. Ferrentino, G. Le Godec, M. Karppinen, D. Perini, E. Ravaioli, and D. Tommasini, "SIGRUM - A Superconducting Ion Gantry with Riboni's Unconventional Mechanics," CERN, Geneva, 2021. https://cds.cern.ch/record/2766876

[142] L. Bottura, E. Felcini, G. D. Rijk, and B. Dutoit, "GaToroid: A novel toroidal gantry for hadron therapy," *Nuclear Instruments and Methods in Physics Research Section A: Accelerators, Spectrometers, Detectors and Associated Equipment,* p. 164588, 2020.

[143] E. Felicini, A. Haziot, A. Louzguiti, T. Lehtinen, G. Vernassa, B. Dutoit, and L. Bottura, “Feasibility study of GaToroid gantries for carbon ions,” in *27th International Conference on Magnet Technology (MT-27)*, Fukuoka, Japan, 2022.

[144] M. G. Pullia, E. Benedetto, L. Dassa, E. D. Matteis, M. Donetti, E. Felcini, G. Frisella, M. Karppinen, C. Kurfürst, S. Mariotto, A. Mereghetti, A. Mirandola, A. Pella, D. Perini, L. Piacentini, M. T. F. Pivi, M. Prioli, A. Ratkus, and Rossi, “Explorative studies of an innovative superconducting gantry,” *Journal of Physics: Conference Series,* vol. 2420, 2023.

[145] L. Piacentini, L. Dassa, D. Perini, A. Ratkus, T. Torims, J. Villcans, and M. Vretenar, Comparative Study on Scenarios for Rotating Gantry Mechanical Structures, Geneva, 2022.

[146] M. Vretenar, A. Mamaras, G. Bisoffi, and P. Foka, “Production of radioisotopes for cancer imaging and treatment with compact linear accelerators,” in *JACoW*.

[147] L. Arnaudon, Linac4 Technical Design Report, CERN, Geneva, 2006.

[148] U. Amaldi, “Oblique raster scanning: An ion dose delivery procedure with variable energy layers,” *Physics in Medicine and Biology,* vol. 64, 2019.

[149] M. Seidel, R. Gehring, E. Jensen, T. I. Parker, P. J. Spiller, and J. Stadlmann, “Improving the energy efficiency of accelerator facilities,” in *Proc. 6th International Particle Accelerator Conference (IPAC'15), Richmond, VA, USA, May 3–8, 2015*, Geneva, 2015.

[150] “Energy Efficiency of Particle Accelerators (EnEfficient)” [Online]. Available: https://www.psi.ch/en/enefficient.

[151] J. Stadlmann, R. Gehring, E. Jensen, T. I. Parker, M. Seidel, and P. J. Spiller, “Energy efficiency of particle accelerators - A networking effort within the EUCARD program,” in *Proc. 5th International Particle Accelerator Conference (IPAC'14), Dresden, Germany, June 15–20, 2014*, Geneva, 2014.

[152] “ARIES Workshop on Energy Efficient RF” [Online]. Available : https://indico.uu.se/event/515/.

[153] G. Bisoffi, E. Benedetto, M. Karppinen, M. R. Khalvati, M. G. Pullia, M. Sapinski, M. Sorbi, L. Rossi, R. U. Valente, R. v. Weelderen, G. Venchi, and M. Vretenar, Energy Comparison of Hadron Therapy facilities based on Normal Conducting and Superconducting Magnet Synchrotrons, NIMMS-Note-021, CERN, Geneva, 2024.

[154] C. Muehle, “Fast-pulsed superconducting magnets,” in *Proc. of the 39th ICFA Advanced Beam Dynamics Workshop (HB2006)*, Japan, 2007.